Evaluation of X-ray Fluorescence Spectroscopy as a Tool for Element Analysis in Pea Seeds

A Thesis Submitted to the College of Graduate and Postdoctoral Studies

In Partial Fulfillment of the Requirements

For the Degree of Master of Science

In the Department of Plant Sciences

University of Saskatchewan

Saskatoon

By

RAMANDEEP KAUR BAMRAH

PERMISSION TO USE

In presenting this thesis in partial fulfillment of the requirements for a graduate degree from the University of Saskatchewan, I agree that the Libraries of this University may make it freely available for inspection. I further agree that permission for copying of this thesis in any manner, in whole or in part, for scholarly purposes may be granted by the professor or professors who supervised my thesis work or, in their absence, by the Head of the Department or the Dean of the College in which my thesis work was done. It is understood that any copying or publication or use of this dissertation or parts thereof for financial gain shall not be allowed without my written permission. It is also understood that due recognition shall be given to me and to the University of Saskatchewan in any scholarly use which may be made of any material in my thesis.

Requests for permission to copy or to make other uses of materials in this thesis in whole or part should be addressed to:

Head, Department of Plant Sciences
University of Saskatchewan
Agriculture Building, 51 Campus Drive Saskatoon
Saskatoon, Saskatchewan S7N 5A8
Canada

OR

Dean
College of Graduate and Postdoctoral Studies
University of Saskatchewan
116 Thorvaldson Building, 110 Science Place
Saskatoon, Saskatchewan S7N 5C9
Canada

ABSTRACT

X-ray fluorescence spectroscopy (XRF) is a powerful analytical tool for the determination of elemental composition of diverse materials. The principal aim of this study was to evaluate and characterize the utility and reliability of synchrotron-based XRF for use in element analysis of field pea seeds for quantification of macro- (K and Ca) and micro- (Mn, Fe, Cu, Zn, Se) elements. Pea seed samples were ground into fine flour and pellets were prepared to collect XRF peak intensities. Seventy-three pea seed samples were selected to cover the expected concentration ranges for each element for developing calibration curves by correlating the results from atomic absorption spectroscopy (AAS) reference method and XRF peak intensities. For all the calibration curves R^2 values were above 0.8 except for K (0.5). XRF results were validated by a systematic comparison with data obtained from AAS on a set of 80 additional and independent pea seed samples (Validation Set). Element concentrations were also predicted using the fundamental parameter approach collectively for 153 samples. Limit of detection was calculated as low as 0.016 mg/kg for Se and 9.54 mg/kg for K. For Mn, Cu, Zn, Se, the XRF method was found to be not statistically different from AAS method at 95% confidence interval; furthermore, the bias between the methods was not significantly different from 0. Relative standard deviation (RSD) was less than 26% in XRF and range of recovery 75-165% for different elements. For the lower energy elements K and Ca, significant negative bias was observed (statistically different from 0) indicating underprediction by XRF method. The intercepts of the validation curve were -1460.3 and -61.27 for K and Ca respectively. Similar results were obtained with the fundamental parameter approach except for Fe for which significant bias of ~6 mg/kg was calculated. The intercept of validation curves was found to be not significantly different from 0 and B (the slope) was found to be not significantly different from 1. This leads to the conclusion that the results obtained using XRF and AAS were statistically not different from AAS method at 95% confidence interval. This study demonstrated that the XRF technique is a fast and reliable tool for element analysis, particularly for high energy elements and does not produce waste and requires no chemical reagents.

ACKNOWLEDGEMENTS

I would like to first and foremost express my sincere appreciation and gratitude to my supervisor, Dr. Tom Warkentin for taking me on as his graduate student, for all the guidance, support and encouragement throughout my M.Sc. program. You have been a great mentor and I could not have had a better supervisor. I will be forever grateful for all the opportunities you have given me, opportunities that I have never imagined. I would also like to thank my advisory committee, Dr. Karen Tanino, Dr. Michael Nickerson, committee chair, Dr. Helen Booker, and defense chair Dr. Kate Congreves for their helpful guidance and direction during this project. Thanks to Dr. Derek Peak, who agreed to act as external examiner. My special thanks go to Dr. Perumal Vijayan and Dr. Emil Hallin for their inspiration, guidance, and help throughout my project.

I am also very thankful to Dr. Chithra Karunakaran for her expertise and inputs to this project. Special thanks to Dr. David Muir for designing a new software for XRF data collection, booking of CLS shifts and with processing and analysis of XRF spectra. I would also like to thank Barry Goetz for his help and guidance in atomic absorption spectroscopy analysis of my samples. I am thankful to everyone who assisted with laboratory analysis and spectroscopic analysis of my samples.

Finally, I am thankful to my friends for their friendship, support, advice and their help in grinding the samples and collection of XRF data. I am especially grateful to my family for their support, and constant encouragement. Financial support provided by Government of Saskatchewan and Western Grains Research Foundation is gratefully acknowledged.

DEDICATION

To my Mother and Father....

TABLE OF CONTENTS

LIST OF TABLES

LIST OF FIGURES

LIST OF ABBREVIATIONS

XRF	**:**	X-ray Fluorescence Spectroscopy
EDXRF	**:**	Energy Dispersive X-ray Fluorescence Spectroscopy
AAS	**:**	Atomic Absorption Spectroscopy
ICP-MS	**:**	Inductively Coupled Plasma Mass Spectroscopy
ICP-AES	**:**	Inductively Coupled Plasma Atomic Emission Spectroscopy
WDXRF	**:**	Wavelength Dispersive X-ray Fluorescence Spectrometer
TXRF	**:**	Total Reflection X-ray Fluorescence
RSD	**:**	Relative Standard Deviation
SD	**:**	Standard Deviation
CV	**:**	Coefficient of Variation
NIR	**:**	Near Infrared Radiation
CLS	**:**	Canadian Light Source
HNO_3	**:**	Nitric acid
H_2O_2	**:**	Hydrogen Peroxide
HCl	**:**	Hydrochloric acid
HF	**:**	Hydrofluoric acid
K	**:**	Potassium
Ca	**:**	Calcium
Mn	**:**	Manganese
Fe	**:**	Iron
Cu	**:**	Copper
Zn	**:**	Zinc
Se	**:**	Selenium

1.0 INTRODUCTION

1.1 Thesis Overview

Increasing agricultural productivity in an environmentally sound manner is a high priority in public policy, along with improving the availability of nutritious foods for a growing world population. Mineral elements are the metals and their derivatives present in body tissues and fluids. Though they do not yield any energy, they play important physiological roles essential for life (Soetan et al., 2010). Mineral elements are important for human and animal nutrition as nutrient sufficiency is the basis of productivity, good health and longevity, however, two-thirds of the world's population suffer from a deficiency in one or more essential mineral elements (White and Broadley, 2009; Welch, 2002). Deficiencies of minerals afflicts a variety of diseases and conditions including iron deficiency that causes anemia, pregnancy complications, child mortality, reduced work capacity, and reduced immunity to infections (Soetan et al., 2010). Strategies to deliver minerals to susceptible populations include mineral supplementation (White and Broadley, 2005) and diet diversification (White and Broadley, 2009), but these approaches have had only moderate success. An alternative approach, 'biofortification' or development of crop varieties with greater mineral bioavailability has been proposed to help combat these dietary deficiencies.

Pulse crop seeds are richer sources of dietary minerals compared to cereals and root crops with a potential to provide 15 of the essential minerals required by humans (Wang et al, 2003; Welch 2002; Ma et al., 2017). Most of the cropping area in Saskatchewan is composed of the Brown, Dark Brown, and Black soil zones and is adequate in mineral composition (Ray et al, 2014). Saskatchewan is a major pulse growing area being the

major exporter of field peas to India, China and Bangladesh (Ray et al., 2014). Pea is an annual, self-pollinated pulse crop and is one of the major legume crops grown in Western Canada along with lentil. The major producers of dry peas were Canada (30.4%), China (13.9%), Russia (13.3%), the United States (6.9%) and India (5.3%) in 2014 (FAOSTAT, 2014). It is grown on over 10 million hectares worldwide annually. An increase of 0.76 million hectares under dry field pea production has been reported in Canada from 2011 to 2016 (Fig. 1.1). Moreover, associated with high nitrogen fixation, it plays a vital role in the prairie crop rotation system and reduces the production cost for farmers.

The major market classes of field pea are those with yellow or green cotyledons. High nutritional value of peas makes them capable of meeting the dietary needs of the undernourished population in the world as, in addition to protein and complex carbohydrates, vitamins and minerals in peas play a key role in the prevention of deficiency related diseases (Dahl et al., 2012). Peas are a rich source of protein, complex carbohydrates, fiber, B vitamins, and minerals including potassium, magnesium, calcium, and iron that have beneficial health effects (Warkentin et al., 2012). Pea has been recognized as a valuable and nutritious food for human diets and is one of the crops targeted for biofortification (Ma et al., 2017). Development of pea varieties with high mineral concentration or decreased anti-nutritional components can be a solution to mineral deficiency all over the world. Phytate is one of the major anti-nutritional components of staple food crops that inhibits Fe and Zn bioavailability. In recent years, to mitigate the nutritional concern arising from phytate-rich cultivars, low-phytate pea breeding mutant lines have been developed and cultivars will be developed in next couple of years (Warkentin et al., 2012; Banger et al., 2017).

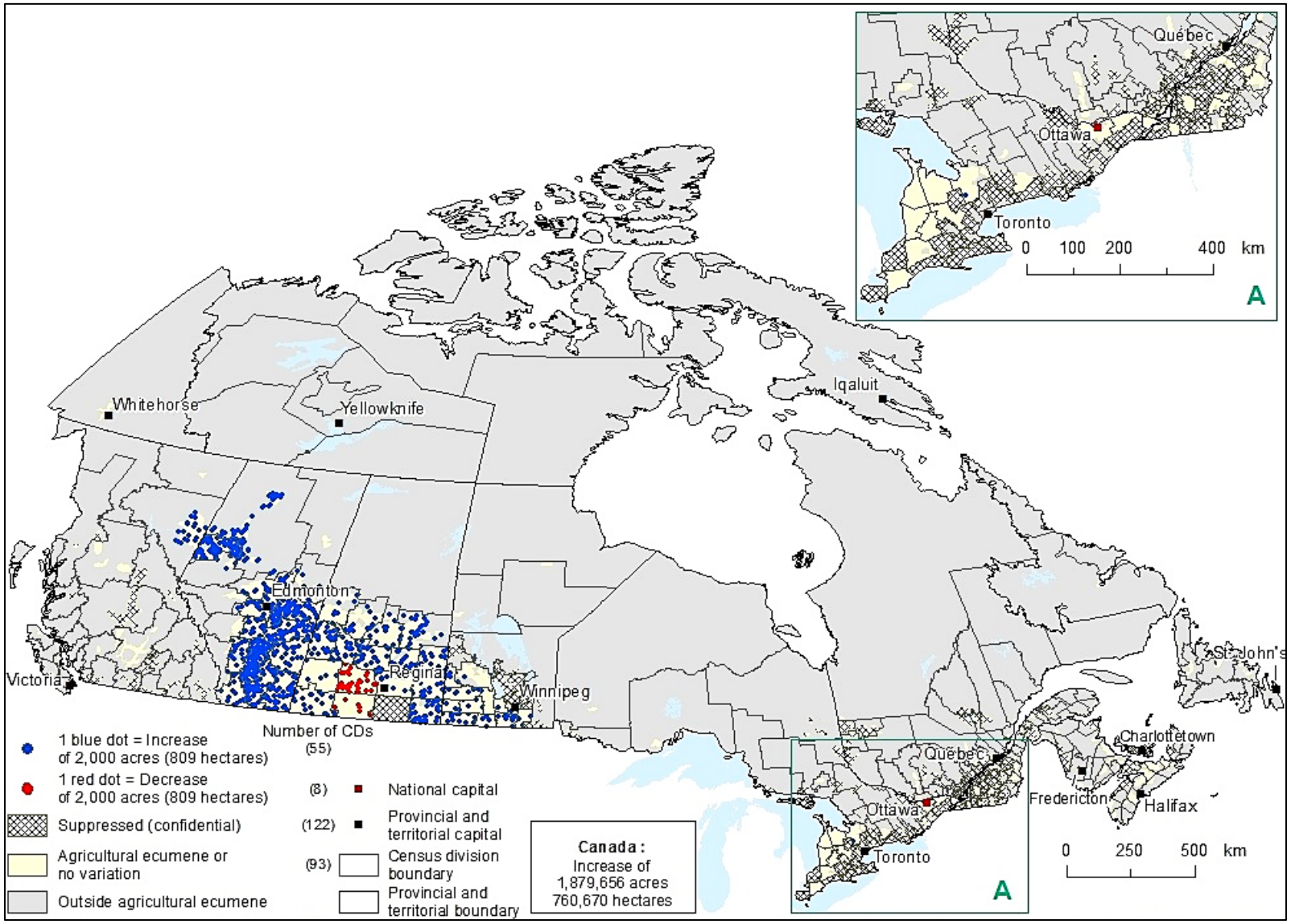

Figure 1.1 Change in dry field pea area by census division (CD) from 2011 to 2016 (from Statistics Canada, 2016).

Although micronutrient deficiency is less prevalent in developed countries (Marx, 1997), vegetable protein sources like peas can be a good option for vegetarians and flexitarians. Thus, assessment of the mineral content of food and animal feed is essential for the formulation of feeding regimes and food processing techniques (Simsek and Aykut, 2007). Determination of elemental composition of plant material is also important for estimating the availability of nutrients in the soil and studying mineral nutrition-related plant growth, development, and maturation processes that can affect yields (Kalra, 1997). However, reporting of heavy metals or permissible limits for the elements is also important as some of the trace elements are toxic for humans at very low levels of intake (Gawalko et al., 2009). As quality control of foods increases, it is a major challenge to provide rapid, multi-element and accurate techniques to obtain control data about toxicity or nutritional value. Therefore, developing and standardizing reliable, cost-effective methods for element analysis is fundamental to these efforts.

There have been considerable efforts to determine the concentrations of elements in plant and food samples using atomic absorption spectroscopy (AAS) and inductively coupled plasma mass spectroscopy (ICP-MS). Though reliable, these methods are digestion-based methods and require contamination free reagents and extensive sample preparation (Perring and Andrey, 2018). X-ray fluorescence (XRF) is an elemental analysis technique that has been established for accurate elemental analysis in several fields including environmental pollution (Borgese et al., 2009), medicine and pharmacy, biochemical research, quality control systems, oil, paints and fuel industries (Howard et al., 2012), forensic sciences (Mamedov, 2012), as well as agriculture and food industries (Krupskaya et al., 2015). This technique is based on the principle that on exposure to

suitable energy X-rays, each element produces secondary fluorescent X-rays and it is possible to identify and quantify the elemental composition of the sample from X-ray spectra by correlating the intensity to the concentration of an element in the sample. A potential advantage of XRF technique compared to chemical methods is that the measurements can be carried out directly on the solid material as milled and ground powder pressed into pellets or directly poured into cups. When optimized, XRF may be simple to use and relatively rapid, but the XRF technique is totally dependent on the reference methods for equipment and method calibration, validation and monitoring. In this study, XRF was evaluated for multi-elemental analysis for quantification of essential macro (K and Ca) and trace elements (Mn, Fe, Cu, Zn, Se) in field pea seeds.

1.2 Research Hypothesis

X-ray fluorescence (XRF) technique can quantify the concentration of elements in pea seeds.

1.3 Research Objectives

Corresponding to the above-mentioned hypothesis, the following were the objectives of this study:

1. To develop a semi-automated method for pea seed sample preparation for XRF analysis.
2. To evaluate a Calibration Set for element concentrations using atomic absorption spectroscopy (AAS) and XRF method and develop a linear relationship between XRF peak areas and AAS concentrations
3. To validate the XRF technique on a Validation Set using empirical and fundamental parameter approaches.

2.0 REVIEW OF LITERATURE

2.1 Element Uptake by Plants

Absorption of element ions by plants is affected by several external factors such as light, temperature, pH and nutrient status of media, oxygen availability and several internal factors like aging, growth and morpho-physiological status (Baldwin, 1975; Miller and Cramer, 2005). Plant cells uptake element ions by two methods:

Passive absorption: Passive transport occurs when a solute is concentrated on one side of a membrane and diffuses from higher to lower concentration. This mechanism does not involve the expenditure of metabolic energy (White, 2012); it is driven by mass flow or diffusion of ions.

Active absorption: In contrast to the passive transport of ions, active transport is an energy consuming process in which the ions are transported against the concentration gradient (White, 2012).

A series of complex processes control the accumulation of elements in seeds and grains such as uptake from rhizosphere, membrane transport in root-shoot cells, translocation and redistribution of elements to vascular phloem which ultimately delivers the nutrients to developing seeds and grains through phloem sap (Ma et al., 2017). Seeds can accumulate micronutrients such as zinc and iron 10-20 times higher than the concentrations in the rest of the plant (Miller and Cramer, 2005).

Several gene families of nutrient transporters specialize in uptake of soil available nutrients and each transport step is mediated by specific transporter proteins (Miller and Cramer, 2005). Some of the plasma membrane transporters sense the external availability of nutrients and are described as ‘transceptors’. Whole plant tissue is used for elemental analysis as the excess nutrients are stored in cell vacuoles (Miller and Cramer, 2005).

Nutrients can be converted into specific forms and can be used as indicators of a plant's nutrient status, for example, phosphorous can be stored as phytate in seeds, and iron storage has been linked to protein ferritin, particularly in legume seeds like peas and beans (Miller and Cramer, 2005). Poorly understood mechanisms of phloem loading and unloading of nutrients need further research to significantly increase certain microelements in staple seeds and grains (Welch, 2002).

The improvement of micronutrient loading in seeds requires knowledge of micronutrient trafficking pathways within the plant, including uptake from soil and remobilization from senescing organs. Most studies have so far focused on micronutrient uptake in root cells, intracellular partitioning, and long-distance transport. In contrast, micronutrient remobilization from vegetative organs during senescence, has received much less attention (Pottier et al., 2014). Senescence of *Arabidopsis thaliana* is associated with decreases by 50% of leaf Fe concentration, in parallel with micronutrient filling in seeds (Himelblau and Amasino, 2001). This finding implies that 50% of micronutrients present in senescent leaves are not remobilized. A better understanding of micronutrient remobilization from senescent organs is therefore likely to highlight new solutions to improve seed micronutrient content. More specifically, mechanisms controlling the availability of nutrients in source organs such as autophagy, could be a matter of great significance for micronutrient loading in seeds (Pottier et al., 2014; Pottier et al., 2018).

2.2 Digestion-based Methods for Element Analysis

Elemental analysis is a valuable tool in several disciplines including mining, manufacturing, soil science ecology, physiology, and agronomy. Therefore, element analysis techniques have rapidly advanced in response to the need for accurate measurements of the elements present in trace amounts (Brown and Milton, 2005). Ash, water, soil, food and plant samples are usually analyzed for the determination of trace, minor and major elements by several techniques such as potentiometry, voltammetry, atomic spectroscopy, X-ray methods and nuclear techniques (Brown and Milton, 2005). Highly sophisticated atomic spectroscopy techniques like Scanning Auger Microprobe, Secondary Ion Mass Spectrometry, Inductively Coupled Plasma Atomic Emission Spectroscopy (ICP-AES) and Inductively Coupled Plasma Mass Spectrometry (ICP-MS) can provide highly accurate results, but atomic absorption spectroscopy is most commonly used for analysis of plant samples. Atomic spectrometry techniques atomize and/or ionize the samples at a very high temperature and then the atomic constituent parts are analyzed by interaction with electromagnetic radiation (absorption and emission) (Brown and Milton, 2005).

2.2.1 Atomic absorption spectroscopy (AAS)

An atomic absorption spectrometer consists of a hollow cathode lamp or electrodeless discharge lamp appropriate for the element(s) of interest, atomizer (flame, graphite tube, and hydride atomizer), monochromator and radiant energy detector system (Kalra, 1997). The sample is introduced in the atomizer where it gets dissociated in its constituent parts (Brown and Milton, 2005). AAS is based on the principle of atomic absorption in which light of a certain wavelength absorbed by free atoms in a gaseous state is measured and

the absorbance is directly proportional to analyze concentration (McIntosh, 2012). The element in the lamp is excited by an electrical current causing radiation to be emitted from the lamp and the sample solution is aspirated into an atomizer converting solution into fine droplets that enter the flame through a burner head (Kalra, 1997). The ground state atoms absorb energy from a hollow cathode lamp and get excited. The energy from the flame strikes a monochromator, which isolates the wavelength of interest. Further, a photomultiplier tube converts the light energy to electrical energy which is related to the concentration of the element (McIntosh, 2012) (Fig. 2.1).

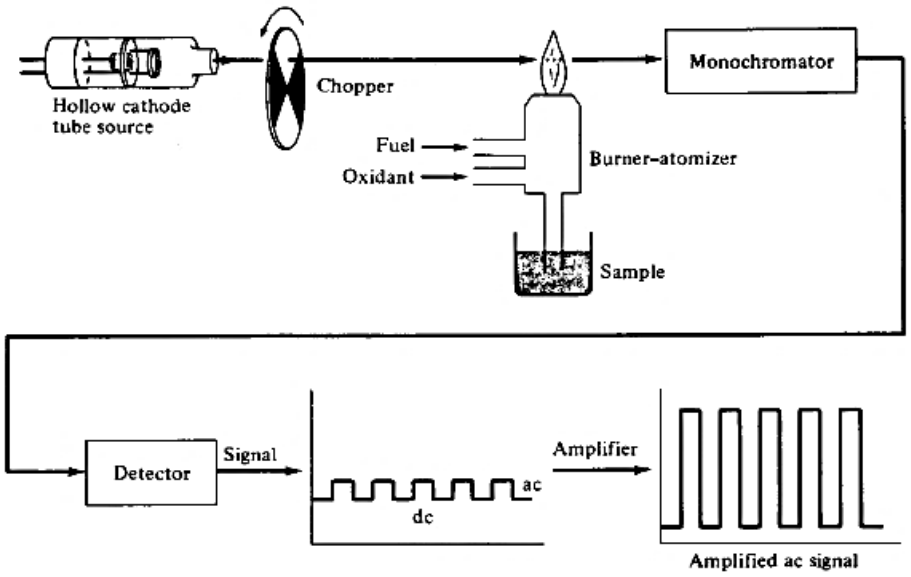

Figure 2.1 Instrumentation of atomic absorption spectroscopy (from McIntosh, 2012).

2.3 Disadvantages of Digestion-Based Techniques

Digestion-based methods for element analysis are hazardous, slow and create a bottleneck in the analysis of some elements when hundreds of samples are to be analyzed. Acid digestion involves the use of nitric, hydrochloric, perchloric, sulphuric or hydrofluoric acid in different proportions according to the sample to be digested

(McLaren et al., 2012). These acids are highly corrosive and produce toxic fumes during the digestion process. Acid handling, heating requirement, incubation time, and sample preparation, in addition to many weighing and serial dilution steps are problems in atomic spectrometry techniques. The accuracy of this method also depends on the extent of destruction of the sample and can lead to elemental loss due to incomplete solubilization of sample or volatilization of elements (Reidinger et al., 2012). Accuracy can be further decreased by oxide formation in the flame (McLaren et al., 2012). Moreover, re-analysis of the samples is not possible if the researcher wishes to analyze the samples at later date. Although ICP-MS offers unsurpassed sensitivity and throughput, the cost of the instrument, its installation, and operation, can be beyond the reach of many laboratories with limited budgets.

2.4 Historical Perspective of X-rays

X-rays were discovered in 1895 by Wilhelm Conrad Röntgen while studying cathode rays in high-voltage, gaseous discharge tubes, and was designated as ‘X’ due to the unknown nature of radiation (Van Grieken and Markowicz, 2001). Röntgen won the Nobel Prize for the discovery of X-rays in 1901. Within a brief time of discovery, there were several attempts to use this radiation for the characterization of matter (Haschke, 2014). The use of X-rays for element characterization started in 1913 when Henry Gwyn Jeffreys Moseley established a specific relationship between the wavelength of characteristic X-ray photons and an atomic number of the excited element (Jenkins, 1999). The X-ray spectrum starts at 0.010 nm (100 eV) and extends to 10 nm (100 KeV). The wavelength of X-ray photons is inversely related to their quantum energies and in the same order of magnitude as the binding energies of inner shell electrons of atoms

(Janssens, 2014). In 1925, X-rays were used for the first time to excite the sample, but the technique was made practical with the development of the first commercial X-ray spectrometer in 1948 (Tsuji et al., 2005). This spectrometer was a wavelength dispersive X-ray spectrometer (WDXRF) and measured the wavelength of one element at a time. Later, energy dispersive X-ray spectrometers (XRF) were discovered which allowed multi-element analysis.

2.5 Interaction of X-rays with Matter

The X-ray beam gets attenuated on interaction with any substance which results in a decrease in intensity of incident beam (Jenkins, 1995). When an X-ray beam passes through a sample, some of the photons might get scattered or absorbed inside the material as illustrated in Fig 2.2.

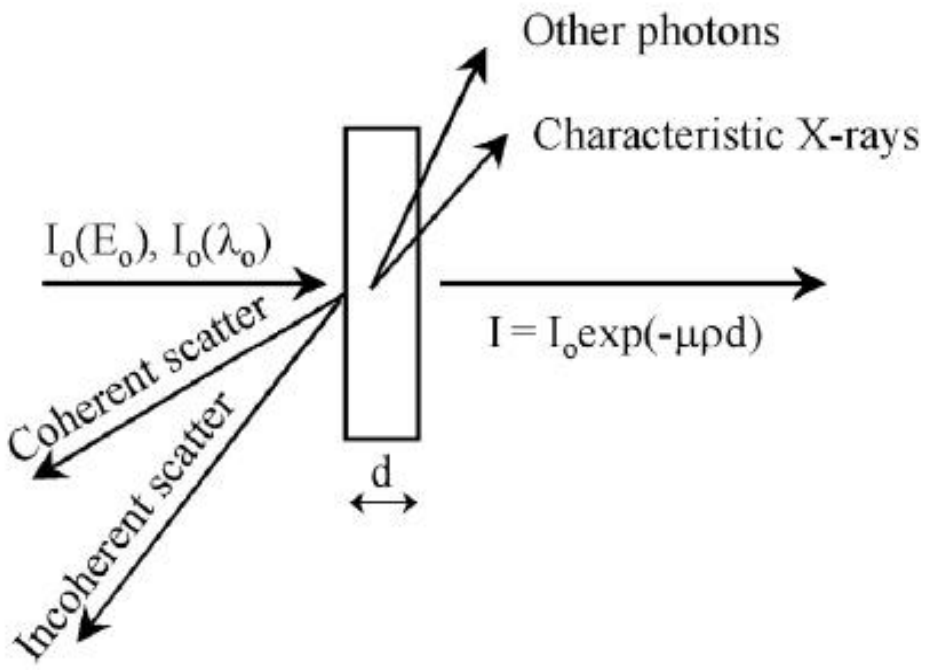

Figure 2.2 Interaction of X-rays with matter (from Jenkins, 1995).

2.5.1 Scattering

The interaction between the radiation and matter can cause the X-rays to change their direction. It is known as elastic or Rayleigh scattering if the energy of the photon remains the same. Scattering occurs when the X-ray photons interact with weakly bound electrons. If the photons lose some energy, it is known as inelastic or Compton scattering (Beckhoff et al., 2007). Compton scattering is the interaction of a photon with a free electron at rest (Van Grieken and Markowicz, 2001). Total cross section of scattering σi can be written as the sum of two components:

$$\sigma i = \sigma R,i + \sigma C,i$$

where $\sigma R,i$ and $\sigma C,i$ respectively denote the cross sections for Rayleigh and Compton scatter of element i.

2.5.2 Photoelectric Effect

Photoelectric absorption, the phenomenon discovered by Albert Einstein in 1905 can only occur if the energy of a photon is equal to or higher than the binding energy of the electron. A photon is completely absorbed, and an inner shell electron is ejected in the case of the photoelectric effect (Fig. 2.3). A portion of the energy of a photon is used to overcome the binding energy of the electron and the rest is transferred as kinetic energy to the ejected electron (Janssens, 2014). The ejection of an electron leaves the atom in an excited state due to the creation of a vacancy, so the atom immediately returns to the stable configuration by emitting an Auger electron or characteristic photon. The ratio of emitted characteristic X-ray photons to the total number of inner shell vacancies created in atomic shell is called fluorescence yield (Beckhoff et al., 2007).

The intensity I_0 of an X-ray beam passing through a layer of thickness d and density ρ is reduced to an intensity I after absorption, according to the well-known law of Lambert-Beer:

$I = I_0 e^{-\mu\rho d}$ where μ is the mass attenuation coefficient

The number of photons (the intensity) is reduced but their energy is generally unchanged (Janssens, 2014).

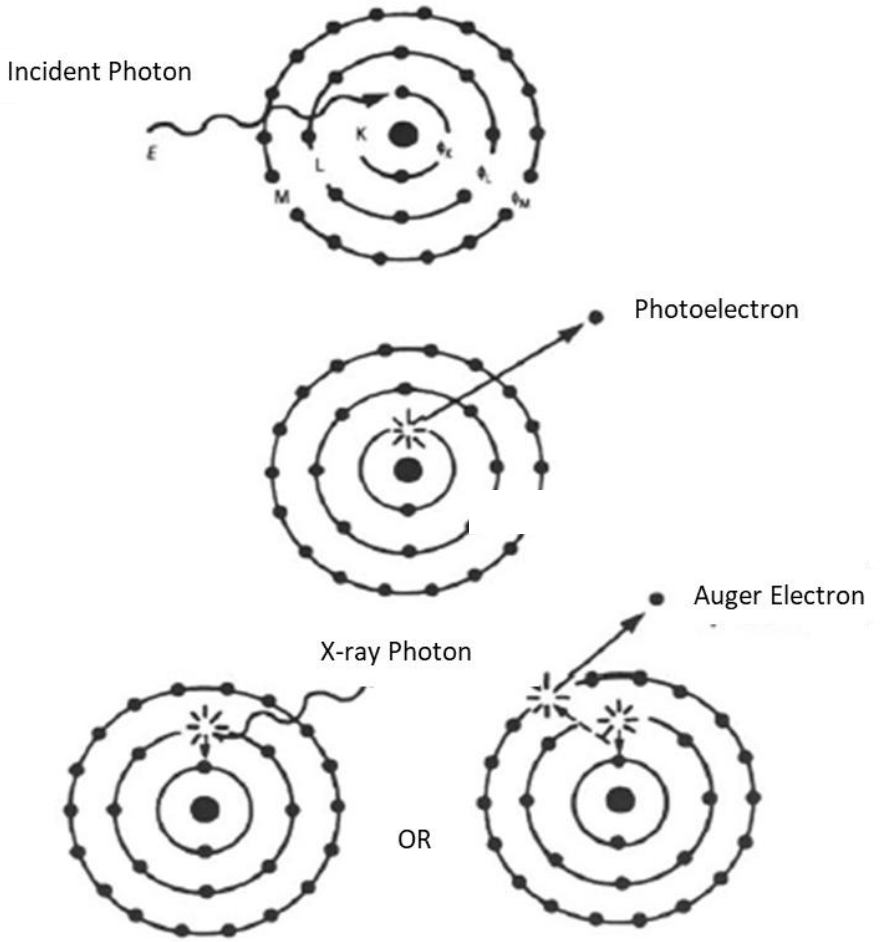

Figure 2.3 Photo-electric absorption effect within the atom (from Janssens, 2014).

The photoelectric cross-section increases as the energy of X-rays decreases as more vacancies are created but a sharp decline in cross-section can be seen at binding energies, as lower energy X-rays are not able to eject the electrons from K shell, but they continue to interact with weakly bound electrons in the L and M shells. This abrupt decrease in cross section is called absorption edge (Beckhoff et al., 2007) and the ratio of the cross-section just above and below the absorption edge is called jump ratio. An efficient absorption process is required for X-ray fluorescence as it is the result of selective absorption of radiation, followed by the spontaneous emission of an electron (Jenkins, 1995).

2.6 X-ray Fluorescence Spectroscopy (XRF)

2.6.1 Basic principle of XRF

The X-ray or Röntgen region starts at 10 nm and extends towards shorter wavelengths. The energy of X-rays is of the same order of magnitude as the binding energies of inner shell electrons and can, therefore, be used to excite or probe these atomic levels (Beckhoff et al., 2007). The electromagnetic wave is emitted and absorbed in a package of discrete energy called photons where energy is proportional to the frequency of radiation (Young and Freedman, 2004). The atom described as Bohr atomic model is composed of a nucleus containing protons and the electrons occupying discrete energy shells. If the energy of a photon is greater than the binding energy of an electron in the shell, the electron will be ejected in a process called the photoelectric effect (Jenkins, 1999). This results in instability of atom as the atom is left in high energy state due to the ejection of an electron from K shell and there are two processes by which the atom can revert into its normal state, auger effect and fluorescence (Van Grieken and Markowicz,

2001). In auger effect, an electron from higher orbital falls into the core hole and in doing so it transfers the energy to another electron from the outer shell, causing the outer electron to eject. Alternatively, when an electron from an outer shell falls into the core hole, the excess energy can be released in the form of an X-ray photon in a process called X-ray fluorescence. The transitions within 100 fs and the one obeying the selection rules for electric dipole radiation can cause the emission of fluorescence radiation (Beckhoff et al., 2007). The emission of this characteristic radiation allows the identification of elements. The elements can be quantified by measurement of the energy of characteristic X-ray photons emitted from the sample from the line spectra with all the characteristic lines superimposed above a certain fluctuating background (Gauglitz and Moore, 2014).

2.6.2 Selection rules and characteristic lines

X-ray spectral series, such as K, L and M series include the allowed transitions that may fill the vacancy in a named atomic shell (Fig 2.4).

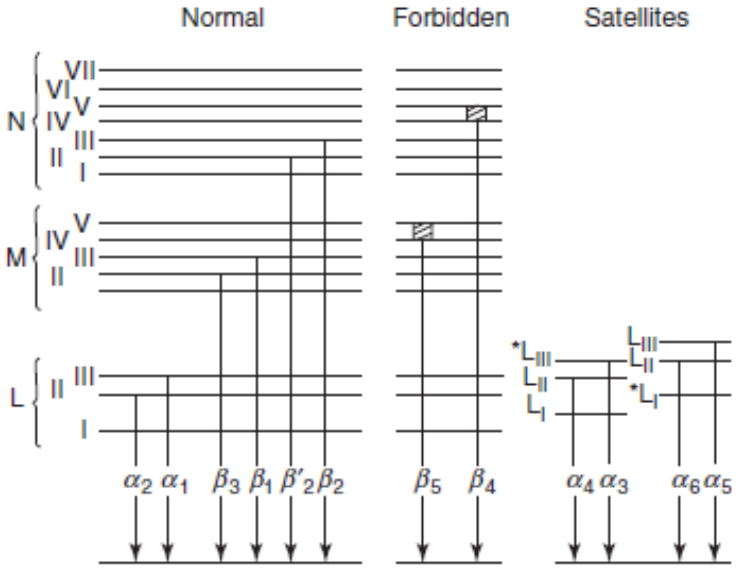

Figure 2.4 Observed characteristic lines in K series for X-ray Fluorescence (from Gauglitz and Moore, 2014).

Additional notions such as α, β and γ indicate which higher energy sub-shell the electron originated from. For example, Kα1 and Kα2 indicate the transitions from L3 and L2 subshells, whereas, K β1, K β2, K β3 lines are produced during the transitions from M3, N2 and M2 subshells (Gauglitz and Vo-Dinh, 2006) (Fig 2.4). Each electron is defined by four quantum numbers, principal quantum number n, which can take all integral values (for K level n=1, for L level n=2 and so on), angular quantum number l that can take all values from (n−1) to 0, m is the magnetic quantum number take values from + l to −l and last is spin quantum number s, with a value of ±1/2. Total momentum J of an electron is given by the vector sum of l+s (Janssens, 2014). For production of normal lines, according to selection rules the principle quantum number must change by at least one, the angular quantum number must change by only one, and total momentum must change by 0 or 1 (Beckhoff et al., 2007). Certain lines that do not abide by the basic selection rules and arise from outer orbital levels may also occur in X-ray spectra which are known as forbidden lines (Fig 2.4). After the ejection of initial electron, the atom can remain in the excited state to such an extent that during this period there is a significant probability of ejection of another electron before the vacancy is filled. The loss of an electron modifies the energies of surrounding electrons and thus X-rays with other energies are emitted. These weak lines known as satellite lines are not analytically significant and may cause confusion in interpretation of spectra (Van Grieken and Markowicz, 2001).

2.6.3 Instrumentation

X-ray spectrometers have similar design, but the use of different components depend upon the analytical task or the type of sample to be analyzed. The general design is presented in Fig 2.5.

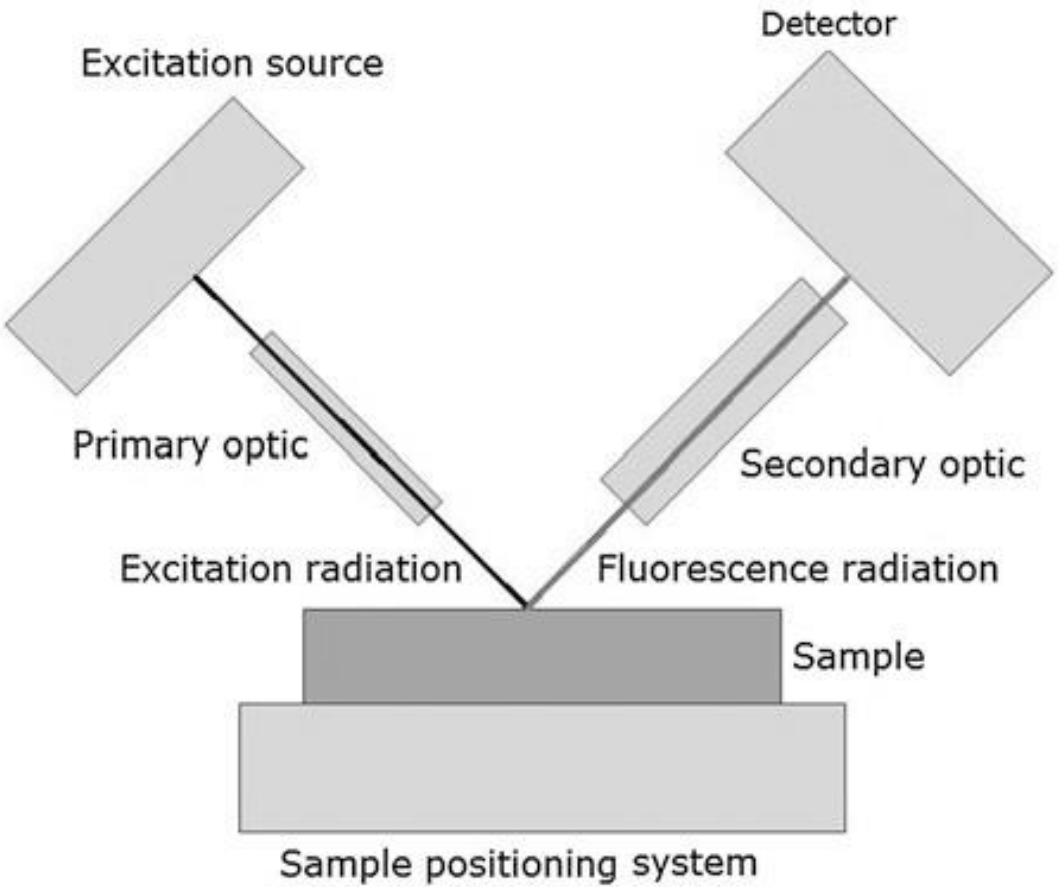

Figure 2.5 General design of XRF spectrometer (from Haschke, 2014).

The main components of XRF spectrometer are:

2.6.3.1 Excitation source

The excitation energy is required more than the bonding energy of the electrons of the atom for production of X-ray fluorescence. The excitation is mostly produced by X-ray tubes in laboratory instruments whereas, radioactive sources, rotating anodes and

synchrotrons (Janssens, 2014) are common in transportable instruments and for highly sophisticated investigations, respectively.

2.6.3.2 Primary optics

Primary optics is positioned between the X-ray source and sample to shape the beam before it hits the sample. These are used to adjust the distribution of source radiation. Similar optics can also be used as secondary optics to shape the secondary beam. Possible primary optics can be the filters for the absorption of special parts of the spectrum, collimators and apertures for defining the beam shape and monochromators for selecting a monochromatic beam (Haschke, 2014).

2.6.3.3 Sample positioning system

The sample can be positioned manually or with a motor driven positioning system if it is in a tray or on a stage, but the position needs to be reproducible in relation to the source and spectrometer. The distance (D) between the source and sample influence the measured intensity by $1/D^2$. (Haschke, 2014). Another influence can be due to tilting the sample surface which can change the absorption for low energetic radiation. Spinning of the sample can be helpful for averaging the sample inhomogeneities. As a small area of the sample is analyzed, it needs to be positioned correctly in the beam. The measurements for the sample can be taken in air, gas flow or vacuum. Generally, vacuum is maintained but for samples that cannot be evacuated, He-flush or other special conditions are used for the analysis of the sample. Different excitation directions of the sample are possible. The sample can be excited from top or bottom (Janssens, 2014).

2.6.3.4 Secondary optics

Secondary optics can be required as a beam shaper which improves the resolution but can also be a dispersive optic that is used as a monochromator (Haschke, 2014).

2.6.3.5 Detector

There are two types of detectors:

2.6.4.5.1 Wavelength Dispersive X-ray Fluorescence Spectrometer (WDXRF)

X-rays emitted from the sample are directed to the crystal which diffracts the X-rays in different directions according to their wavelengths. The detector is placed at a fixed position, but the crystal is rotated so that different wavelengths are picked up by the detector (Beckhoff, 2007). The resolution of WDXRF lies between 5 eV to 20 eV. Higher resolution reduces spectral overlaps and allows the analysis of complex samples with higher accuracy. It also reduces the background and improves the detection limits and sensitivity but use of additional optical components can reduce the efficiency and is more expensive (Janssens and Van Grieken, 2004).

2.6.4.5.2 Energy Dispersive X-ray Fluorescence Spectrometer (EDXRF)

In EDXRF, the entire spectra are acquired simultaneously and the elements across most of the periodic table can be detected within a few seconds (Haschke, 2014). As EDXRF takes less time for generation of spectra, it is widely used in element mapping to build up detailed element images with high spatial resolution for thousands of pixels (Beckhoff, 2007).

2.6.4 Sample preparation

Accurate analysis by XRF requires adequate sample preparation. Samples must be prepared according to the method of analysis and should be representative of the bulk material being tested (Beckhoff et al., 2007). Samples should fit into chamber of XRF spectrometer. Therefore, the sample used for X-ray spectroscopy needs to be effectively homogenized and mostly in fine powder form, but may also be liquid (Janssens, 2014). Lack of sample homogeneity is the most important factor which can cause inaccuracy in X-ray assessment-based element quantification methods larger than matrix effects (Beckhoff et al., 2007), as only a small amount as well as area of sample is analyzed (Haschke, 2014).

2.6.4.1 Solid samples

A solid sample can be analyzed as a bulk sample without any preparation, fused with glass, as a loose powder or powder pressed in pellets (Jenkins, 1995). However, most solid samples require pre-treatment such as cutting, grinding or polishing before analysis to meet the requirement of homogeneity and ensure accurate and quality analysis (Margui and Van Grieken, 2013).

Direct measurement is used when any type of sample preparation may damage its structure. This method of analysis is used for characterizing cultural heritage material that is usually fragile, and in the study of gems and jewelry (Margui and Van Grieken, 2013). Direct measurement is also used for the analysis of layer systems, corrosion layers, contamination and non-homogeneities of valuable samples (Haschke, 2014). Fusion of sample with glass minimizes matrix and surface effects, but not all samples fuse with glass without prior treatment (Jenkins, 1995).

The most common method of analysis is powder preparation. The sample is ground to a fine powder, mixed with binder/matrix and pressed into pellets or tablets resulting in a homogenous sample with a flat surface (Haschke, 2014). Pellets must be compacted and ideally presented as a pellet so that the angle of incidence of the X-rays is uniform and the emitted fluorescence can be captured without bias from all parts of the sample.

2.6.4.2 Liquid samples

Liquid samples can be analyzed directly, by taking few milliliters placed in a cup made of polyethylene or polytetrafluoroethylene with a thin film at the bottom to allow the penetration of X-rays (Margui and Van Grieken, 2013). For top-down measurement, a film is not required, and measurement can be made without any absorbing material in between (Haschke, 2014). In liquid samples, the light matrices generate higher scatter background which reduces the sensitivity compared to solid samples (Margui and Van Grieken, 2013), but the sample is homogeneous and negligible particle size effects are present (Jenkins, 1995). Sometimes, the powdered suspension of water-insoluble material is mixed a with few milliliters of water and filtered through cellulose, glass or plastic filters resulting in a thin layer on the filter which is directly measured by XRF (Margui and Van Grieken, 2013).

2.6.5 Factors Influencing XRF measurements

2.6.5.1 Matrix Effect

The X-ray matrix effect is the most basic and key component in analytical accuracy. The accumulated counts of X-ray photons are always accompanied by statistical fluctuations. As the incident beam passes through the sample it is absorbed due to interaction with atoms and emits fluorescence in all directions (Beckhoff et al., 2007). The fluorescence

radiation in the direction of the detector is collected directly but can also be absorbed in its way by matrix (Haschke, 2014).

The simple linear relation between the observed element counts and the concentration is only valid in a limited number of cases. Beyond the critical depth below the surface of the sample, any emitted photons are absorbed and will not contribute to the fluorescence intensity (Janssens, 2014). This critical depth varies according to the matrix composition and the energy of primary and secondary radiation. The samples thicker than critical penetration depth are called infinitely thick or massive samples. Matrix effects are caused by attenuation and enhancement phenomena that influence X-ray fluorescence intensity. Due to the matrix effect, the observed XRF intensity will no longer be proportional to the concentration of the element.

2.6.5.2 Atomic number of elements

The elements with a low atomic number are difficult to detect as compared to the elements with a high atomic number as their excitation probability is very low (Haschke, 2014). If the fluorescence radiation emitted is of low energy, it may be absorbed in the sample itself.

2.6.5.3 Sample morphology (particle size and homogeneity)

The detected concentration of elements depends upon the exact position of measurement as X-rays can penetrate only a few mm into the sample (Hou et al., 2004). Sample inhomogeneity can drastically affect the results of quantification of elements and result in a low accuracy of quantification (Haschke, 2014). Particle size effects are generally classified as grain size effects, inter-element effects or mineralogical effects (Krusberski, 2006). Within the powdered samples analyzed by XRF, particle size effects are a serious

source of analytical errors contributing >30% deviation if the samples have highly heterogeneous particle size distributions (Mzyk et al., 2002).

2.6.5.4 Sample moisture

Moisture content in the sample is considered one of the most important sources of error especially in soil analysis (Bastos et al., 2012). Water absorbs as well as scatters the primary radiation which results in an exponential decrease in characteristic X-rays (Ge et al., 2005). Effect of moisture on XRF intensity can differ from one element to another and is known to influence light elements (K and below) more as compared to heavier elements (Schneider et al., 2016).

2.6.6 Quantitative Spectra analysis

Spectra evaluation is one of the most critical steps in X-ray analysis, especially in XRF. It involves the techniques for extracting the most accurate information possible about the characteristic lines (Jenkins, 1995). In general, it is possible to distinguish between the amplitude noise, which is the result of the statistical nature of the counting process, and the energy noise which causes the X-ray lines in the spectra to appear much wider than their natural widths (Janssens, 2014). X-ray lines appear as narrow well-defined peaks in WDXRF, and net as well as background intensities can be determined with great accuracy (Gauglitz and Vo-Dinh, 2006). In both, XRF and WDXRF net number of counts under a characteristic line is proportional to the concentration of analyte, which is also true for concentration and net peak height. In XRF as the detector resolution is low, peaks may be low in intensity so peak area as analytical signal is preferred as this results in lower statistical uncertainty for small peaks (Haschke, 2014).

2.6.6.1 Smoothing

Smoothing is a pre-treatment technique applied to a spectrum to remove insignificant noise to reveal important signals. It involves removing oscillatory functions with high frequency and transforming the data back to spectrum form (Kokalj et al., 2011). Smoothing can reduce the statistical fluctuations in the background and make it easier to notice the small peaks near the limit of detection as shown in Fig 2.6 (Tominaga et al., 1972), but smoothing the spectrum to reduce the statistical fluctuations prior to quantitative analysis is not recommended due to low precision associated with the integration of peaks (Jenkins, 1995).

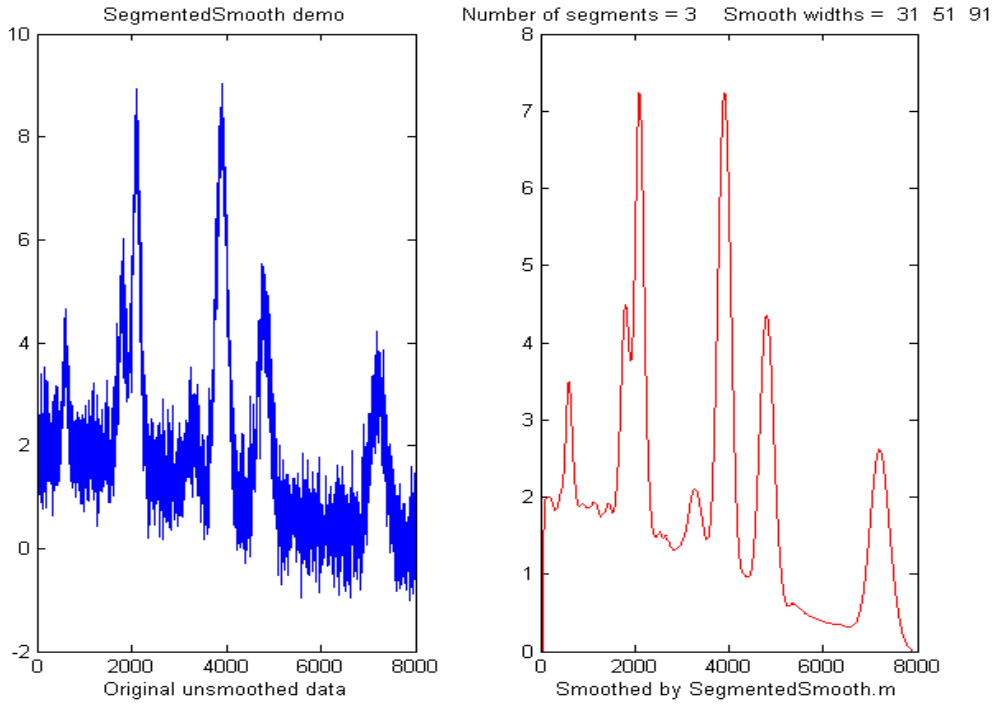

Figure 2.6 Comparison of unsmoothed and smoothed spectrum showing that smoothing can reduce the statistical fluctuations in the background (from Jenkins, 1995).

2.6.6.2 Background Estimation

Background radiation is a limiting factor for determining detection limits, repeatability and reproducibility (Li, 2008). Electron beam excited samples are not perfectly flat, the background shape is not fully predictable, so questions arise concerning how much of the available spectrum should be used to measure the peak area (Statham, 1977). In spectra in which severe peak overlap is not encountered, and well-defined background regions are detected on both sides of peak, simple background subtraction methods can be used. If the neighboring peaks lie too close to the peak of interest, background is estimated through least square fitting of background or quantitative regression analysis models (Jenkins, 1995). Background is estimated by least square polynomial fitting performed on user defined subsets of points, which should belong to the background. If those points are correctly selected, the fitting yields satisfactory results for background estimation (Mazet et al., 2005). When regression models are developed using calibration curves, the background of the spectrum can be included to account for lack of accurate background subtraction in the sample (Jenkins, 1995).

2.6.6.3 Treatment of Peak overlaps

Overlapping of peaks occur when the energies of two or more elements are close to each other. Peak overlap can significantly reduce the accuracy of X-ray spectrum quantification (Jalas et al., 2002). To determine accurate net area under each peak, overlap must be addressed (Jenkins, 1995). Deconvolution refers to assigning the areas to peaks of interest (Brouwer, 2006).

2.6.7 Methods and models for quantitative analysis

Data analysis in XRF requires the conversion of experimental data into analytically useful information and this process can be divided into two parts – evaluation of spectral data and conversion of X-ray data into concentrations (Janssens, 2014). Most of the XRF instruments use software that automatically calculates the results for multiple elements in a variety of matrices without any calibration by the user, but appropriate corrections for matrix effect is a critical issue (Haschke, 2014).

This part can be further divided into two parts – quantification of single elements and quantification of multiple elements (Gauglitz and Vo-Dinh, 2006). The situation may become complex when the matrix is unknown and almost all the elements are to be quantified. Various methods employed for quantification of elements when the matrix is unknown are listed in Table 2.1. The correlation between the concentration of that element and characteristic count rate of the element may be nonlinear over wide ranges of concentration because of interelement effects between the analyte element and other elements making up the sample matrix (Haschke, 2014).

Table 2.1 Methods employed for quantification of elements when the matrix is unknown.

Single element methods	Internal standardization
	Standard addition
	Type standardization
Multiple-element methods	Use of influence coefficients
	Fundamental parameter techniques

The most common method of developing a prediction model is preparation of standard and calibration curves. Standard curves involve use of a series of standard samples to prepare a standard curve that plots peak intensity (area of peak/count rate) against a range of elemental concentrations. In calibration curves, samples with similar matrix properties, but diverse element concentrations are employed to prepare calibration plots. Standard regression equations are derived with a reasonable linear fit of spectral data points (element concentrations). These equations can then be used for predicting the concentrations of elements from measured intensities of appropriate XRF peaks in unknown samples. Matching the matrix of standard or calibration curve with that of samples helps to reduce the matrix effects, also known as in-type or type-matching analysis, which is the most common method of quantitative analysis (Jenkins, 1995). This method is still widely employed today, even with its inherent limitations and need for many calibration standards. Its popularity stems from its ease of application and minimal requirement for computational facilities. If the sample and standard curves differ in matrix, the curves need to be corrected for matrix effects (Jenkins, 1995).

Another type of prediction model involves use of *ab initio* methods such as the Fundamental Parameter (FP) approach that eliminates the need for standards.

Fundamental Parameters (FP) analysis

FP method is a mathematical approach to determine the concentration of elements in variable matrix types as a function of X-ray intensities measured. This approach was independently developed by Shiraiwa and Fujino in 1966, as well as Criss and Birks in 1968, though it was brought into use after the introduction of the personal computer (Van Grieken and Markowicz, 2001). This method is based on the physical theory of X-ray

production rather than empirical relations between observed count rates and concentrations of standard samples (Janssens, 2014). FP equations describe the intensity of fluorescent radiation as a function of sample composition, incident spectrum and spectrometer configuration (Van Grieken and Markowicz, 2001). Various physical constants are used in FP equations such as incidence and exit angles, energy of incident beam, mass attenuation coefficients, fluorescence yield, absorption jump ratios, intensity ratios and energy of absorption edges and emission lines (Van Grieken and Markowicz, 2001) which can be looked up in appropriate tables. FP equations are used to predict the intensity of characteristic lines for the composition of the sample. A set of equations, one for each element to be determined, is written and solved in an iterative way, making the method computationally complex (Janssens, 2014). When an unknown is measured, the calibration data is used to estimate what the intensity would be if each of the elements present were pure. The measured and calculated intensities for the sample are then compared (Van Grieken and Markowicz, 2001). An accurate knowledge of the shape of the excitation spectrum and detector efficiency is required (Janssens, 2014). Use of standards dissimilar in composition to the unknown samples is likely to contribute to inaccuracy. In XRF analysis, once the sample composition is known, intensities of generated fluorescent X-rays can be theoretically calculated by measuring the conditions and physical constants. The FP method utilizes these characteristics in a reverse manner, i.e., it obtains the composition from measured intensities. The fundamental formula for calculation of fluorescence X-ray intensity was derived by Sherman and improved by Shiraiwa and Fujino (Shiraiwa and Fujino, 1966). FP parameters can be used with no reference, if all the parameters in the employed mathematical model are known. The

accuracy obtained depends on all statistical and systematical errors of FP, systematical errors introduced by deficiencies of mathematical models, numerical and statistical computational errors, and statistical errors of the experiment (Mantler and Kawahara, 2004).

2.6.8 Errors in XRF

There are four main categories of random and systematic errors in XRF (Table 2.2). The first category includes the selection and preparation of the sample to be analyzed which is done before the actual prepared sample is presented to the spectrometer (Janssens, 2014). Inadequate sample preparation can not only add to large random error, but heterogeneity of sample can result in greater than 50% systematic error. The second category includes errors arising from the X-ray sources which can be reduced to less than 0.1% using the ratio counting technique. The third category involves the actual counting process and these errors can be both random and systematic.

System errors due to detector dead time can be corrected either by use of electronic dead time correctors or by mathematical approaches. The fourth category includes all errors arising from interelement effects. Each of these effects can give large systematic errors that must be controlled by the calibration and correction scheme.

Table 2.2 Sources of error in X-ray Fluorescence analysis (Janssens, 2014).

Source	Random (%)	Systematic (%)
Sample preparation	0-1	0-5
Sample inhomogeneity	-	0-50
Excitation source fluctuations (Benchtop XRF)	0.05-0.2	0.05-0.5
Spectrometer instability	0.05-0.1	0.05-0.1
Counting statistics	Time dependent	-
Dead time correction	-	0-25
Primary absorption	-	0-50
Secondary absorption	-	0-25
Enhancement	-	0-15
Third-element effects	-	0-2

2.6.9 Statistical Theory for Method Validation

Accuracy

Accuracy refers to the degree of agreement of a measurement made from a sample being analyzed with the 'true result' obtained from an accepted reference standard.

Precision

Precision refers to the degree of agreement between the repeated individual measurements made on the same sample. The precision of a method may be excellent, but its accuracy may be very poor. The terms accuracy and precision are often misused and frequently interchanged.

Bias or Systematic Error

Bias is a consistent deviation of the experimental results from the accepted reference level. The sources of systematic errors such as environmental factors can cause systematic errors.

True Value

The true value is the value of a characteristic obtained from an accepted reference standard.

Confidence Limit

The confidence limits are upper and lower bounds between which the sample values will fall with given probability P.

Random Error

Random error refers to nonsystematic fluctuations in experimental conditions and measurements methods. These may arise from the machine or the operator.

2.6.10 Applications of XRF

2.6.10.1 Food products

XRF has been applied in numerous studies to characterize the elemental content of many foods. Toxic and essential elements were measured by XRF in seafood, which is known to bio-accumulate metals (Manso et al., 2007; Desideri et al., 2009). XRF has been used for the accurate determination of macro-elements (Na, Mg, P, Cl, K, and Ca) and trace elements (Fe and Zn) by XRF in commercial dehydrated bouillon and sauce base products (Perring and Andrey, 2018). For more than a decade, XRF has been successfully investigated, developed and validated in various finished food/feed products like powdered milk (Perring and Andrey, 2003), freeze-dried milk and dairy products (Pashkova, 2009), infant cereals (Perring and Blanc, 2007), and dry pet food (Ávila et al., 2016; Perring et al., 2017). XRF was shown to be adequate for the determination of multiple elements in Mexican candies at mg/kg levels (Martinez et al., 2010).

2.6.10.2 Plant samples

Considerable efforts have been made to determine the concentrations of trace elements in plant leaves. Tobacco and its ash were quantitatively analyzed for K, Ca, Ti, Fe, Cu, Br, Sr and Ba using XRF method (Çevik et al., 2003). XRF was applied to characterize the elemental content of lichens and cole (*Brassica oleraceae* var. *acephale*); cole samples were collected from 11 stations and analyzed using 50 mCi Fe-55 and Am-241 radioactive sources (Tıraşoğlu et al., 2005). Tıraşoğlu et al. (2006) used XRF technique to analyze the samples of plants including *Mentha spp.*, *Campanula spp., Galium spp.,* and *Heriat popium.* In an interesting study of Syrian medicinal plants, conventional bulk-sample EDXRF was compared with Total Reflection X-ray Fluorescence (TXRF), and

for similar operating parameters the two approaches were found to be comparable (Khuder et al., 2009). Obiajunwa (2002) reported accurate and precise analysis of fourteen elements, namely K, Ca, Ti, V, Cr, Mn, Fe, Ni, Cu, Zn, Se, Br, Rb, Sr in twenty Nigerian medicinal plants by XRF. Loose powder of coffee (*Coffea arabica* L.) leaves was successfully analyzed by XRF (Tezotto et al., 2013). XRF has been used for the accurate determination of iron and zinc in common bean, maize and cowpea seeds (Guild et al., 2017), determination of iron, zinc, and selenium in whole wheat grains (Paltridge et al., 2012a), determination of iron and zinc in rice and pearl millet grain (Paltridge et al., 2012b). Brazilian scientists used XRF method to define the content of potassium, calcium, iron, copper, and zinc in potatoes, bananas, salad, rice, beans, and oranges (Krupskaya et al., 2015).

2.6.10.3 Soil samples

Soil can be measured *in situ* with portable XRF instrumentation, though it is more commonly analyzed as a bulk material either in a sample cup or as a pressed pellet. The analysis of street dust using XRF was used to characterize heavy metal contamination from atmospheric deposition (Yeung et al., 2003). XRF method was used for the determination of nine elements (V, Cr, Mn, Fe, Ni, Cu, Zn, As and Pb) in the soil, grape and wine samples in the wine producing area of Vrbnik on the island Krk and it was found that over the years extensive grape cultivation had doubled the Cu concentration in soil (Orescanin et al., 2003). Koz et al. (2012) investigated the use of XRF spectrometer (Epsilon 5, PANalytical, Almelo, The Netherlands) for heavy metal contamination around one of the most important mining areas in Turkey, the Murgul mining region, by

analyzing moss and soil samples collected around the copper mining at different distances.

2.6.10.4 Other sample types

Ayurvedic herbal medicine products (HMP) have been associated with numerous heavy metal poisoning cases in recent decades and have therefore been the focus of several EDXRF studies (Saper et al., 2004; Saper et al., 2008; Mahawatte et al., 2006; Al-Omari, 2011). The use of XRF in the assessment of air quality was demonstrated in a quantitative study of aerosol particles deposited on filters (Spolnik et al., 2005). The use of XRF for the determination of elemental content in water may not be considered practical compared with other analytical procedures such as ICP-MS because sensitivity is not enough for direct analysis (Marguí et al., 2012; Melquiades et al., 2011). The latest developments in XRF have improved the accuracy and made it possible to analyze alloys, metals such as gold jewelry using a few or no reference samples (Jalas et al., 2002).

3.0 MATERIALS AND METHODS

3.1 Sample Selection

3.1.1 Calibration Set

A panel of 73 pea seed samples (Appendix - A) was selected from three pea mapping populations developed at the Crop Development Centre (CDC), University of Saskatchewan which had previously been characterized for seed quality traits. Out of these 73 pea seed samples, 40 were selected from the 2016 Saskatchewan pea regional variety trial (PVRT), conducted at 4 locations (Sutherland, Rosthern, Lucky Lake and Kamsack). To represent the widest range of concentrations of elements (Fe, Zn, K and Se) available within the CDC pea breeding program, 33 additional seed samples originating from the plots of the CDC Pea Association Mapping panel (PAM), PR-07 – a population segregating for traits including element composition, and the CDC Pea Genome Wide Association Study (GWAS) population were included in the Calibration Set. These samples were sourced from field trials grown at Sutherland (Saskatoon), Rosthern, SPG (Floral), Saskatchewan nurseries in 2010 to 2013. These pea seed samples had the widest contrasting nutritional profiles with respect to four elements Fe, Zn, K and Se available in the CDC pea breeding program (unpublished source) (Table 3.1).

Table 3.1 Range of K, Fe, Zn, and Se concentrations in Calibration Set pea seed samples as per previous AAS data available.

Element	Minimum Conc. (mg/L)	Maximum Conc. (mg/L)
K	8715.87	14313.54
Fe	25.71	93.68
Zn	14.39	53.78
Se	0.08	6.94

3.1.2 Validation Set

A Validation Set of 80 samples (Appendix - B) was selected for validation of XRF protocols. Ten widely grown market classes were deliberately selected from the Saskatchewan pea regional variety trial (PVRT) field experiment conducted in 2016. The 10 pea varieties included yellow, green, dun, red, maple, forage and wrinkled market classes, each grown in two replicated plots at four separate locations in Saskatchewan: Sutherland (Saskatoon), Lucky Lake, Rosthern and Kamsack.

3.2 Optimization of Seed Grinding Method

3.2.1 Grinding methods and strategies

Several grinding methods including cryogrinding, cyclone milling - Retsch mill (Ultra Centrifugal Mill ZM 200, Retsch, Germany) and UDY cyclone mill (Model: 3010-014, UDY Corporation, Fort Collins, U.S), and Geno Grinder 10 (SPEX SamplePrep, LLC, UK) were evaluated to obtain the desired fineness of pea flour (particle size < 20 microns) for XRF analysis. The detailed description of the optimization of experimental method is provided in Appendix - C. Various sample preparation variables were considered for XRF analysis (Table 3.2).

Table 3.2 Optimization of sample preparation variables for XRF analysis.

1. Grinder type (cryogrinding, manual, Geno Grinder, mill grinding)
2. Grinding time and speed
3. Particle size distribution
4. Container specifications (strength, durability) and dimensions
5. Ease of cleaning and minimization of contamination from container and sample carry over
6. Sample volume
7. Matrix for pelleting and dilution of standard compounds
8. Preparation of pellets

3.2.2 Optimized grinding method for pea seeds

Pea seeds for all the experiments in this project were ground using a Geno Grinder 10 (SPEX SamplePrep, LLC, UK) in 50 mL flat bottom polycarbonate tubes (OPS Diagnostics LLC, Lebanon, USA). Thirty pea seeds, considered as suitable sample size, were ground in 2 batches of 15 seeds at a time. The first grinding was conducted using 1 steel ball (13 mm diameter) at 1350 rpm for 2 minutes, and the second grinding using 30 zirconia balls (6.5 mm diameter) at 1650 rpm for 2 minutes (Fig 3.1). After each grinding, the tubes were thoroughly washed with distilled water twice, then rinsed with ethanol before drying. Metal contamination in pea flour due to grinding media was not detectable (Appendix - C, Table C5).

Optimization of the above-mentioned sample preparation parameters resulted in the desired quality of pea flour suitable for XRF analysis, but the 50 mL flat bottom polycarbonate tubes (OPS Diagnostics LLC, Lebanon, New Jersey, USA) cracked at the base when reused for grinding >3 times. This problem was resolved later after fabricated polycarbonate tubes with a hard polycarbonate base were obtained from a local manufacturing company (Metal Shapes).

Figure 3.1 Optimized grinding method for XRF analysis in pea seeds.

3.3 Reference Wet Bench Method (AAS)

3.3.1 AAS protocol

Acid digestion of pea flour

Atomic absorption spectroscopy is the most common technique used for metal determination in most laboratories. Three replicate samples were extracted into solution by acid digestion using nitric acid (HNO_3), hydrogen peroxide and hydrochloric acid (HCl) before introduction to the instrument for analysis. Each seed sample (0.5 g) was weighed into a digestion tube and the digestion block was preheated to 86^{o}C. Digestion tubes were lowered into the digestion block and 6 mL HNO_3 was added to each tube. The samples were shaken after 5 minutes to allow the gas to escape from any foam generated in the digestion tubes. Five mL of hydrogen peroxide (H_2O_2) was added to digestion tubes after 45 minutes while they were still in the digestion block and again incubated for another 65 minutes. Subsequently, 3 mL of 6 M HCl was added and digestion was allowed for another 5 minutes. The fully digested sample was diluted to 25 mL using

distilled water and stored in plastic vials with closed lids until injection, to avoid evaporation losses. Blanks and a routine check sample (yellow cotyledon lentil) were also digested in a similar fashion. Reference standard solutions were used for preparation of standard curves (Table 3.5). Digestion was completed one day prior to instrumental analysis. Digested solution (25 mL) was diluted separately for the analysis of different elements. The results reported are average of three replications for each sample. The concentration of elements was computed using the standard curves. A sample of lentil seed powder was analyzed after every 21 samples, as a check. Digested solutions were injected into an Atomic Absorption Spectrometer novAA 300 (Analytik Jena AG) for determination of the concentrations of elements in pea seeds in the Tissue Culture Laboratory, Department of Plant Sciences, University of Saskatchewan. AAS lamp and calibration settings and spectrometer parameters employed for seed sample analysis are summarized in Tables 3.3 and 3.4.

Table 3.3 AAS lamp and calibration settings.

Photometer	- Single-beam - Wavelength range for monochromator: 185-900 nm
Deuterium Hollow cathode lamp correction (Zn and Ca)	- Lamp Current- 5 to 35 mA - Mode - Electrical timing 50 Hz
Measurement value Processing	- Measuring Frequency - 25 Hz - Signal evaluation - Mean for all elements except Se - Area calculation for Se - Confidence interval - 95.4%
Calibration	
Calibration method	- Standard calibration
Fit sample curve	- Non-linear
Number of standards	- 1 to 5
Recalibration	- Two-point recalibration with display of the recalibration factor

Table 3.4 AA spectrometer parameters employed for the analysis of pea seed samples.

Element	Absorption Wavelength (nm)	Optimal Spectral Bandpass (nm)	Flame Stoichiometry	Lamp Current (mA)	Characteristic concentration (mg/L)	Check Concentration (0.1 Abs) (mg/L)
K	766.5	0.8	C_2H_2/Air	4.0	0.02	0.4
Mn	279.5	0.2	C_2H_2/Air	7.0	0.03	0.6
Fe	248.3	0.2	C_2H_2/Air	6.0	0.08	1.6
Cu	324.8	1.2	C_2H_2/Air	3.0	0.04	0.7
Zn	213.9	0.5	C_2H_2/Air	4.0	0.01	0.3
Se	196.0	1.2	Hydride	6.0	0.03	0.7

Optimal Spectral Bandpass gives the size of wave component, after it has passed the dispersive device that can go through the monochromator. Characteristic concentration is defined as the concentration of an element (expressed as mg/L) required to produce a signal of 1% absorption (0.0044). If the measurements are made in the linear working range, characteristic concentration allows the operator to predict the absorbance range which will be observed for a known concentration range of the element of interest. Check concentration value is the concentration of the element (mg/L) that will produce the signal of ~ 0.1 absorbance units. Using the check concentration, the operator can determine whether the instrument parameters are optimized and whether the instrument is performing up to specifications.

Se analysis: Selenium was analyzed using the hydride system. The digested sample was diluted 6-fold by 0.72M HCl solution. Reducing agent was prepared by mixing 1.5 g NaOH and 5 g of sodium borohydride in 1 L of distilled water. Se present in the sample reacts with sodium borohydride and HCl to produce a volatile hydride. Gaseous hydride and hydrogen are then swept by argon purge into a heated quartz cell where absorption by Se is measured. A series of standards were prepared in mock digested blank solutions and assayed in the same fashion as the seeds.

Ca and K analysis: Samples as well standard solution were diluted in lanthanum solution prepared by dissolving 1.2 g consisting of lanthanum oxide (L_2O_3) in 30 mL of 12 M HCl. The same samples were further diluted 5-fold in lanthanum solution for K analysis.

Zn, Mn, Fe and Cu analysis: Acid digested samples were directly used for Zn, Mn, Fe and Cu analysis without any dilution. Standard curves were prepared in digested blank.

The samples higher in concentration than the upper concentration limit of the standards, were further diluted in mock blank solution before analysis.

Table 3.5 Concentration of standards for different elements prepared in AAS analysis.

Standards	Se (mg/L)	Ca (mg/L)	K (mg/L)	Zn (mg/L)	Fe (mg/L)	Mn (mg/L)	Cu (mg/L)
Reference standard	Se (LOT 4602E15, RICCA chemical	Ca (LOT 155739, Fisher Chemical)	K (LOT 4602E13, RICCA chemical company)	Zn (LOT 144773R, Fisher Chemical)	Fe (LOT 152270, Fisher Chemical)	Mn (LOT 150412 Fisher Chemical)	Cu (LOT 154837, Fisher Chemical)
Standard 1	1	2.5	0.62	0.2	0.5	0.2	0.1
Standard 2	2	5	1.25	0.4	1	0.4	0.2
Standard 3	5	10	2.5	1.2	3	1.2	0.6
Standard 4	10	20	5	1.6	4	1.6	0.8

3.4 XRF Analysis of Seed Samples

The primary technique utilized in this study was X-ray fluorescence Spectroscopy (XRF) at Industry Development Education Applications Students (IDEAS) beamline at Canadian Light Source, Saskatoon, which is a 3rd generation light source with a storage ring of ~3 GeV.

3.4.1 XRF beamline setup

IDEAS is a beamline on port 08B2-1 of the Canadian Light Source. The beamline produces a constant X-ray beam that passes through a double crystal monochromator using InSb (111), Ge (220), Si (311) crystal pairs with an energy output in the range of 1.8 KeV – 15 KeV. XRF experiments were performed in air, at room temperature and

pressure, with the available ion chambers to estimate incident and transmitted beams. A silicon drift detector (KETEK GmbH, model AXAS-M, Germany) with active area of 0.8 cm^2 and beryllium window of 0.0025 cm was used to collect and analyze XRF emission spectra. The detector was positioned at 90° to the incident beam to avoid interference from scattered beam. Beamline specifications are summarized in Table 3.6

Table 3.6 IDEAS beamline specifications at Canadian Light Source.

Source	1.35T Bending magnet, 7.14m radius
Optics	-White Beam slits (4-jaw) -600 mm Rh coated bent cylindrical white beam (focusing/collimating)
Monochromator	Constant exit height Double Crystal Monochromator (DCM) with a wide 15-65^o incident angle range. Available crystal pairs include InSb (111), Ge (220) and Si (311).
Energy Range	InSb (111) crystals: 1.8 keV-6.4keV Ge (220) crystals: 3.4 keV-13.4 keV Si (311) crystals: 4 keV-15keV
Flux	5E10-7E11 ph/s @100mA
Resolution (Focused)	0.4 eV-14 eV (focused) 0.1 eV-1.5 eV (collimated)
Beam spot size (Horizontal × Vertical)	10 mm × 0.3 mm (focused) 10 mm × 2 mm (collimated)

3.4.2 Sample preparation

Three circular discs, referred to as 'pellets' in this document, per sample were prepared using a 13 mm stainless steel pellet die in a hydraulic pellet press (PIKE Technologies, Auto-CrushIR, Wisconsin, U.S) at the Canadian Light Source (CLS). The pellet die compresses sample powders between two flat polished discs to form a pellet. Forty mg of pea flour was pressed into pellets of thickness 0.2 mm and diameter of 13 mm. As pellets were robust and did not show any tendency to desegregate, no binder was added to the Calibration Set and Validation Set. The pelletizing die was wiped using ethanol after each sample preparation. The pellets were stored in the dark in a vacuum desiccator until further use.

3.4.3 Spectra collection and instrument configuration

XRF based elemental analysis of the Calibration Set and the Validation Set was performed by an Energy Dispersive X-ray Fluorescence (EDXRF) spectrometer at IDEAS beamline at Canadian Light Source, Saskatoon using beamline settings already described in the previous section 3.4.1 and instrumentation setup as shown in Fig 3.2. The energy of the incident beam was 13000 eV for Calibration and Validation Set. The measurement conditions for the analysis of seed samples at IDEAS beamline are summarized in Table 3.7.

Three replicate pellets from each sample were irradiated for 260 seconds each and 13 spectra were recorded from 13 different points on each pellet. Slit width and slit height employed were 1.5 mm and 0.5 mm respectively, irradiating a total of 9.75 mm^2 for each pellet. The peak areas calculated from 39 spectra recorded for each sample were averaged for all further prediction calculations.

Since the stainless-steel vacuum chamber in the spectrometer caused external interferences in signal of Fe, Mn, Ni and Cr (Appendix - D), it was decided to irradiate the samples outside the vacuum chamber in air at room temperature at atmospheric pressure.

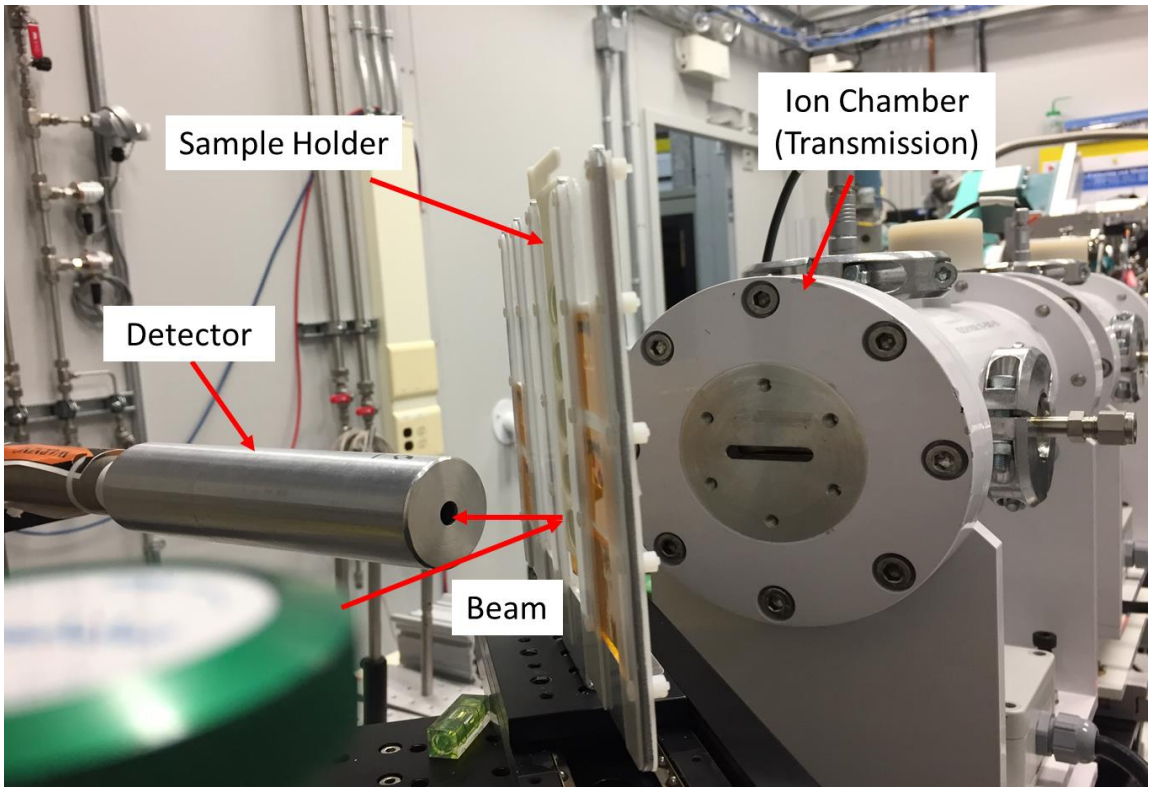

Figure 3.2 XRF instrument set up at IDEAS beamline at Canadian Light Source, Saskatoon.

Table 3.7 XRF instrument set up and conditions for the analysis of K, Ca, Mn, Fe, Cu, Zn, and Se.

Condition	Set Up (Validation Set)
Atmosphere	Room pressure
Voltage (eV)	13000
Highest beam Current (mA)	220
Acquisition time (secs)	260
Detector	Silicon Drift

3.4.4 Processing of XRF emission spectra

As the beam current, and hence the intensity, of the incident X-ray beam changes with time at the CLS, all spectra were normalized to incident beam energy (I_0). All the spectra were processed using PyMca software (Solé et al., 2007) and the areas of element specific peaks were calculated. A configuration and a calibration fit were developed in the software which overlaps the original spectra and calculates the areas of individual elemental peaks. Overlapping peaks were deconvoluted before area calculation (Fig 3.3).

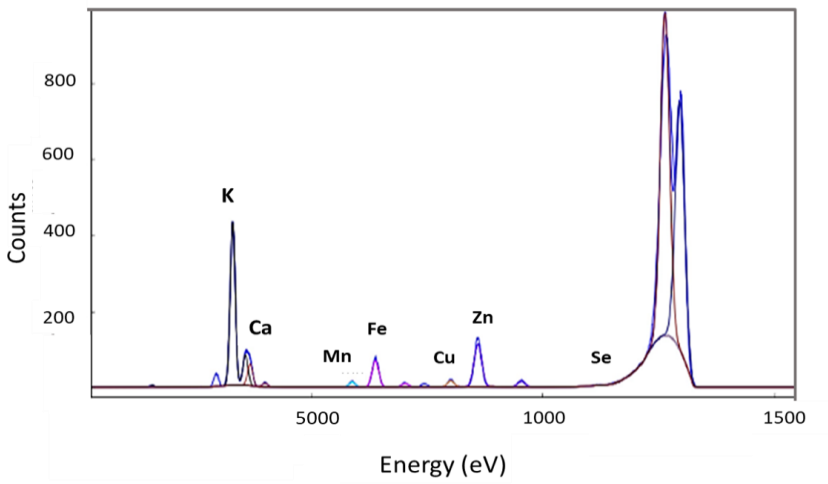

Figure 3.3 Overlapping and deconvolution of peaks before area calculation in PyMca.

3.4.5 Development of calibration curves and validation

Quantitative XRF analysis of samples is accomplished using a comparative procedure. Therefore, a calibration procedure must be performed before proceeding to the calculation of unknown sample compositions. The calibration procedure known as 'empirical' directly compares the net intensity of the analyte peaks with their concentrations, without making any correction for inter-element or matrix effects. It is possible to use this type of calibration only when the analyte concentration range is limited, and the standards are normally typical 'samples' that have been analyzed by a technique other than XRF. With this calibration type, it is assumed that the net intensity (y-axis) is linearly related to concentration (x- axis). Calibration curves were developed using the Calibration Set. The area of peaks were correlated to AAS concentrations and standard equations were obtained. These calibration curves were validated on the Validation Set.

3.4.6 Fundamental parameter approach (FP)

The FP quantification is based on the theoretical relation between the measured X-ray intensities and the concentrations of the elements in the sample. It considers all interactions between incident and emitted X-ray photons and the atoms of the analytes as well as the matrix. Therefore, the contribution of factors like the thickness of atomic layer of elements, thickness of the sample pellet and the composition of the sample are considered in this method.

PyMca, a user-friendly program for XRF analysis developed by the European Synchrotron Radiation Facility, France has an inbuilt FP algorithm that allows the users to achieve 'standard-less' analysis. The FP program in PyMca uses the parameters

provided by the user and predicts the concentrations of analytes based upon the precise modeling of the sample itself, the incident X-ray beam, the detector, and instrumental geometry using theoretical equations and the fundamental parameter database. Users can choose the parameters relating to all the sample properties and instrumental set up for their specific experiment.

The theoretical calculations of the intensity of fluorescent X-rays are made based on the following premises:

1. All elements are evenly distributed in the sample.
2. The intensity of generated X-rays is proportional to the concentration of the measured element. However, the intensity is affected by the absorption and enhancement effects of the matrix elements.
3. The concentrations of the matrix elements are known, and their effects can be calculated using physical constants, e.g., absorption coefficients.
4. The intensity of the fluorescent X-rays produced from the sample and thus detected by the instrument are dependent on the instrumental configuration and measurement conditions.

Since plant samples are mainly composed of organic substances (C, H, O, N), the ratio of these elements was calculated using percentage of protein, starch and fiber in the Validation Set pea seed samples, obtained by near Infrared radiation (NIR) predictions within the University of Saskatchewan pea breeding program. Yatkin et al. (2011) concluded that the XRF-FP analysis was more efficient than linear calibration for the quantification of most elements. Hence, we decided to evaluate the standard-less analysis in our study. A configuration and a calibration fit were developed in PyMca including all the above-mentioned necessary parameters as input measures. XRF concentrations were directly obtained from the software, normalized to I_0 and correlated to the concentration

values of reference method (AAS) for all 153 seed samples (Calibration Set and Validation Set).

3.4.7 Statistical analysis

Statistical evaluation of XRF based prediction of element concentrations was based on the 'robust statistics' approaches (Rousseeuw and Croux, 1993) used in Perring & Andrey (2003), Perring et al., 2005. "Robust statistics are statistical methods, insensitive to the effects of outliers. These methods rely on medians instead of means and use more information from the central than from the outlying observations (Hampel et al., 2011). The average of three replicates for XRF method and AAS method were routinely used for analysis as follows:

Reference method value (AAS)	Yi
XRF value	$\hat{Y}i$
Number of samples	n
Difference	$di = \hat{Y}i - Yi$
Bias	$\bar{d} = \frac{\sum_{i=1}^{n}(\hat{Y}i - Yi)}{n}$
Difference standard deviation	$SD\ (d) = \sqrt{\frac{\sum_{i=1}^{n}(di - \bar{d})^2}{n-1}}$
Standard error of prediction	$SEP = \sqrt{\frac{\sum_{i=1}^{n}(\hat{Y}i - Yi)^2}{n}}$
Residual standard deviation	$RSD = \sqrt{\frac{\sum_{i=1}^{n}(x\hat{} - x)^2}{n-1}}$ where x^ is predicted concentration from the equation and x is the known concentration.

4.0 RESULTS

4.1 Estimation of element concentrations in pea seed samples by AAS

Table 4.1 lists the macro- (K, Ca) and micro-elements (Mn, Fe, Cu, Zn, and Se) determined in this study. In the table are also reported some basic statistics {mean, minimum, maximum and coefficient of variation (CV)} to gain a better understanding of the nature of the sample sets. Mean, maximum and minimum concentrations in mg/L and CV in % is reported according to the reference method (AAS).

Table 4.1 Mean, minimum and maximum concentrations (mg/L) of pea seed samples according to AAS method (Calibration Set and Validation Set).

	K	Ca	Mn	Fe	Cu	Zn	Se
Mean	9859	806	10.4	44.9	6.2	32.4	0.93
Minimum	7230	418	7.2	30.0	3.1	17.3	0.16
Maximum	12495	1917	17.8	90.1	14.2	46.7	8.93
***CV (%)**	4.4	3.9	2.5	3.2	7.4	2.2	2.7

n=153; No. of replicates = 3
*Coefficient of variation

A total of 153 pea seed samples representing a wide range of concentrations in different analytes were selected. The spread of concentrations of all the data points is given by box and whisker plots (Fig 4.1). The vertical boxes represent 25 to 75 percentiles, error bars represent 10 to 90 percentiles, and lines in vertical boxes represent median values. For Ca, Mn, Fe, Cu, and Se the outliers are present beyond the 90th percentiles, for Zn one outlier is present below the 10th percentile, and for K outliers are present above the 90th and below the 10th percentiles. Since some outliers are present for all the analytes, the data are not normally distributed.

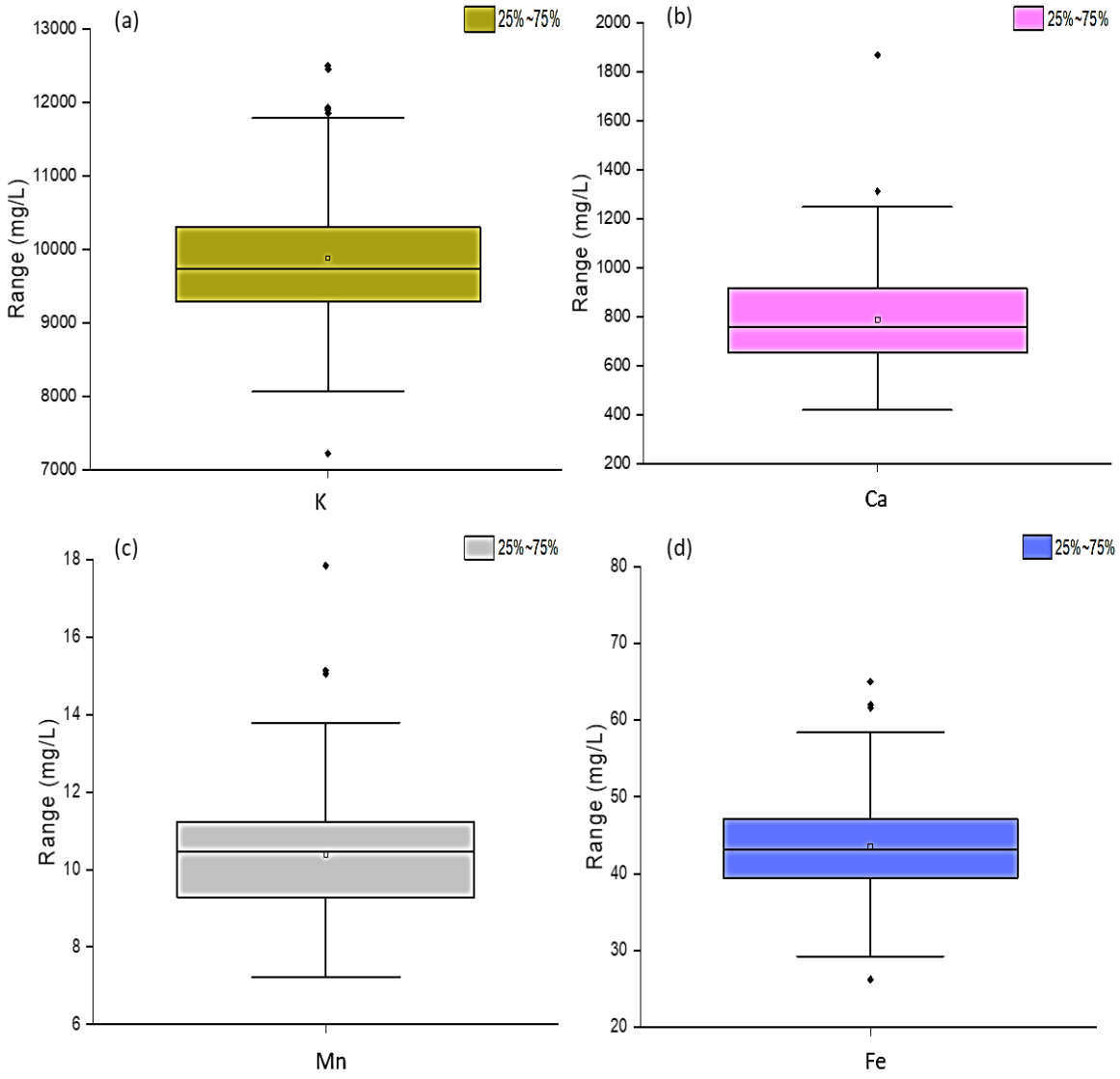
(a)
25%~75%
Range (mg/L)
13000
12000
11000
10000
9000
8000
7000
K
(b)
25%~75%
Range (mg/L)
2000
1800
1600
1400
1200
1000
800
600
400
200
Ca
(c)
25%~75%
Range (mg/L)
18
16
14
12
10
8
6
Mn
(d)
25%~75%
Range (mg/L)
80
70
60
50
40
30
20
Fe

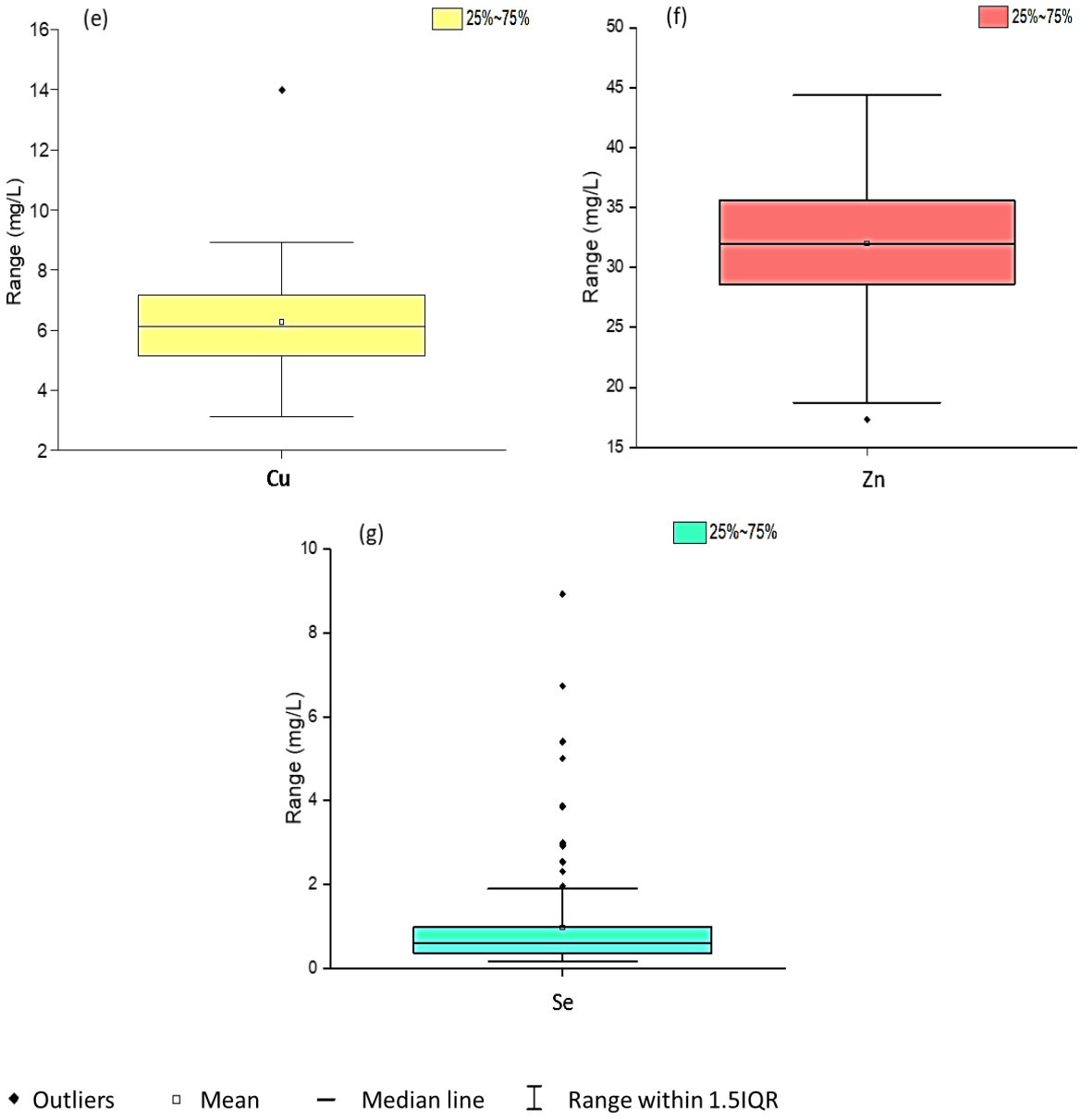

Figure 4.1 **Distribution of pea seed sample concentrations for (a) K (b) Ca (c) Mn (d) Fe (e) Cu (f) Zn (g) Se.**

Reference standard solutions were used for the preparation of standard curves in AAS. R^2 is the proportion of variation in AAS values explained by the correlation between absorbance values and concentrations (Fig 4.2). For all the standard curves R^2 value was reported above 0.99. The concentration of elements was computed using the standard curves.

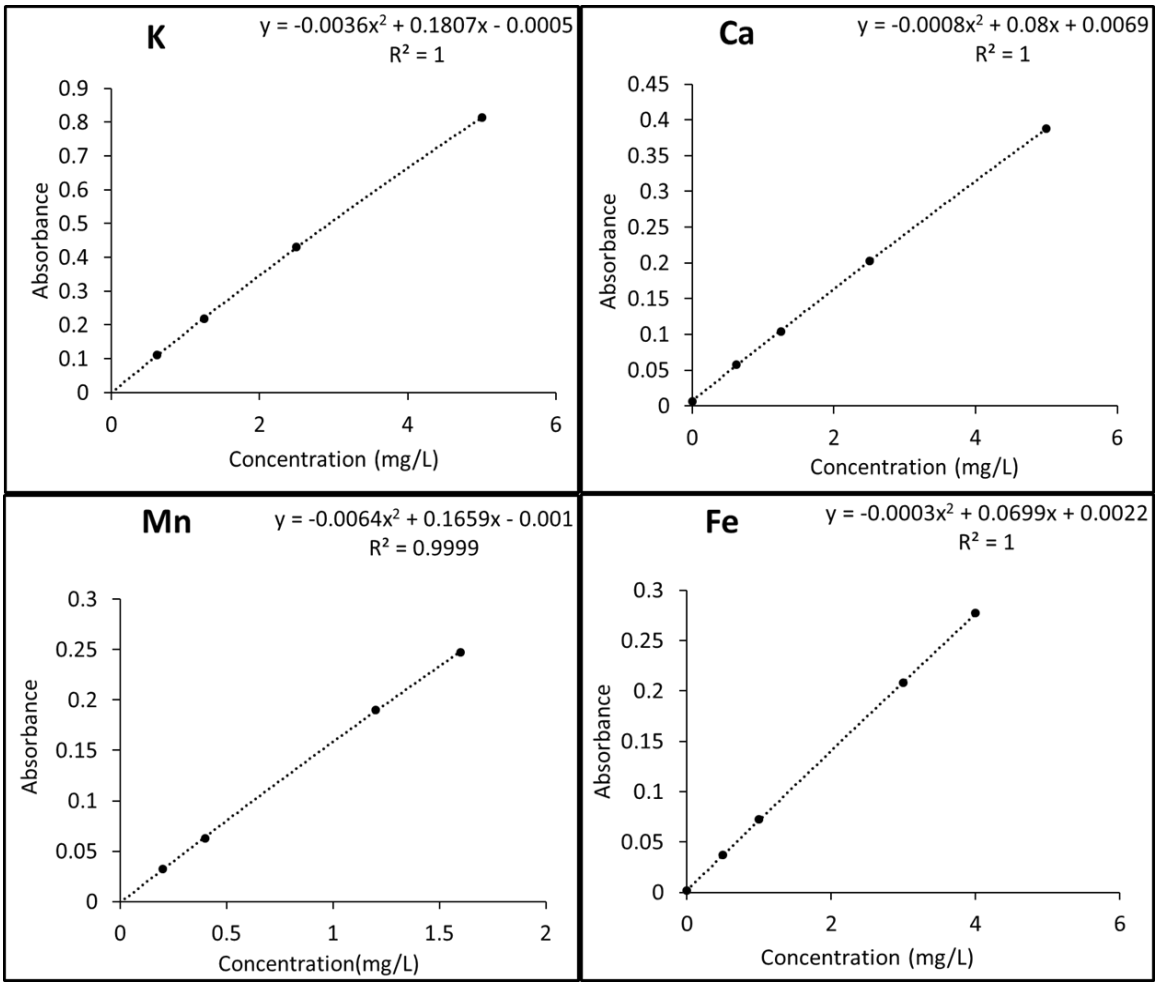

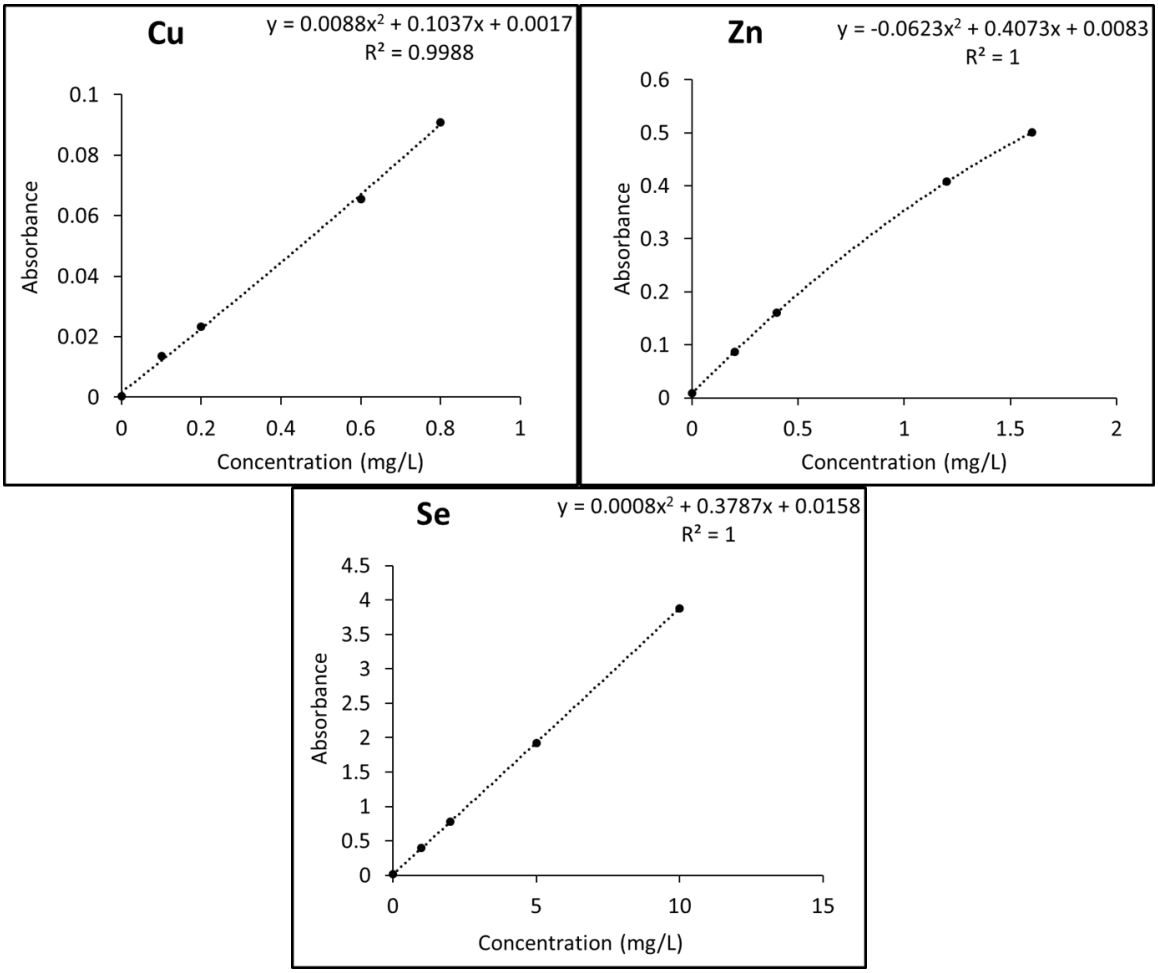

Figure 4.2 AAS standard curves used for prediction of concentration in seed samples.

4.2 XRF Method

4.2.1 Calibration curves

Calibration curves were developed with the Calibration Set of 73 seed samples (Fig 4.3). These samples were selected to cover the maximum range of concentrations and spread over the entire range of analytes. The measured intensities (areas) of XRF were plotted on the y-axis and the concentrations obtained from AAS method on the x-axis to calculate the slope and the intercept of calibration curves by regression analysis.

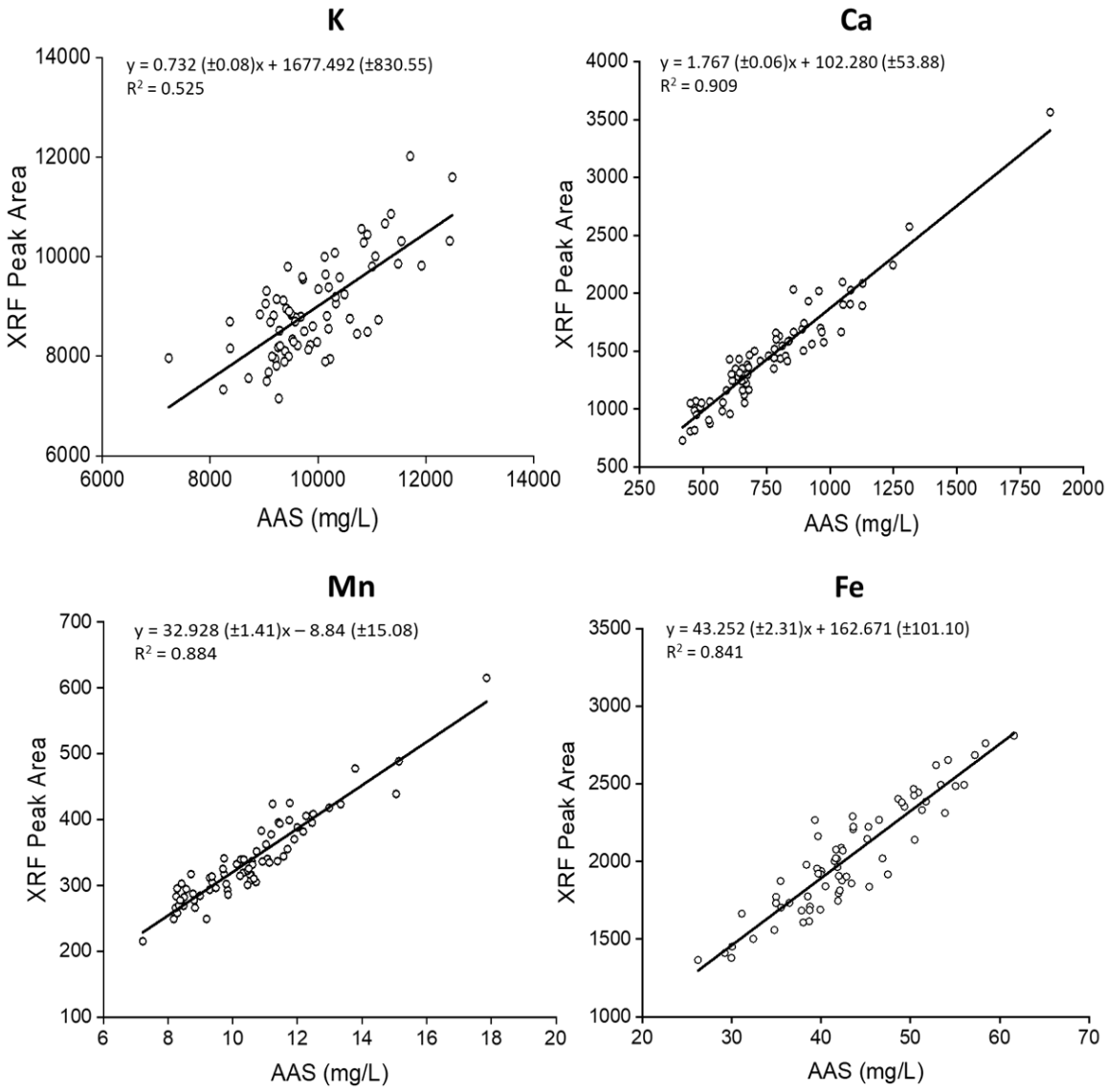
K
y = 0.732 (±0.08)x + 1677.492 (±830.55)
R2 = 0.525
XRF Peak Area
AAS (mg/L)
Ca
y = 1.767 (±0.06)x + 102.280 (±53.88)
R2 = 0.909
XRF Peak Area
AAS (mg/L)
Mn
y = 32.928 (±1.41)x – 8.84 (±15.08)
R2 = 0.884
XRF Peak Area
AAS (mg/L)
Fe
y = 43.252 (±2.31)x + 162.671 (±101.10)
R2 = 0.841
XRF Peak Area
AAS (mg/L)

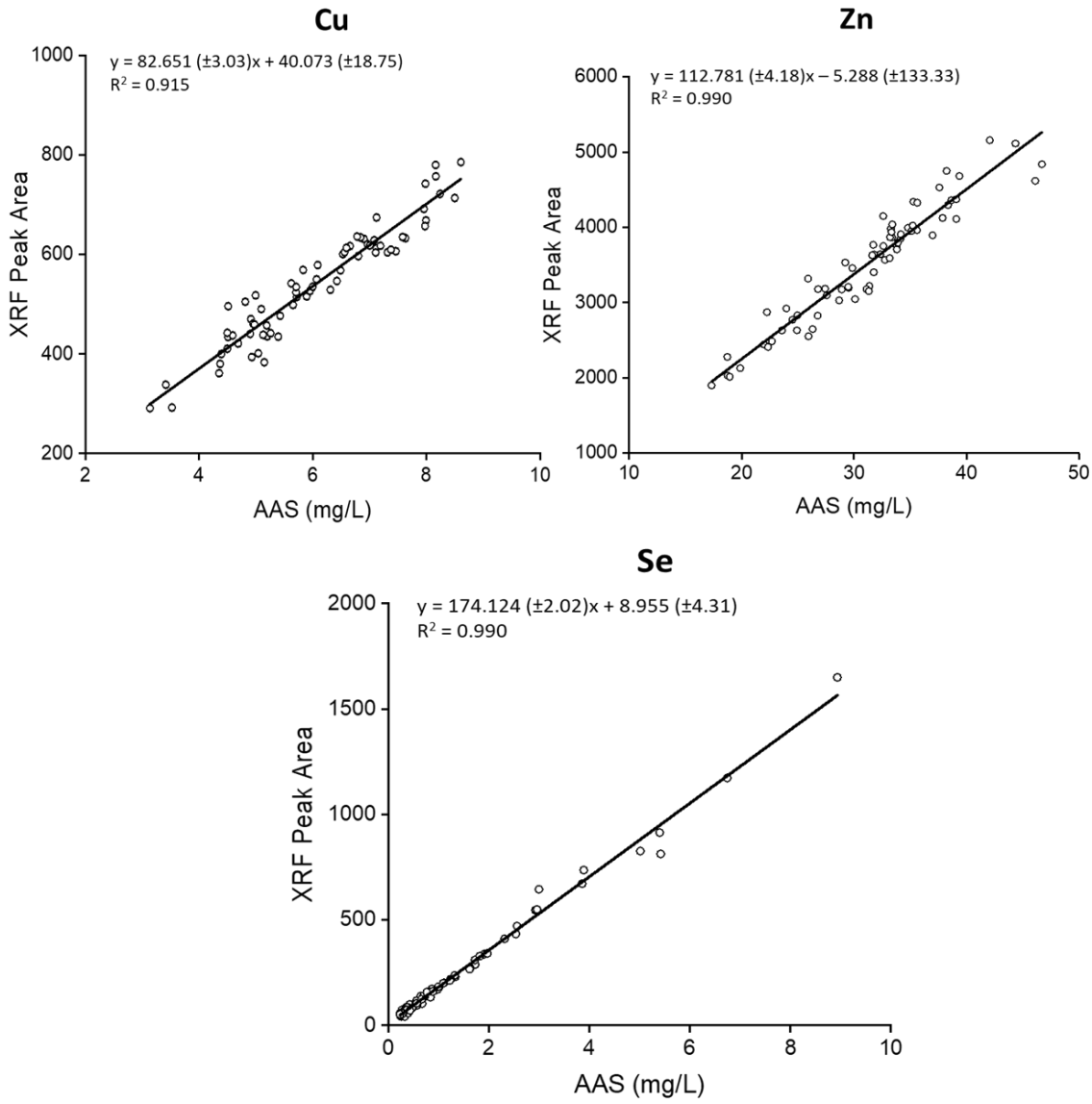

Figure 4.3 Calibration curves developed by correlating area of XRF peak and AAS concentrations for Calibration Set.

The calibration characteristics for K, Ca, Mn, Fe, Cu, Zn and Se are given in Table 4.2. For all the calibration curves, R^2 is greater than 0.84, except K for which R^2 is 0.525. Standard error of calibration which is the measure of dispersion of data around regression model was highest for K among all the analytes followed by Ca. Table 4.3 indicates slopes and intercepts of linear calibration equations obtained from the calibration plots. These equations were used to predict the concentrations in the Validation Set.

Table 4.2 Calibration characteristics with units expressed in mg/L for min, max, SEC (standard error of calibration), R^2, and N = number of samples

Analyte	Min	Max	Median	N	R^2	SEC
K	7230	12495	9717	73	0.525	920.57
Ca	418	1868	725	73	0.909	75.50
Mn	7.2	17.8	10.4	73	0.884	0.67
Fe	26.2	61.6	41.9	73	0.841	3.13
Cu	3.1	8.6	5.9	73	0.915	0.39
Zn	17.3	46.7	31.7	73	0.990	1.92
Se	0.20	8.90	0.60	73	0.990	0.15

Table 4.3 Parameters obtained with the formula between XRF signals (area of peak) and analyte concentrations from reference method

Analyte	Slope=a	Intercept=b
K	0.7328	1677.49
Ca	1.7679	102.28
Mn	32.928	-8.84
Fe	43.252	162.67
Cu	82.651	40.073
Zn	112.781	-5.28
Se	174.124	8.95

4.2.2 Validation curves

The Validation Set of 80 samples was used for validating the calibration model obtained from the calibration curves. The validation of the XRF method was accomplished by a systematic comparison between the concentration values predicted by XRF with those obtained by AAS and correlation analysis with linear regression method (Fig 4.4). The data were utilized only if the reference method concentrations were included in the calibration ranges or very similar to their extrema.

Statistical evaluation of the XRF performance was done using robust statistics and formulae described in the statistical analysis section 3.4.7. The results for validation are reported in Table 4.4. For the model XRF (area) = A + B* [Reference Method (mg/kg)], for all analytes, at 95% of confidence, R, intercept (A) and slope (B) were computed. If the XRF predicted concentrations and AAS determination of the concentrations of elements are consistently equal for the Validation Set, these parameters should have the values R ~ 1, B = 1 and A = 0. As shown in Table 4.4, for Mn, Fe, Cu, Zn and Se, the intercept was found to be not significantly different from 0 and B (the slope) was found to be not significantly different from 1. This leads to the conclusion that the results obtained using two methods were found not to be significantly different for Mn, Fe, Cu, Zn and Se.

On the contrary, at the same confidence levels, statistically significant differences were found for XRF predicted element concentrations of K and Ca. Though the slopes of the validation curves for K and Ca were not significantly different from 1, the intercept was found to be significantly different from zero. Bias and standard deviation of differences

was also relatively high and significantly different from zero for K and Ca. Additionally, for all analytes, the ratio SEP/SEC is lower than 1.5.

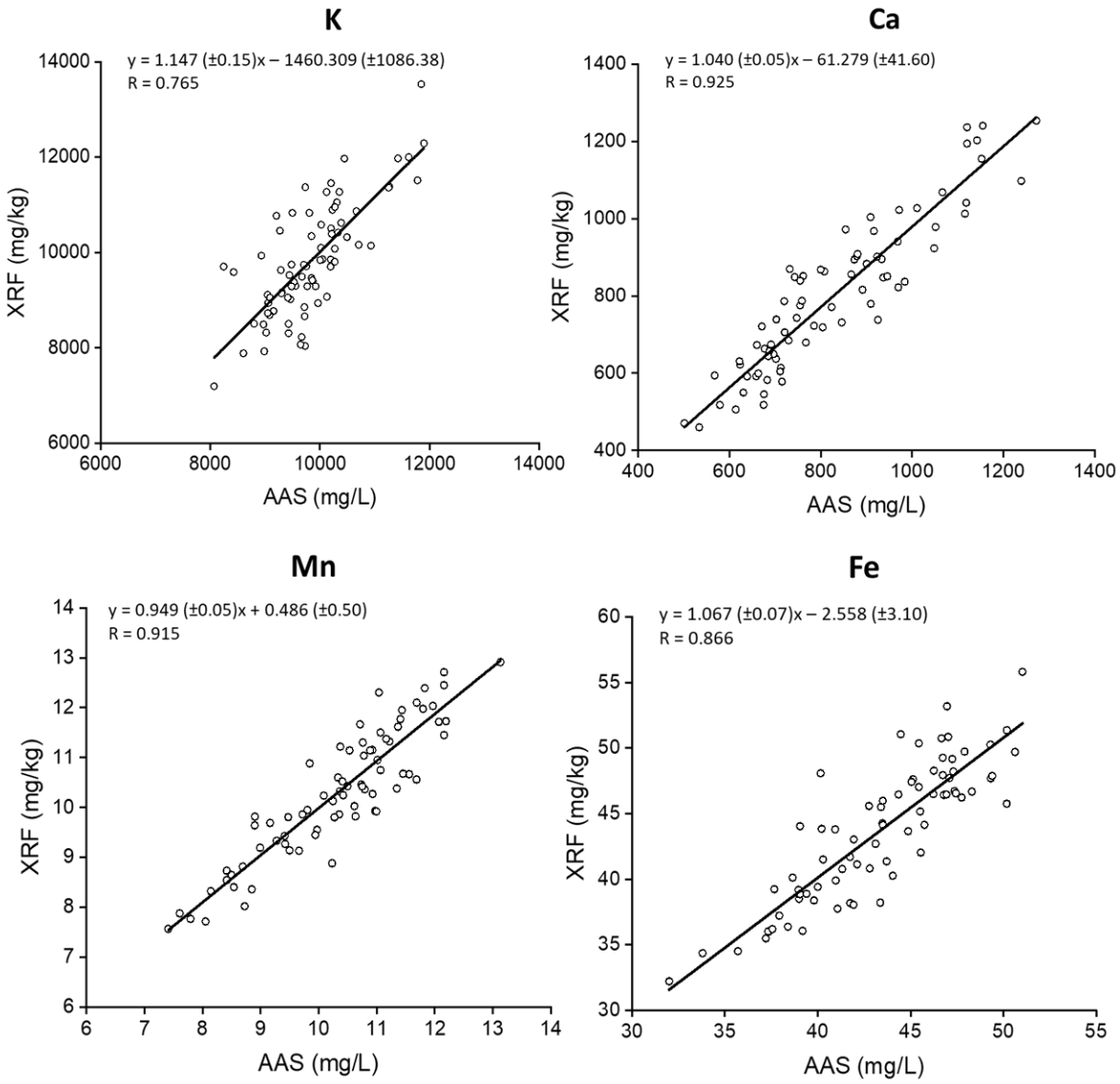

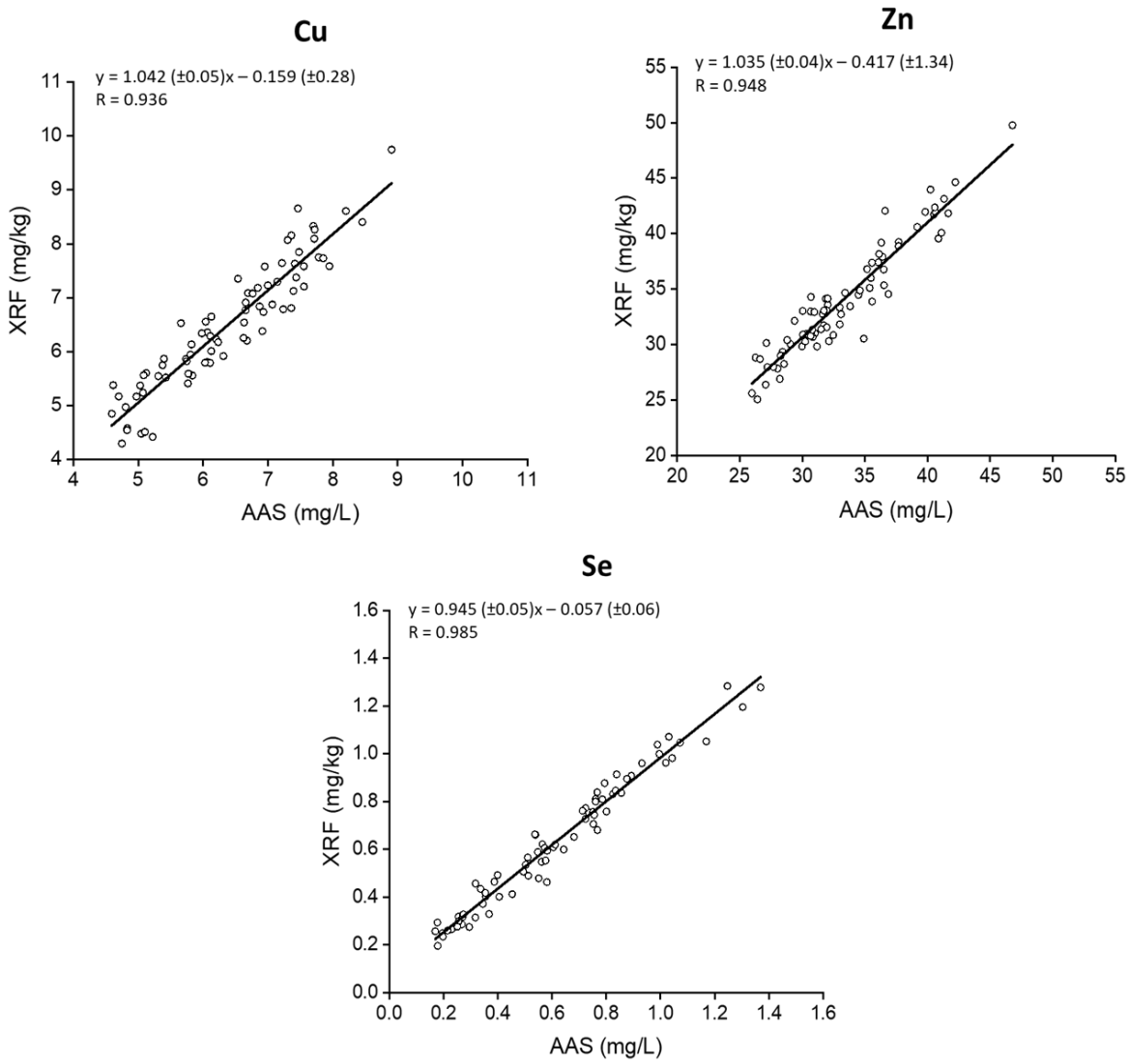

Figure 4.4 Validation curves plotted by correlating area of XRF predicted concentrations and concentrations measured by the reference method (AAS) for Validation Set.

Table 4.4 Validation characteristics with units expressed in mg/kg, n = number of samples, SEP = standard error of prediction, and SD (d) = standard deviation of differences.

Analyte	N	Min	Median	Max	SD(d)	Bias	R	Slope	Slope=1 (Y/N)	Intercept	Intercept=0 (Y/N)	SEP	SEP/ SEC
K	80	8066	9751	11897	766.0	-6.62	0.765	1.147	Y	-1460.30	N	761.2	0.83
Ca	80	501	776	1272	80.83	-26.98	0.925	1.040	Y	-61.27	N	80.32	1.06
Mn	80	7.4	10.5	13.1	0.54	-0.007	0.915	0.949	Y	0.48	Y	0.54	0.81
Fe	80	31.9	43.4	57.5	2.57	0.260	0.866	1.067	Y	-2.55	Y	2.57	0.82
Cu	80	4.6	6.4	8.9	0.416	0.005	0.936	1.042	Y	-0.15	Y	0.415	1.05
Zn	80	25.9	32.1	46.7	1.74	0.804	0.948	1.035	Y	-0.41	Y	1.728	0.90
Se	80	0.20	0.60	2.10	0.09	0.004	0.985	0.945	Y	0.05	Y	0.094	0.63

4.2.3 XRF Percentage Recovery

The analytical term "recovery" describes whether the expected value can be measured accurately. If the recovered value differs significantly from the expected, this can be a sign that some factor in the sample matrix may be causing a falsely elevated or falsely depressed predicted value. Recovery was calculated using three replicates of the 80 samples in the Validation Set:

$$\text{Recovery} = \left(\frac{\text{Average of the 3 estimated concentrations}}{\text{Reference method concentration}}\right)*100$$

The range of recovery was above 75% for all the analytes (Table 4.5).

Table 4.5 Range of recovery for different analytes calculated from three replicates of Validation Set.

Analyte	Recovery (%)
K	82-117
Ca	76-118
Mn	86-113
Fe	88-119
Cu	84-116
Zn	87-114
Se	79-165

4.2.4 Limit of Detection and Limit of Determination of XRF based Method

The limit of detection and limit of determination in this study, determined according to Rousseau (2006), are given in Table 4.6. It is apparent that energy dispersive X-ray fluorescence is a sensitive technique for detection of elements in plant samples at mg/kg concentration levels. Limits of detection and determination for K and Ca (light elements) were higher than the other elements, but they are low enough if we consider that both elements are present at very high concentrations in plant tissues and the limits. The

concentrations of all the analytes in pea seed samples were higher than reported limits of detection at 95% confidence interval.

Table 4.6 Calculated limits of detection and determination (mg/kg) in pea seed samples and comparison with reference method (AAS).

	Limit of Detection (mg/kg)		Limit of Determination (mg/kg)	
Analyte	**XRF**	**AAS**	**XRF**	**AAS**
K	9.54	0.058	2363	0.084
Ca	3.5	0.216	153	0.381
Mn	0.5	0.009	1.85	0.013
Fe	0.54	0.180	6.6	0.66
Cu	0.35	0.021	0.84	0.049
Zn	0.2	0.007	5.2	0.018
Se	0.016	0.0002	0.3	0.0006

4.2.5 XRF Repeatability and Relative Standard Deviation (RSD)

The repeatability, SD(r), was calculated using robust statistics (Rousseeuw and Croux, 1993). Robust statistics are statistical methods, insensitive to the effect of outliers. These methods rely on medians instead of mean. To see the dispersion of intensity measurements, 10 samples were prepared and measured in same batch.

The repeatability, SD(r) calculated for each analyte using the triplicate values of all validation samples are listed in Table 4.7. SD(r) was calculated using the formula:

$SD(r) = 1.2011^{*} \text{Med}\ \{SD(i)\}$

Relative standard deviation was calculated by following formula:

$$RSD = \left(\frac{\text{Standard deviation of the 3 estimated concentrations}}{\text{Average of 3 estimated concentrations}}\right) * 100$$

Table 4.7 Robust SD(r) of repeatability and Relative standard deviation (RSD) for AAS and XRF method

Analyte	AAS		XRF	
	SD(r) (mg/L)	RSD (%)	SD(r) (mg/kg)	RSD (%)
K	367.1	5	572.2	26
Ca	27.5	4	65.9	20
Mn	0.2	2.5	0.5	15
Fe	1.2	3	2.4	19
Cu	0.4	7	0.3	19
Zn	0.6	2	1.8	16
Se	0.1	3	0.06	10

Consequently, the standard deviation of repeatability for AAS and XRF method for analytes was comparable. Slightly higher standard deviation is observed for the XRF method as compared to AAS for Mn, Fe, Cu, Zn, and Se. For K and Ca standard deviation of repeatability increased to 66 and 572 mg/kg in XRF as compared to 28 and 367 mg/kg in AAS, respectively. Relative standard deviation (RSD %) was 3-7% for all the analytes in AAS. The RSD% for each element from three replicate analyses were generally less than 20%, except for K for which RSD was 26% in XRF method indicating relatively higher error among three replicate values. However, except this, the XRF method showed good repeatability.

4.2.6 Fundamental Parameter

To compare the data obtained by applying fundamental parameters-based prediction (XRF-FP) of element concentrations with results from the reference AAS method, linear correlation analysis of the AAS based results and XRF-FP based results was carried out (Fig 4.5). For the model XRF-FP (mg/kg) = A + B* [AAS (mg/L)], for all analytes, at 95% of confidence, correlation coefficient (R), intercept (A) and slope (B) were evaluated (Table 4.8). For Mn, Cu, Zn and Se, the intercept was found to be not significantly different from 0 and B (the slope) was found to be not significantly different from 1. Thus, the results obtained using XRF and AAS methods were found not to be significantly different for Mn, Cu, Zn and Se. On the contrary, at the same confidence levels, statistically significant differences between the XRF- calibration and XRF-FP based methods were found for K, Ca and Fe. Though the slopes the plots correlating XRF predicted K, Ca and Fe concentrations AAS measurements was not significantly different from one, the intercepts were found to be significantly different from zero. The results reported for XRF-FP are similar to those reported by using calibration curves, except for Fe. Fe concentrations predicted using empirical method (calibration curves) are not significantly different from AAS concentrations.

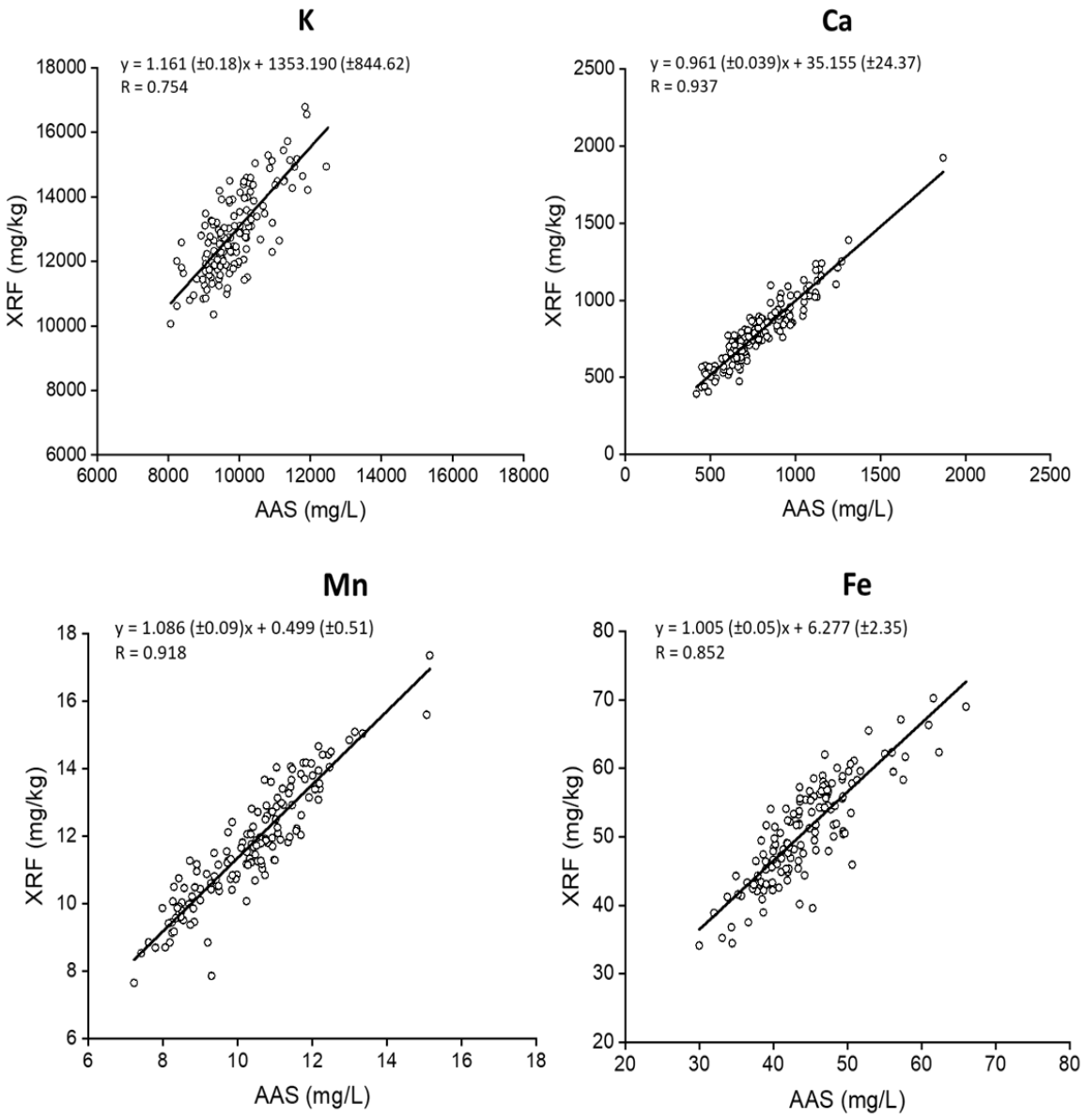
K
y = 1.161 (±0.18)x + 1353.190 (±844.62)
R = 0.754
XRF (mg/kg)
AAS (mg/L)
Ca
y = 0.961 (±0.039)x + 35.155 (±24.37)
R = 0.937
XRF (mg/kg)
AAS (mg/L)
Mn
y = 1.086 (±0.09)x + 0.499 (±0.51)
R = 0.918
XRF (mg/kg)
AAS (mg/L)
Fe
y = 1.005 (±0.05)x + 6.277 (±2.35)
R = 0.852
XRF (mg/kg)
AAS (mg/L)

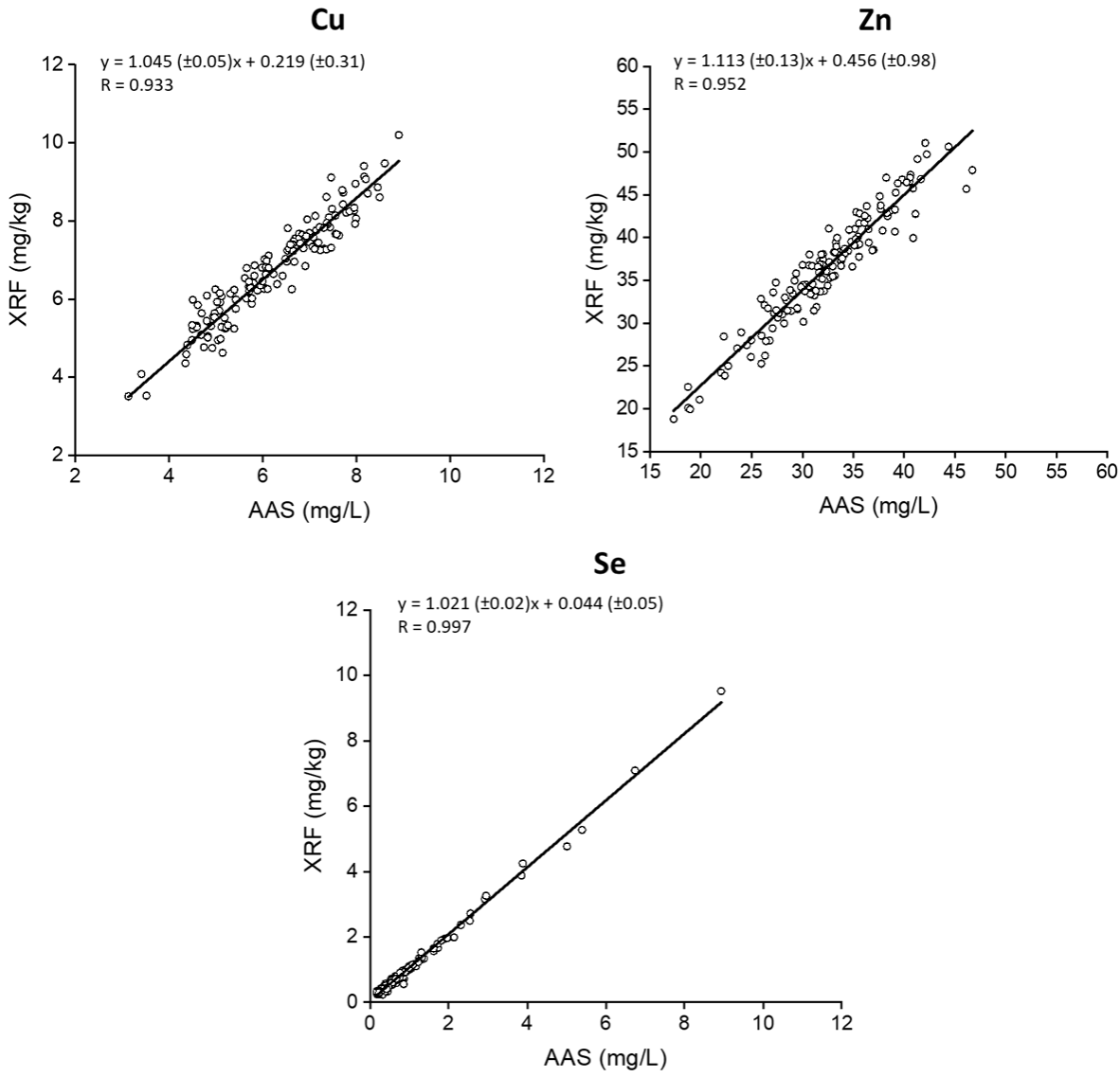

Figure 4.5 Correlation of XRF predicted concentrations using Fundamental parameter and AAS concentrations for 153 pea seed samples (Calibration Set and Validation Set).

Table 4.8 Validation characteristics with units expressed in mg/kg, n = number of samples, SEP = standard error of prediction, and SD(d) = standard deviation of differences

Analyte	N	Min	Median	Max	SD(d)	Bias	R	Slope	Slope=1 (Y/N)	Intercept	Intercept=0 (Y/N)	SEP
K	153	7230	9749	12495	1158.11	2666.31	0.754	1.161	Y	1353.19	N	2666.02
Ca	153	418	759	1917	148.35	11.82	0.937	0.961	N	35.15	N	311.67
Mn	153	7.2	10.5	17.8	0.88	1.25	0.918	1.086	Y	0.49	Y	1.41
Fe	153	30.1	44.1	90.1	8.95	6.90	0.852	1.005	Y	6.27	N	7.62
Cu	153	3.1	6.1	14.2	0.69	0.51	0.933	1.045	Y	0.21	Y	1.10
Zn	153	17.3	32.2	46.7	3.52	3.89	0.952	1.113	Y	0.45	Y	4.62
Se	153	0.16	0.60	8.90	0.22	0.08	0.997	1.021	Y	0.04	Y	0.15

SD(d) = standard deviation of differences and SEP = standard error of prediction

5.0 DISCUSSION

Accuracy and Precision of XRF predictions

The hypothesis was that the X-ray fluorescence (XRF) technique can quantify the concentration of elements in pea seeds. One of the first characteristic one would like to know about any method is whether the results reflect the true value of the analyte or not. One of the approaches for checking the accuracy or trueness of the method is by comparing the results with those of a reference method. Trueness or accuracy of the method can be sensitive to varying conditions including the level of an analyte in the sample, matrix effects, and temperature. This study reports statistically significant bias in predicted values of K and Ca, whereas bias was not significantly different from 0 for the other elements. XRF based prediction of element concentrations in food products have been reported (e.g., Perring and Andrey 2003; Perring et al. 2005; Perring and Blanc 2007). For different analytes including K, Ca, and Fe, bias has not been reported significantly different from 0 in several previous studies (Perring and Andrey, 2003 in milk-based products; Perring and Andrey, 2018 in dehydrated bouillon and sauce based products; Perring et al., 2017 in dry pet food samples; Perring and Blanc, 2008 in milk powders), for Zn, Mn and Cu too bias has been reported significantly not different from 0 (Perring et al., 2017 in dry pet food samples; Perring and Blanc, 2008 in milk powders). In some studies, on food products and plants, bias has been reported significantly different from 0 for prediction of Zn (Perring and Andrey, 2003 in milk-based products), K, Ca and Fe (Marguí et al., 2005 in plant sample) indicating the inaccuracy in prediction of these elements. The appreciable content of silicon in plant samples has also been reported which is generally involved as silica and may be present in the colloidal form. In these conditions, some elements are not fully recovered (especially Al, Mn, Fe, and Cu)

due to the binding of analytes with this silica residue (Hoenig and De Borger, 1983). To dissolve the elements, which may be retained by the insoluble residue Marguí et al. (2005) included a hydrofluoric acid treatment during digestion of samples for element analysis. It was observed that after applying hydrofluoric acid treatment a new precipitate appeared, mainly composed of calcium and fluoride. Thus, the poor recoveries of elements of interest could be explained by co-precipitation of the analytes with this solid residue remaining after sample digestion.

Replicate analysis on the sample yields a standard deviation of the mean as a measure of precision. Precision is numerically expressed as an absolute value of standard deviation (SD) or more universally, by relative standard deviation (RSD). In this study relative standard deviation (RSD) between the replicates was 26% among the triplicates which was higher than 10% (Perring et al., 2005) reported in infant cereal matrices using WDXRF, 13% in dry pet food samples (Perring et al., 2017), 20% (Perring and Blanc, 2008) in milk powders, but lower than 31% RSD reported in dehydrated bouillon and sauce base products (Perring and Andrey, 2018). Robust standard deviation (SD) of repeatability in this study was reported as K (572.2 mg/kg), Ca (65.9 mg/kg), Mn (0.5 mg/kg), Fe (2.4 mg/kg), Cu (0.3 mg/kg), Zn (1.8 mg/kg), and Se (0.06 mg/kg), respectively. Perring and Blanc (2008) reported the standard deviation of repeatability as K (57 mg/kg), Ca (56 mg/kg), Fe (4.8 mg/kg), Cu (0.39 mg/kg), and Zn (1.3 mg/kg), respectively. Another study reported the standard deviation of repeatability as K (7.1 mg/kg), Ca (79.4 mg/kg), Mn (0.18 mg/kg), Fe (0.77 mg/kg), Cu (0.04 mg/kg), and Zn (0.13 mg/kg), respectively (Perring et al., 2017). Except for the higher standard deviation of repeatability for K in this study, for the rest of the elements, SD was of the same order

of magnitude as reported in previous studies. In general, the higher the standard deviation, the higher the heterogeneity in the samples. The degree of homogeneity of processed products such as milk powder and pet food is high as these are subjected to wet blending prior to spray drying ensuring a high degree of homogeneity of raw material which reduces the RSD and SD among the replicates. In comparison, in this study ground pea flour was less homogenous. The presence of seed coat makes it comparatively difficult to achieve the desired homogeneity level. Use of dehulled seeds in future studies may be advantageous. Pea flour used for the preparation of pellets was relatively coarse compared to milk powder, thus, RSD and SD values were higher in this study.

In this study, the range of recovery for the elements was reported from 76% to 165%. Previous XRF studies have reported range of recovery between 80 and 120% (Perring and Blanc, 2008 in fortified milk powders) for quantification of macro (Na, Mg, P, Cl, K and Ca) and micronutrients (Fe, Cu and Zn) and 82-117% in coffee plants (Tezotto et al., 2013). Bias and recovery are mostly treated as synonyms and indicators of accuracy. The difference in recovery reported in different studies may be the function of analyte content and matrix mismatch (Linsinger, 2008). This study reports similar recovery percentage for all the elements as reported in previous studies except for Se being high energy element, percentage recovery can be obtained as high as 165% for few samples.

The detection limits of different elements were K (9.54 mg/kg), Ca (3.5 mg/kg), Mn (0.5 mg/kg), Fe (0.54 mg/kg), Cu (0.35 mg/kg), Zn (0.2 mg/kg), Se (0.016 mg/kg) in this study in comparison to the detection limits reported by Tezotto, 2013 for K (27.5 mg/kg), Ca (27.6 mg/kg), Mn (2.6 mg/kg), Fe (2.3 mg/kg), Cu (5.8 mg/kg), and Zn (2.1 mg/kg). The detection limits are higher in the study conducted by Tezotto as that experiment was

conducted using benchtop energy dispersive X-ray fluorescence spectrometer Shimadzu EDX-720, whereas this study was conducted in a synchrotron due to which the instrumental detection limits are lower. The limit of detection of the proposed approach has the same order of magnitude compared to those observed in other reports.

The limit of determination in this study was reported as K (2363 mg/kg), Ca (153 mg/kg), Mn (1.85 mg/kg), Fe (6.6 mg/kg), Cu (0.84 mg/kg), Zn (5.2 mg/kg), and Se (0.3 mg/kg), respectively. Previous studies in milk-based products reported the determination limits as K (1135 mg/kg), Ca (656 mg/kg), Fe (28 mg/kg) and Zn (9 mg/kg) (Perring and Andrey, 2003). Limit of determination was reported as K (500 mg/kg), Ca (600 mg/kg), Mn (6 mg/kg), Fe (30 mg/kg), and Zn (10 mg/kg) in infant cereal matrices (Perring and Blanc, 2007). Paltridge et al. (2012b) estimated limit of determination for Zn and Fe in rice as ~12 and ~3 mg/kg, respectively, while the corresponding limit of determination in pearl millet were ~16 and ~5 mg/kg, respectively.

Due to higher standard deviation of repeatability in samples for K, the limit of determination was higher as compared to the values reported in previous studies. For high energy elements, the limits were reported lower than the values reported in previous studies. Detection limits for light elements (K and Ca) was higher than those for Mn, Fe, Cu, and Zn.

A disadvantage of XRF, relative to AAS analysis, is that the elements typically used to check for soil contamination in grain, Al, Ti, and Cr, are either too light (Al), or present at levels too low to be detected by XRF (Ti, Cr). This is not a major concern for Zn analysis since soil and dust usually contain little Zn but may be of concern for Fe analysis since soil and dust contain enough Fe to compromise screening programs (Paltridge et al.,

2012b). It would, therefore, be essential to check for soil contamination. As with any analytical method relying on electronic detection of spectra (including AAS), drift can occur in XRF results over time as subtle changes occur in detection sensitivity. Thus, the running of samples with known elemental concentrations (check samples) is necessary to monitor such drift.

AAS measurement of element concentrations as a reference method and the effect of its error on the evaluation of XRF predictions

The XRF validations and calibrations presented in this study relied on reference measurements of seed element concentrations obtained by triplicate AAS analyses. Minor errors in these reference concentration values may have occurred due to sample inhomogeneity, errors in sample digestion, operator errors and instrumental instability in the AAS based analyses. These errors would be expected to further compound the XRF error estimates. Thus, the true SEC and SEP calculated for XRF analysis are likely to be smaller than reported here.

Wet digestion using strong acids is the most common method used for destruction of organic matter in AAS (reference method). Improper digestion may cause analytical bias and block the sample introduction system. In this study, the digestion of samples was carried out in an open system. Wet digestion carried out in closed vessels has several advantages relative to open systems, including reduced risk of contamination and loss of volatile analytes. Use of HNO_3 and H_2O_2 allows complete digestion of biological samples except if they have a high content of silicates. In the presence of high silicates, hydrogen fluoride is added. The digested solution may appear fully transparent but residual carbon may persist at lower temperatures and cause analytical bias as non-oxidized carbon has been reported to act as a surfactant, changing the efficiency of the nebulizer. Hydrogen

peroxide is known to reduce the temperature requirements but most of the matrices still must be digested in a closed system to elevate the temperature (Hansen et al., 2009). Chen and Ma (2001) indicated that on a comparison of different digestion methods (hotplate aqua regia, microwave aqua regia, and microwave aqua regia + HF) to determine elemental concentrations in soil, microwave aqua regia + HF had better precision (3.7%) and elemental recoveries (94%). The aqua regia digestion technique failed to accurately quantify more than 20 elements in soil samples, especially K and Al which are part of clay mineral structures.

Since the aim of this research was the comparison between XRF and AAS, the homogeneity of the high amount of digested sample required by AAS is a prerequisite for the correct XRF concentration evaluation. The large difference in the analyzed samples quantity in XRF (40 mg) and AAS (0.5 g) may also be the cause of some differences in the quantification.

ICP-MS analysis was conducted on the Validation Set to check for possible errors in the AAS values obtained for K since we observed low Pearson correlation coefficient (0.72) for XRF predicted concentration of K and AAS in empirical and FP models. On correlating AAS and ICP-MS data, it was observed that the R‾value was only 0.5 for K indicating unreliability, or error in K concentrations from digestion-based methods, i.e., errors in either the AAS or the ICP-MS approaches (Fig 5.1) but on correlating AAS and ICP-MS data for Ca, Mn, Fe, Cu, Zn and Se the R values obtained were 0.97, 0.95, 0.95, 0.96, 0.94 and 0.99 respectively.

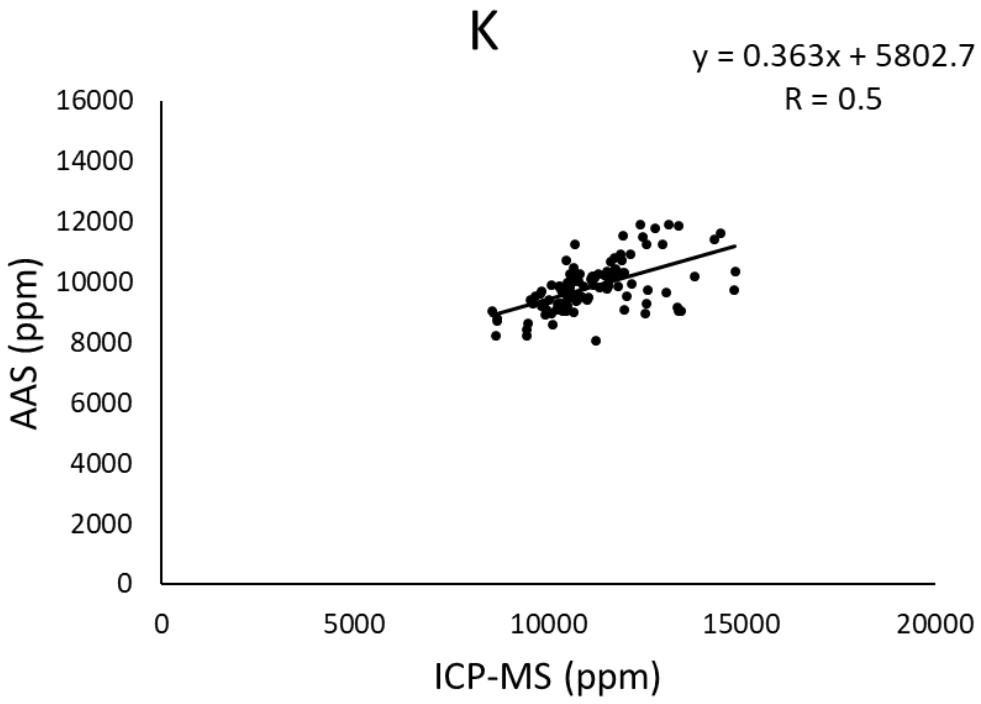

Figure 5.1 Correlation between AAS and ICP-MS concentrations for K in Validation Set.

Conventional wet digestion methods involve inconsistent digestion from the edges in heating blocks and require constant monitoring of acid consumption to avoid sample drying and burning. Transfer of digest into another volumetric container introduces error for final quantification. Repeated use of glassware for HNO_3 digestion may result in the unacceptably high background, leading to unreliable estimation of trace elements (Cu, Zn) especially when the plants are deficient in these elements (Huang, 2004).

Effect of XRF measurement conditions and its effect on the prediction of element concentrations

Pellet thickness

After compressing pea flour into pellets, the pellets were weighed. It was observed that there were minor differences in weight of pellets that could result in minor differences in thickness of pellets. Pellet thickness is also expected to increase with decreased pressure on the sample powder and with decreasing particle size (Demir et al., 2006). The characteristic X-rays have different penetration depths. The dependence of results on sample weight and thickness can be significant for high energy X-rays (Lutz and Pernicka, 1996).

Sample surface

The intensity of Compton and Rayleigh scatter peaks vary according to the energy of photons emitted from the excitation source and mass attenuation coefficient of the target sample. If the changes in the intensity of a scattering peak are to be used to correct for surface irregularity effects, the measured intensity should ideally be independent of sample composition. Potts et al. (1997) observed that the scatter intensities were influenced by small variations in the thickness of the powder pellets from which the measurements were made. Scatter peak data showed significant variation in the mass attenuation coefficient.

Air vs. vacuum

In an analysis of rock samples using portable XRF, large errors were obtained with even small air gaps of 1-2 mm between the analyzer and sample, unless an appropriate correction is applied to measured intensities (Potts et al., 1997). For K lines of higher atomic number elements, a simple scatter peak normalization can be used to correct for

surface irregularities and is known to be effective for air gaps up to 3 mm (Potts et al., 1997). The main limitations to the larger air gaps are the enhanced air attenuation of K lines of elements with atomic numbers lower than Fe. Increase in the distance between analyzer and sample causes a relative increase in total to scatter intensity.

Light elements including K and Ca, are mostly measured under vacuum conditions in XRF (Mittal, 2001). The absence of a vacuum makes a reliable analysis of either of the light elements much more difficult. Matrix corrections are necessary when samples are of enough thickness to absorb fluorescent radiation which causes a systemic reduction in experimentally measured fluorescence amplitude also called self- absorption or reabsorption (Reynolds, 1963). The elemental concentrations will, of course, vary with nutrient availability, plant species, growing conditions and time of sampling. Monte Carlo regressions indicate that the most reliable analytical conditions for light elements are under internal vacuum conditions (Li, 2008).

Particle size and sample homogeneity

Particle size effects in the analysis of powdered samples by XRF method are a serious source of analytical errors (>30%). Mean particle size limits the accuracy of XRF method and these particle size effects are very significant for light elements (Reynolds Jr, 1963). K, Ca and another low energy radiation is more sensitive to sample particle size changes than high energy radiation (Mzyk et al., 2002). Use of mill or hand grinding has proved impossible to grind the samples to the same particle size resulting in non-standard mean particle size (Evans, 1970). As the intensity of emitted X-radiation is related to the particle size, use of a ball mill (Geno grinder) is reported for grinding to obtain homogenous particle size (Evans, 1970). The relationship between the X-ray intensity

and grain size is even more complicated when strong matrix effects exist (Mzyk et al., 2002).

Evaluation of XRF calibration curve-based prediction of pea seed element concentrations

A general principle of empirical calibration in XRF is that the calibration and test samples be as similar as possible and cover a similar range of concentrations, and this range is reflective of the actual range of analyte concentrations expected in the samples on which the method would be applied in the future. The calibration relationships developed in this research should be robust enough to be applied on pea samples beyond the pea samples tested here (e.g., on varieties grown in different environments). Although plant species-specific calibrations are recommended (Paltridge et al., 2012b), there may be cases where analysts have limited access to grain samples with a wide range of accurately known elemental concentrations.

The empirical regression method, which has been in use for many years, represents absorption and enhancement effects of each element on each other element by parameters independent of mass concentrations. The calibration relationships between XRF peak areas and AAS concentrations for all the elements except K were strong with the R^2 value above 0.8 except for K (0.5). Standard error of calibration (SEC) which is based on the differences between each reference value and those calculated using the calibration model was reported as K (920 mg/kg), Ca (75.5 mg/kg), Mn (0.67 mg/kg), Fe (3.13 mg/kg), Cu (0.39 mg/kg), Zn (1.92 mg/kg), and Se (0.15 mg/kg) respectively in this study. Several other studies in food products have reported different standard error values for calibrations such as Fe (792 mg/kg), Cu (82 mg/kg) and Zn (468 mg/kg), respectively (Perring et al., 2005 in food premixes); K (252 mg/kg), Ca (262 mg/kg), Fe (4.1 mg/kg)

and Zn (2.7 mg/kg), respectively (Perring and Andrey, 2003 in milk products); K (~646 mg/kg), Ca (57 mg/kg), Fe (1.28 mg/kg) and Zn (0.9 mg/kg), respectively (Perring and Andrey, 2018 in dehydrated bouillon and sauce-based products); K (28 mg/kg), Ca (106 mg/kg), Mn (0.33 mg/kg), Fe (1.45 mg/kg), Cu (0.06 mg/kg) and Zn (0.57 mg/kg), respectively (Perring et al., 2017 in dry pet food samples). Except for K, standard error of calibration reported in this study were in comparison to the values reported in previous studies. Differences in the standard error of calibration reported in several studies appear to be the function of instruments used and matrix differences in samples.

Furthermore, the empirical coefficients calculated by multiple regression analysis contain many potential pitfalls. Not only do empirical coefficients correct for matrix effects, but they can also conceal other error types that may be present, such as errors on measured intensities, poor standard chemical data, poor sample preparation, a variation of particle size effects, of mineralogical effects, of surface effects, and so on. Unfortunately, all these effects tend to change from sample to sample, so that unknown samples analyzed using such calibration curves often may yield inferior quality analytical results. These errors might contribute to the significant bias obtained for K and Ca in this study.

Evaluation of XRF Fundamental parameter-based prediction (XRF-FP) of pea seed element concentrations

The Fundamental Parameter method has been recently used for quantitative analysis. This method uses measured primary spectral distributions, rather than theoretical expression and accounts for matrix effects by means of measured mass absorption coefficients μ and fluorescent yields. For quantitative analysis, the fundamental parameter method has proven to be very useful and accurate. The fundamental parameter method relies on the accurate estimation of the net intensities of the characteristic lines in the spectrum. The

use of an incorrect or incomplete fitting function results in considerable bias in the estimates of the net peak areas (systematic errors), especially for small peaks near large ones. The reason for the relatively high bias for K and Ca in the FP approach in comparison to the empirical method may be the overlapping of the fluorescent X-rays. For example, Ca-Kβ overlaps with K-Kα and may cause adverse effects on the analytical results since the FP algorithm uses not only α X-rays but also, β ones for the calculation (Marguí et al., 2005).

The combination of spectrum evaluation by nonlinear least-squares fitting and quantitative analysis using the fundamental parameter method delivers accurate concentration estimates for a large variety of samples and experimental conditions but still has one major disadvantage. The theoretical background of the method is difficult, and any decision of the operator can drastically influence the outcome of the method. Except for Fe, the reason for which might be inaccurate fitting of Fe peak, the fundamental parameter approach was observed to be equally as good as the empirical method for all other elements.

Automation of sample preparation and data collection steps and its effect on sample throughput

The emphasis in this study was placed on developing methods with high throughput and analytical performance for use in the evaluation of seed samples from a plant breeding program. A major advantage of XRF is the simplicity of sample preparation and analysis and the associated ease of high throughput analysis of several samples and multiple elements at a time. Most of the commercial spectrometers can determine all the elements from atomic number 9 to 92. The large capacity of a sample holder allows unattended multiple and a wide variety of samples such as soil, rock, plants, liquids and airborne

particulates (O'connell, 1977). Wet bench analysis requires time-consuming steps associated with labor requirement for monitoring acid levels and transfer of digest solution, and high background levels in trace elements (e.g. Cu, Mn) (Huang et al., 2004). Analyzing the samples at the same irradiation time (20 sec/spectra), would take around two weeks to prepare and analyze 1000 samples using XRF by a single person, equating to daily throughput of 150 samples in 8 hours a day. Using AAS, the same number of samples would require a month for analysis. Technicians can be trained to conduct XRF analysis in days, as the technology requires less sample preparation than wet bench analysis.

6.0 CONCLUSION AND RECOMMENDATION

The aim of this research was the comparison between XRF and AAS for element analysis in pea seeds. We determined that the XRF technique could be considered as a valuable and comparable alternative to the conventional analytical technique (AAS) for analysis of Mn, Cu, Zn and Se in pea seeds. For Mn, Cu, Zn and Se, the intercept was found to be not significantly different from 0 and B (the slope) was found to be not significantly different from 1 with empirical (XRF) as well as fundamental parameter approach (XRF-FP). Nevertheless, for some elements including K and Ca, relative uncertainties of measurement were found higher than 20% and being low energy elements, the intensities need to be corrected for self-absorption; since the incident beam passes through the sample it is absorbed due to interaction with other atoms.

The key point for the efficient application and then successful implementation of the described approach is to firstly constitute a suitable collection of samples containing a broad range of analyte concentrations to ensure robust calibrations. The setup of the calibration standards is a crucial step in the utilization of XRF. Considering several other facts, it could be concluded that sample decomposition procedure (grinding in XRF and sample digestion in AAS) used influences the results of element determination and this depends on the analyte of interest and the main matrix element composition of the sample. In contrast, the XRF method allows obviating the matrix destruction stage and the poor recoveries of some elements. Moreover, this method is less time consuming, requires fewer amounts of reagents and large capacity of a sample holder allows unattended and multiple sample analysis. This is of significance in studies where conclusions are drawn based on many samples. Nevertheless, there are several factors

that influence the results from XRF analysis and need to be investigated before finalizing the protocol. Detection limits, matrix effects, sample preparation and instrument configuration, and measuring time need to be investigated before setting up the final protocol. Future work may include addressing low energy elements (K and Ca) issues and methods to correct the self-absorption in the XRF method. The samples can be analyzed under vacuum to check the attenuation due to air molecules. As the literature indicates, binding of K and Ca to silicates can be solved by using hydrofluoric acid (HF). Samples digested using HF can be then be tested for K and Ca. Future research could also investigate limitations in the accuracy and repeatability of digestion-based issues in the AAS method.

7.0 LITERATURE CITED

Adrjanowicz, K., Kaminski, K., Grzybowska, K., Hawelek, L., Paluch, M., Gruszka, I., Zakowiecki, D., Sawicki, W., Lepek, P., Kamysz, W. and Guzik, L., 2011. Effect of cryogrinding on chemical stability of the sparingly water-soluble drug furosemide. *Pharmaceutical Research*, 28(12), pp.3220-3236.

Al-Omari, S., 2011. Determination of essential and toxic trace elements in ten herbal medicines using energy-dispersive EDXRF analysis. *X-Ray Spectrometry*, 40(1), pp.31-36.

Ávila, D.V.L., Souza, S.O., Costa, S.S.L., Araujo, R.G.O., Garcia, C.A.B., Alves, J.D.P.H. and Passos, E.A., 2016. Determination of Zn in dry feeds for cats and dogs by energy-dispersive X-ray fluorescence spectrometry. *Journal of AOAC International*, 99(6), pp.1572-1575.

Baldwin, J.P., 1975. A quantitative analysis of the factors affecting plant nutrient uptake from some soils. *European Journal of Soil Science*, 26(3), pp.195-206.

Bangar, P., Glahn, R.P., Liu, Y., Arganosa, G.C., Whiting, S. and Warkentin, T.D., 2017. Iron Bioavailability in Field Pea Seeds: Correlations with Iron, Phytate, and Carotenoids. *Crop Science*, 57(2), pp.891-902.

Bastos, R.O., Melquiades, F.L. and Biasi, G.E.V., 2012. Correction for the effect of soil moisture on in situ EDXRF analysis using low-energy background. *X-Ray Spectrometry*, 41(5), pp.304-307.

Beckhoff, B., Kanngießer, B., Langhoff, N., Wedell, R. and Wolff, H. eds., 2007. *Handbook of Practical X-ray Fluorescence Analysis*. Springer Science & Business Media.

Borgese, L., Zacco, A., Bontempi, E., Colombi, P., Bertuzzi, R., Ferretti, E., Tenini, S. and Depero, L.E., 2009. Total reflection of x-ray fluorescence (TXRF): a mature technique for environmental chemical nanoscale metrology. *Measurement Science and Technology*, 20(8), p.084027.

Brouwer, P., 2006. Theory of EDXRF. *Almelo, Netherlands: PANalytical BV*.

Brown, R.J. and Milton, M.J., 2005. Analytical techniques for trace element analysis: an overview. *TrAC Trends in Analytical Chemistry*, 24(3), pp.266-274.

Çevik, U., Ergen, E., Budak, G., Karabulut, A., Tiraşoğlu, E., Apaydin, G. and Kopya, A.I., 2003. Elemental analysis of Akcaabat tobacco and its ash by EDXRF spectrometry. *Journal of Quantitative Spectroscopy and Radiative Transfer*, 78(3-4), pp.409-415.

Chen, M. and Ma, L.Q., 2001. Comparison of three aqua regia digestion methods for twenty Florida soils. *Soil Science Society of America Journal*, 65(2), pp.491-499.

Dahl, W.J., Foster, L.M. and Tyler, R.T., 2012. Review of the health benefits of peas (Pisum sativum L.). *British Journal of Nutrition*, 108(S1), pp. S3-S10.

Demir, F., Budak, G., Baydaş, E. and Şahin, Y., 2006. Standard deviations of the error effects in preparing pellet samples for WDXRF spectroscopy. *Nuclear Instruments and Methods in Physics Research Section B: Beam Interactions with Materials and Atoms*, 243(2), pp.423-428.

Desideri, D., Meli, M.A., Roselli, C. and Feduzi, L., 2009. A biomonitoring study: 210Po and heavy metals in mussels. *Journal of Radioanalytical and Nuclear Chemistry*, 279(2), pp.591-600.

Evans, C.C., 1970. X-ray fluorescence analysis for light elements in plant and faecal materials. *Analyst*, 95(1136), pp.919-929.

Gauglitz, G. and Moore, D.S. eds., 2014. *Handbook of Spectroscopy, 4 Volume Set*. John Wiley & Sons.

Gauglitz, G. and Vo-Dinh, T. eds., 2006. *Handbook of Spectroscopy*. John Wiley & Sons.

Gawalko, E., Garrett, R.G., Warkentin, T., Wang, N. and Richter, A., 2009. Trace elements in Canadian field peas: a grain safety assurance perspective. *Food Additives and Contaminants*, 26(7), pp.1002-1012.

Ge, L., Lai, W. and Lin, Y., 2005. Influence of and correction for moisture in rocks, soils and sediments on in situ XRF analysis. *X-Ray Spectrometry: An International Journal*, 34(1), pp.28-34.

Guild, G.E., Paltridge, N.G., Andersson, M.S. and Stangoulis, J.C., 2017. An energy-dispersive X-ray fluorescence method for analysing Fe and Zn in common bean, maize and cowpea biofortification programs. *Plant and Soil*, 419(1-2), pp.457-466.

Hansen, T.H., Laursen, K.H., Persson, D.P., Pedas, P., Husted, S. and Schjoerring, J.K., 2009. Micro-scaled high-throughput digestion of plant tissue samples for multi-elemental analysis. *Plant Methods*, 5(1), pp.12.

Hampel, F.R., Ronchetti, E.M., Rousseeuw, P.J. and Stahel, W.A., 2011. *Robust statistics: the approach based on influence functions*. John Wiley & Sons, 196.

Haschke, M., 2014. Laboratory Micro-X-Ray Fluorescence Spectroscopy. *Laboratory Micro-X-Ray Fluorescence Spectroscopy: Instrumentation and Applications, Springer Series in Surface Sciences,* Volume 55. ISBN 978-3-319-04863-5. Springer International Publishing Switzerland.

Himelblau, E. and Amasino, R.M., 2001. Nutrients mobilized from leaves of Arabidopsis thaliana during leaf senescence. *Journal of Plant Physiology*, 158(10), pp.1317-1323.

Hoenig, M. and De Borger, R., 1983. Particular problems encountered in trace metal analysis of plant material by atomic absorption spectrometry. *Spectrochimica Acta Part B: Atomic Spectroscopy*, 38(5-6), pp.873-880.

Hou, X., He, Y. and Jones, B.T., 2004. Recent advances in portable X-ray fluorescence spectrometry. *Applied Spectroscopy Reviews*, 39(1), pp.1-25.

Howard, D.L., de Jonge, M.D., Lau, D., Hay, D., Varcoe-Cocks, M., Ryan, C.G., Kirkham, R., Moorhead, G., Paterson, D. and Thurrowgood, D., 2012. High-definition X-ray fluorescence elemental mapping of paintings. *Analytical Chemistry*, 84(7), pp.3278-3286.

Huang, L., Bell, R.W., Dell, B. and Woodward, J., 2004. Rapid nitric acid digestion of plant material with an open-vessel microwave system. *Communications in Soil Science and Plant Analysis*, 35(3-4), pp.427-440.

Jalas, P., Ruottinen, J.P. and Hemminki, S.A.R.I., 2002. EDXRF analysis of jewelry using fully standardless fundamental parameter approach. *Gold technology*, 35, p.28.

Janssens, K., 2014. X-Ray Fluorescence Analysis, in Handbook of Spectroscopy: Second, Enlarged Edition (eds G. Gauglitz and D. S. Moore), Wiley-VCH Verlag GmbH & Co. KGaA, Weinheim, Germany.

Janssens, K. and Van Grieken, R. eds., 2004. *Non-destructive micro analysis of cultural heritage materials*. Elsevier.

Jenkins, R., 1995. *Quantitative X-ray spectrometry*. CRC Press.

Jenkins, R., 1999. X-ray fluorescence spectrometry. *Chemical Analysis: A series of Monographs on analytical chemistry and its applications*, 152, pp.12.

Kalra, Y. ed., 1997. *Handbook of reference methods for plant analysis*. CRC press.

Khuder, A., Sawan, M.K., Karjou, J. and Razouk, A.K., 2009. Determination of trace elements in Syrian medicinal plants and their infusions by energy dispersive X-ray fluorescence and total reflection X-ray fluorescence spectrometry. *Spectrochimica Acta Part B: Atomic Spectroscopy*, 64(7), pp.721-725.

Kokalj, M., Rihtarič, M. and Kreft, S., 2011. Commonly applied smoothing of IR spectra showed unappropriate for the identification of plant leaf samples. *Chemometrics and Intelligent Laboratory Systems*, 108(2), pp.154-161.

Koz, B., Cevik, U. and Akbulut, S., 2012. Heavy metal analysis around Murgul (Artvin) copper mining area of Turkey using moss and soil. *Ecological Indicators*, 20, pp.17-23.

Krupskaya, T.K., Loseva, L. and Anufrik, S., 2015. Possibilities of the method of an X-ray fluorescence analysis when evaluating essential element concentrations in food raw materials of plant origin. *Papers on Anthropology*, 24(1), pp.101-106.

Krusberski, N., 2006. Exploring potential errors in XRF analysis. *Analytical Challenges in Metallurgy. Johannesburg, South Africa: The Southern African Institute of Mining and Metallurgy*, pp.1-8.

Li, F., 2008. *Monte Carlo simulation of energy-dispersive x-ray fluorescence and applications*. Doctoral dissertation. North Carolina State University.

Linsinger, T.P., 2008. Use of recovery and bias information in analytical chemistry and estimation of its uncertainty contribution. *TrAC Trends in Analytical Chemistry*, 27(10), pp.916-923.

Lutz, J. and Pernicka, E., 1996. Energy dispersive X-ray fluorescence analysis of ancient copper alloys: empirical values for precision and accuracy. *Archaeometry*, 38(2), pp.313-323.

Ma, Y., Coyne, C.J., Grusak, M.A., Mazourek, M., Cheng, P., Main, D. and McGee, R.J., 2017. Genome-wide SNP identification, linkage map construction and QTL mapping for seed mineral concentrations and contents in pea (Pisum sativum L.). *BMC Plant Biology*, 17(1), pp.43.

Mahawatte, P., Dissanayaka, K.R. and Hewamanna, R., 2006. Elemental concentrations of some Ayurvedic drugs using energy dispersive EDXRF. *Journal of Radioanalytical and Nuclear Chemistry*, 270(3), pp.657-660.

Mamedov, S., 2012. Application of micro-XRF in forensic science. *Microscopy and Microanalysis*, 18(S2), pp.956-957.

Mantler, M. and Kawahara, N., 2004. *How accurate are modern fundamental parameter methods? The Rigaku Journal*, 21(2), pp.17–25.

Manso, M., Carvalho, M.L. and Nunes, M.L., 2007. Characterization of essential and toxic elements in cephalopod tissues by EDXRF and AAS. *X-Ray Spectrometry*, 36(6), pp.413-418.

Marguí, E., Hidalgo, M., Queralt, I., Van Meel, K. and Fontas, C., 2012. Analytical capabilities of laboratory, benchtop and handheld X-ray fluorescence systems for detection of metals in aqueous samples pre-concentrated with solid-phase extraction disks. *Spectrochimica Acta Part B: Atomic Spectroscopy*, 67, pp.17-23.

Marguí, E., Queralt, I., Carvalho, M.L. and Hidalgo, M., 2005. Comparison of EDXRF and ICP-OES after microwave digestion for element determination in plant samples from an abandoned mining area. *Analytica Chimica Acta*, 549(1-2), pp.197-204.

Margui, E. and Van Grieken, R., 2013. *X-ray fluorescence spectrometry and related techniques: an introduction*. Momentum Press.

Martinez, T., Lartigue, J., Zarazua, G., Avila-Perez, P., Navarrete, M. and Tejeda, S., 2010. Total reflection X-ray fluorescence analysis of trace-elements in candies marketed in Mexico. *Spectrochimica Acta Part B: Atomic Spectroscopy*, 65(6), pp.499-503.

Marx, J.J.M., 1997. Iron deficiency in developed countries: prevalance, influence of lifestyle factors and hazards of prevention. *European Journal of Clinical Nutrition*, 51(8), pp.491-494.

Mazet, V., Carteret, C., Brie, D., Idier, J. and Humbert, B., 2005. Background removal from spectra by designing and minimising a non-quadratic cost function. *Chemometrics and Intelligent Laboratory Systems*, 76(2), pp.121-133.

McIntosh, K.G., 2012. *Trace Element Analysis of Environmental and Clinical Materials Using Novel Instrumentation Based on X-ray Fluorescence Spectrometry: New Capabilities for Public Health Laboratories*, Doctoral dissertation, University at Albany. Department of Environmental Health sciences.

McLaren, T.I., Guppy, C.N. and Tighe, M.K., 2012. A rapid and nondestructive plant nutrient analysis using portable x-ray fluorescence. *Soil Science Society of America Journal*, 76(4), pp.1446-1453.

Melquiades, F.L., Parreira, P.S., Appoloni, C.R., Silva, W.D. and Lopes, F., 2011. Quantification of metals in river water using a portable EDXRF system. *Applied Radiation and Isotopes*, 69(2), pp.327-333.

Miller, A.J. and Cramer, M.D., 2005. Root nitrogen acquisition and assimilation. In: Lambers H., Colmer T.D. (eds) Root Physiology: from Gene to Function. Plant Ecophysiology, vol 4. Springer, Dordrecht

Mittal, R., 2001. Matrix effects during potassium and calcium determinations in rice saplings using X-ray spectrometery. *Applied Radiation and Isotopes*, 54(3), pp.377-382.

Mzyk, Z., Baranowska, I. and Mzyk, J., 2002. Research on grain size effect in XRF analysis of pelletized samples. *X-Ray Spectrometry: An International Journal*, 31(1), pp.39-46.

Obiajunwa, E.I., Adebajo, A.C. and Omobuwajo, O.R., 2002. Essential and trace element contents of some Nigerian medicinal plants. *Journal of Radioanalytical and Nuclear Chemistry*, 252(3), pp.473-476.

O'connell, A.M., 1977. *Automated X-ray fluorescence analysis* (No. INIS-MF--3950). Commonwealth Scientific and Industrial Research Organization.

Orescanin, V., Katunar, A., Kutle, A. and Valkovic, V., 2003. Heavy metals in soil, grape, and wine. *Journal of Trace and Microprobe Techniques*, 21(1), pp.171-180.

Paltridge, N.G., Milham, P.J., Ortiz-Monasterio, J.I., Velu, G., Yasmin, Z., Palmer, L.J., Guild, G.E. and Stangoulis, J.C., 2012a. Energy-dispersive X-ray fluorescence spectrometry as a tool for zinc, iron and selenium analysis in whole grain wheat. *Plant and Soil*, 361(1-2), pp.261-269.

Paltridge, N.G., Palmer, L.J., Milham, P.J., Guild, G.E. and Stangoulis, J.C., 2012b. Energy-dispersive X-ray fluorescence analysis of zinc and iron concentration in rice and pearl millet grain. *Plant and Soil*, 361(1-2), pp.251-260.

Pashkova, G.V., 2009. X-ray fluorescence determination of element contents in milk and dairy products. *Food Analytical Methods*, 2(4), p.303.

Perring, L. and Andrey, D., 2003. ED-XRF as a tool for rapid minerals control in milk-based products. *Journal of Agricultural and Food Chemistry*, 51(15), pp.4207-4212.

Perring, L. and Andrey, D., 2018. Multi-elemental ED-EDXRF Determination in Dehydrated Bouillon and Sauce Base Products. Food Analytical Methods, 11(1), pp.148-160.

Perring, L., Andrey, D., Basic-Dvorzak, M. and Blanc, J., 2005. Rapid multimineral determination in infant cereal matrices using wavelength dispersive X-ray fluorescence. *Journal of Agricultural and Food Chemistry*, 53(12), pp.4696-4700.

Perring, L. and Blanc, J., 2007. EDXRF determination of iron during infant cereals production and its fitness for purpose. *International Journal of Food Science & Technology*, 42(5), pp.551-555.

Perring, L. and Blanc, J., 2008. Validation of quick measurement of mineral nutrients in milk powders: comparison of energy dispersive X-ray fluorescence with inductively coupled plasma-optical emission spectroscopy and potentiometry reference methods. *Sensing and Instrumentation for Food Quality and Safety*, 2(4), pp.254-261.

Perring, L., Nicolas, M., Andrey, D., Rime, C.F., Richoz-Payot, J., Dubascoux, S. and Poitevin, E., 2017. Development and validation of an ED-XRF method for the fast quantification of mineral elements in dry pet food samples. *Food Analytical Methods*, 10(5), pp.1469-1478.

Pottier, M., Dumont, J., Masclaux-Daubresse, C. and Thomine, S., 2018. Autophagy is essential for optimal Fe translocation to seeds in Arabidopsis. *BioRxiv*, pp.313254.

Pottier, M., Masclaux Daubresse, C., Yoshimoto, K. and Thomine, S., 2014. Autophagy as a possible mechanism for micronutrient remobilization from leaves to seeds. *Frontiers in Plant Science*, 5, pp.11.

Potts, P.J., Webb, P.C. and Williams-Thorpe, O., 1997. Investigation of a correction procedure for surface irregularity effects based on scatter peak intensities in the field analysis of geological and archaeological rock samples by portable X-ray fluorescence spectrometry. *Journal of Analytical Atomic Spectrometry*, 12(7), pp.769-776.

Ray, H., Bett, K., Tar'an, B., Vandenberg, A., Thavarajah, D. and Warkentin, T., 2014. Mineral micronutrient content of cultivars of field pea, chickpea, common bean, and lentil grown in Saskatchewan, Canada. *Crop Science*, 54(4), pp.1698-1708.

Reidinger, S., Ramsey, M.H. and Hartley, S.E., 2012. Rapid and accurate analyses of silicon and phosphorus in plants using a portable X-ray fluorescence spectrometer. *New Phytologist*, 195(3), pp.699-706.

Reynolds Jr, R.C., 1963. Matrix corrections in trace element analysis by X-ray fluorescence: estimation of the mass absorption coefficient by Compton scattering. *American Mineralogist: Journal of Earth and Planetary Materials*, 48(9-10), pp.1133-1143.

Rousseau, R.M., 2006. Corrections for matrix effects in X-ray fluorescence analysis—A tutorial. *Spectrochimica Acta Part B: Atomic Spectroscopy*, 61(7), pp.759-777.

Rousseeuw, P.J. and Croux, C., 1993. Alternatives to the median absolute deviation. *Journal of the American Statistical Association*, 88(424), pp.1273-1283.

Saper, R.B., Kales, S.N., Paquin, J., Burns, M.J., Eisenberg, D.M., Davis, R.B. and Phillips, R.S., 2004. Heavy metal content of ayurvedic herbal medicine products. *Jama*, 292(23), pp.2868-2873.

Saper, R.B., Phillips, R.S., Sehgal, A., Khouri, N., Davis, R.B., Paquin, J., Thuppil, V. and Kales, S.N., 2008. Lead, mercury, and arsenic in US-and Indian-manufactured Ayurvedic medicines sold via the Internet. *Jama*, 300(8), pp.915-923.

Schneider, A.R., Cancès, B., Breton, C., Ponthieu, M., Morvan, X., Conreux, A. and Marin, B., 2016. Comparison of field portable EDXRF and aqua regia/ICP-AES soil analysis and evaluation of soil moisture influence on FPEDXRF results. *Journal of Soils and Sediments*, 16(2), pp.438-448.

Shiraiwa, T. and Fujino, N., 1966. Theoretical Calculation of Fluorescent X-Ray Intensities in Fluorescent X-Ray Spectrochemical Analysis. *Japanese Journal of Applied Physics*, 5(10), p.886.

Simsek, A. and Aykut, O., 2007. Evaluation of the microelement profile of Turkish hazelnut (Corylus avellana L.) varieties for human nutrition and health. *International Journal of Food Sciences and Nutrition*, 58(8), pp.677-688.

Soetan, K.O., Olaiya, C.O. and Oyewole, O.E., 2010. The importance of mineral elements for humans, domestic animals and plants-A review. *African Journal of Food Science*, 4(5), pp.200-222.

Solé, V.A., Papillon, E., Cotte, M., Walter, P. and Susini, J., 2007. A multiplatform code for the analysis of energy-dispersive X-ray fluorescence spectra. *Spectrochimica Acta Part B: Atomic Spectroscopy*, 62(1), pp.63-68.

Spolnik, Z., Belikov, K., Van Meel, K., Adriaenssens, E., De Roeck, F. and Van Grieken, R., 2005. Optimization of measurement conditions of an energy dispersive X-ray fluorescence spectrometer with high-energy polarized beam excitation for analysis of aerosol filters. *Applied Spectroscopy*, 59(12), pp.1465-1469.

Statistics Canada, Agriculture Division, Census of Agriculture, 2016. Map produced by Remote Sensing and Geospatial Analysis, Agriculture Division, Statistics Canada, 2018.

Statham, P.J., 1977. Deconvolution and background subtraction by least-squares fitting with prefiltering of spectra. *Analytical Chemistry*, 49(14), pp.2149-2154.

Tezotto, T., Favarin, J.L., Paula Neto, A., Gratão, P.L., Azevedo, R.A. and Mazzafera, P., 2013. Simple procedure for nutrient analysis of coffee plant with energy dispersive X-ray fluorescence spectrometry (EDXRF). *Scientia Agricola*, 70(4), pp.263-267.

Tıraşoğlu, E., Cevik, U., Ertuğral, B., Apaydın, G., Baltaş, H. and Ertuğrul, M., 2005. Determination of trace elements in cole (Brassica oleraceae var. acephale) at Trabzon region in Turkey. *Journal of Quantitative Spectroscopy and Radiative Transfer*, 94(2), pp.181-187.

Tıraşoğlu, E., Söğüt, Ö. Apaydın, G., Aylıkcı, V. and Damla, N., 2006. Elemental concentration analysis in some plant samples by EDXRF at Trabzon. *Journal of Quantitative Spectroscopy and Radiative Transfer*, 102(3), pp.396-401.

Tominaga, H., Dojyo, M. and Tanaka, M., 1972. Effect of spectrum smoothing on peak area determinations. *Nuclear Instruments and Methods*, 98(1), pp.69-76.

Tsuji, K., Injuk, J. and Van Grieken, R. eds., 2005. *X-ray spectrometry: recent technological advances*. John Wiley & Sons.

Van Grieken, R. and Markowicz, A. eds., 2001. *Handbook of X-ray Spectrometry*. CRC Press.

Warkentin, T.D., Delgerjav, O., Arganosa, G., Rehman, A.U., Bett, K.E., Anbessa, Y., Rossnagel, B. and Raboy, V., 2012. Development and characterization of low-phytate pea. *Crop Science*, 52(1), pp.74-78.

Wang, T.L., Domoney, C., Hedley, C.L., Casey, R. and Grusak, M.A., 2003. Can we improve the nutritional quality of legume seeds? *Plant Physiology*, 131(3), pp.886-891.

Welch, R.M., 2002. The impact of mineral nutrients in food crops on global human health. *Plant and Soil*, 247(1), pp.83-90.

White, P.J. and Broadley, M.R., 2005. Biofortifying crops with essential mineral elements. *Trends in Plant Science*, 10(12), pp.586-593.

White, P.J. and Broadley, M.R., 2009. Biofortification of crops with seven mineral elements often lacking in human diets–iron, zinc, copper, calcium, magnesium, selenium and iodine. *New Phytologist*, 182(1), pp.49-84.

White, P.J., 2012. Ion uptake mechanisms of individual cells and roots: short-distance transport. In *Marschner's Mineral Nutrition of Higher Plants (Third Edition)*.

Yatkin, S., Gerboles, M. and Borowiak, A., 2012. Evaluation of standardless EDXRF analysis for the determination of elements on PM10 loaded filters. *Atmospheric Environment*, 54, pp.568-582.

Yeung, Z.L.L., Kwok, R.C.W. and Yu, K.N., 2003. Determination of multi-element profiles of street dust using energy dispersive X-ray fluorescence (EDXRF). *Applied Radiation and Isotopes*, 58(3), pp.339-346.

Young HD, Freedman RA., 2004. Sears and Zemansky's University Physics with Modern Physics vol 1714 11th edn (San Francisco) (Pearson Addison Wesley).

8.0 APPENDICES

Appendix A: List of Calibration Set Used for Preparation of Calibration Curves.

Sample No.	Year	Expt.	Location	Genotype	Market class
1800001	2016	PVRT	Sutherland	CDC Golden	Yellow
1800002	2016	PVRT	Sutherland	CDC Striker	Green
1800003	2016	PVRT	Sutherland	CDC Meadow	Yellow
1800004	2016	PVRT	Sutherland	CDC Dakota	Dun
1800005	2016	PVRT	Sutherland	Redbat 88	Red
1800006	2016	PVRT	Sutherland	CDC Blazer	Maple
1800007	2016	PVRT	Sutherland	CDC 3548-2	Forage
1800008	2016	PVRT	Sutherland	CDC 4140-4	Wrinkled
1800009	2016	PVRT	Sutherland	AAC Carver	Yellow
1800010	2016	PVRT	Sutherland	CDC Pluto	Green
1800031	2016	PVRT	Lucky Lake	CDC Golden	Yellow
1800032	2016	PVRT	Lucky Lake	CDC Striker	Green
1800033	2016	PVRT	Lucky Lake	CDC Meadow	Yellow
1800034	2016	PVRT	Lucky Lake	CDC Dakota	Dun
1800035	2016	PVRT	Lucky Lake	Redbat 88	Red
1800036	2016	PVRT	Lucky Lake	CDC Blazer	Maple
1800037	2016	PVRT	Lucky Lake	CDC 3548-2	Forage
1800038	2016	PVRT	Lucky Lake	CDC 4140-4	Wrinkled
1800039	2016	PVRT	Lucky Lake	AAC Carver	Yellow
1800040	2016	PVRT	Lucky Lake	CDC Pluto	Green
1800061	2016	PVRT	Rosthern	CDC Golden	Yellow
1800062	2016	PVRT	Rosthern	CDC Striker	Green
1800063	2016	PVRT	Rosthern	CDC Meadow	Yellow
1800064	2016	PVRT	Rosthern	CDC Dakota	Dun
1800065	2016	PVRT	Rosthern	Redbat 88	Red
1800066	2016	PVRT	Rosthern	CDC Blazer	Maple
1800067	2016	PVRT	Rosthern	CDC 3548-2	Forage
1800068	2016	PVRT	Rosthern	CDC 4140-4	Wrinkled
1800069	2016	PVRT	Rosthern	AAC Carver	Yellow
1800070	2016	PVRT	Rosthern	CDC Pluto	Green
1800091	2016	PVRT	Kamsack	CDC Golden	Yellow
1800092	2016	PVRT	Kamsack	CDC Striker	Green
1800093	2016	PVRT	Kamsack	CDC Meadow	Yellow
1800094	2016	PVRT	Kamsack	CDC Dakota	Dun
1800095	2016	PVRT	Kamsack	Redbat 88	Red
1800096	2016	PVRT	Kamsack	CDC Blazer	Maple
1800097	2016	PVRT	Kamsack	CDC 3548-2	Forage

1800098	2016	PVRT	Kamsack	CDC 4140-4	Wrinkled
1800099	2016	PVRT	Kamsack	AAC Carver	Yellow
1800100	2016	PVRT	Kamsack	CDC Pluto	Green
1700001	2013	GWAS Sutherland	Sutherland	KASPA	Yellow
1700002	2013	GWAS Sutherland	Sutherland	Avantgarde	Yellow
1700009	2013	GWAS Sutherland	Sutherland	AMPLISSIMOZAZERSKIJ	Green
1700010	2013	GWAS Sutherland	Sutherland	MPG87	Green
1700016	2013	PAM_Rosthern	Rosthern	Trapper	Yellow
1700017	2013	PAM_Rosthern	Rosthern	MPG87	Green
1700019	2013	PAM_Rosthern	Rosthern	MPG87	Green
1700022	2012	PAM_Rosthern	Rosthern	CDCAcer	Yellow
1700023	2012	PAM_Rosthern	Rosthern	Rally	Green
1700024	2012	PAM_Rosthern	Rosthern	MI3391	Green
1700025	2011	PAM_Sutherland	Sutherland	Lucky	Green
1700047	2011	PAM_Sutherland	Sutherland	MI3360	Green
1700050	2011	PAM_Sutherland	Sutherland	Orb	Green
1700053	2011	PAM_Sutherland	Sutherland	Laxtons Superb	Yellow
1700065	2011	PAM_Sutherland	Sutherland	FDP2010	Yellow
1700068	2011	PAM_Sutherland	Sutherland	CDC Golden	Yellow
1700105	2010	PR-07_SPG	SPG	3005-51	Yellow
1700109	2010	PR-07_SPG	Rosthern	3005-40	Yellow
1700120	2011	PR-07_SPG	SPG	3005-8	Yellow
1700122	2011	PR-07_SPG	SPG	3005-93	Yellow
1700123	2011	PR-07_SPG	SPG	3005-100	Yellow
1700126	2011	PR-07_SPG	Rosthern	3005-140	Yellow
1700128	2012	PR-07_SPG	SPG	3005-1	Green
1700131	2012	PR-15_Rosthern	Rosthern	CDC Meadow	Yellow
1700135	2012	PR-15_Rosthern	Rosthern	PR-15-24	Yellow
1700142	2011	PR-15_Sutherland	Sutherland	PR-15-70	Yellow
1700145	2011	PR-15_Sutherland	Sutherland	PR-15-336	Yellow
1700150	2012	PR-15_Sutherland	Sutherland	PR-15-113	Yellow
1700151	2012	PR-15_Sutherland	Sutherland	PR-15-93	Yellow
1700152	2012	PR-15_Sutherland	Sutherland	PR-15-246	Yellow
1700153	2012	PR-15_Sutherland	Sutherland	1-2347-144	Yellow
1700154	2012	PR-15_Sutherland	Sutherland	CDC Meadow	Yellow
1700156	2012	PR-15_Sutherland	Sutherland	PR-15-307	Yellow

SPG: Saskatchewan Pulse Growers located near Floral, Saskatchewan
PVRT: Pea Variety Regional Trial
PAM: Pea Association Mapping panel, Crop Development Centre, University of Saskatchewan

Appendix B: List of Validation Set

Sample No.	Year	Expt.	Location	Genotype	Market Class
1800011	2016	PVRT	Sutherland	CDC Golden	Yellow
1800012	2016	PVRT	Sutherland	CDC Striker	Green
1800013	2016	PVRT	Sutherland	CDC Meadow	Yellow
1800014	2016	PVRT	Sutherland	CDC Dakota	Dun
1800015	2016	PVRT	Sutherland	Redbat88	Red
1800016	2016	PVRT	Sutherland	CDC Blazer	Maple
1800017	2016	PVRT	Sutherland	CDC 3548-2	Forage
1800018	2016	PVRT	Sutherland	CDC 4140-4	Wrinkled
1800019	2016	PVRT	Sutherland	AAC Carver	Yellow
1800020	2016	PVRT	Sutherland	CDC Pluto	Green
1800021	2016	PVRT	Sutherland	CDC Golden	Yellow
1800022	2016	PVRT	Sutherland	CDC Striker	Green
1800023	2016	PVRT	Sutherland	CDC Meadow	Yellow
1800024	2016	PVRT	Sutherland	CDC Dakota	Dun
1800025	2016	PVRT	Sutherland	Redbat88	Red
1800026	2016	PVRT	Sutherland	CDC Blazer	Maple
1800027	2016	PVRT	Sutherland	CDC 3548-2	Forage
1800028	2016	PVRT	Sutherland	CDC 4140-4	Wrinkled
1800029	2016	PVRT	Sutherland	AAC Carver	Yellow
1800030	2016	PVRT	Sutherland	CDC Pluto	Green
1800041	2016	PVRT	Lucky Lake	CDC Golden	Yellow
1800042	2016	PVRT	Lucky Lake	CDC Striker	Green
1800043	2016	PVRT	Lucky Lake	CDC Meadow	Yellow
1800044	2016	PVRT	Lucky Lake	CDC Dakota	Dun
1800045	2016	PVRT	Lucky Lake	Redbat88	Red
1800046	2016	PVRT	Lucky Lake	CDC Blazer	Maple
1800047	2016	PVRT	Lucky Lake	CDC 3548-2	Forage
1800048	2016	PVRT	Lucky Lake	CDC 4140-4	Wrinkled
1800049	2016	PVRT	Lucky Lake	AAC Carver	Yellow
1800050	2016	PVRT	Lucky Lake	CDC Pluto	Green
1800051	2016	PVRT	Lucky Lake	CDC Golden	Yellow
1800052	2016	PVRT	Lucky Lake	CDC Striker	Green
1800053	2016	PVRT	Lucky Lake	CDC Meadow	Yellow
1800054	2016	PVRT	Lucky Lake	CDC Dakota	Dun
1800055	2016	PVRT	Lucky Lake	Redbat88	Red
1800056	2016	PVRT	Lucky Lake	CDC Blazer	Maple
1800057	2016	PVRT	Lucky Lake	CDC 3548-2	Forage
1800058	2016	PVRT	Lucky Lake	CDC 4140-4	Wrinkled
1800059	2016	PVRT	Lucky Lake	AAC Carver	Yellow
1800060	2016	PVRT	Lucky Lake	CDC Pluto	Green
1800071	2016	PVRT	Rosthern	CDC Golden	Yellow
1800072	2016	PVRT	Rosthern	CDC Striker	Green
1800073	2016	PVRT	Rosthern	CDC Meadow	Yellow
1800074	2016	PVRT	Rosthern	CDC Dakota	Dun
1800075	2016	PVRT	Rosthern	Redbat88	Red

1800076	2016	PVRT	Rosthern	CDC Blazer	Maple
1800077	2016	PVRT	Rosthern	CDC 3548-2	Forage
1800078	2016	PVRT	Rosthern	CDC 4140-4	Wrinkled
1800079	2016	PVRT	Rosthern	AAC Carver	Yellow
1800080	2016	PVRT	Rosthern	CDC Pluto	Green
1800081	2016	PVRT	Rosthern	CDC Golden	Yellow
1800082	2016	PVRT	Rosthern	CDC Striker	Green
1800083	2016	PVRT	Rosthern	CDC Meadow	Yellow
1800084	2016	PVRT	Rosthern	CDC Dakota	Dun
1800085	2016	PVRT	Rosthern	Redbat88	Red
1800086	2016	PVRT	Rosthern	CDC Blazer	Maple
1800087	2016	PVRT	Rosthern	CDC 3548-2	Forage
1800088	2016	PVRT	Rosthern	CDC 4140-4	Wrinkled
1800089	2016	PVRT	Rosthern	AAC Carver	Yellow
1800090	2016	PVRT	Rosthern	CDC Pluto	Green
1800101	2016	PVRT	Kamsack	CDC Golden	Yellow
1800102	2016	PVRT	Kamsack	CDC Striker	Green
1800103	2016	PVRT	Kamsack	CDC Meadow	Yellow
1800104	2016	PVRT	Kamsack	CDC Dakota	Dun
1800105	2016	PVRT	Kamsack	Redbat88	Red
1800106	2016	PVRT	Kamsack	CDC Blazer	Maple
1800107	2016	PVRT	Kamsack	CDC 3548-2	Forage
1800108	2016	PVRT	Kamsack	CDC 4140-4	Wrinkled
1800109	2016	PVRT	Kamsack	AAC Carver	Yellow
1800110	2016	PVRT	Kamsack	CDC Pluto	Green
1800111	2016	PVRT	Kamsack	CDC Golden	Yellow
1800112	2016	PVRT	Kamsack	CDC Striker	Green
1800113	2016	PVRT	Kamsack	CDC Meadow	Yellow
1800114	2016	PVRT	Kamsack	CDC Dakota	Dun
1800115	2016	PVRT	Kamsack	Redbat88	Red
1800116	2016	PVRT	Kamsack	CDC Blazer	Maple
1800117	2016	PVRT	Kamsack	CDC 3548-2	Forage
1800118	2016	PVRT	Kamsack	CDC 4140-4	Wrinkled
1800119	2016	PVRT	Kamsack	AAC Carver	Yellow
1800120	2016	PVRT	Kamsack	CDC Pluto	Green

PVRT: Pea Variety Regional Trial

Appendix C: Grinding Methods and Strategies Tested

Cryogrinding

Grinding of pea seeds was tested using liquid nitrogen. Twelve pea seeds of CDC Bronco were placed in capped 50 mL polycarbonate round bottom tubes and were ground at room temperature, using 2 zirconia cylinders (12*12 mm) and 4 zirconia balls (6.5 mm) in a Geno Grinder 10 (SPEX SamplePrep, LLC, UK) for 2 minutes at 1650 rpm. The seeds were partially broken by this process. The inhomogeneous meal was transferred to pre-chilled mortar and pestle and liquid nitrogen was added before grinding it into fine powder. The first Geno Grinder step of cryogrinding was also evaluated in pre-frozen polycarbonate tubes in a Geno Grinder 10 which is designed to hold cryo-blocks and keep the samples cold during processing.

Cyclone milling

Retsch mill (Ultra Centrifugal Mill ZM 200, Retsch, Germany) and UDY cyclone mill (Model: 3010-014, UDY Corporation, Fort Collins, U.S) were evaluated for grinding pea seeds (Table C1). These mills were tested on twelve pea seeds of three genotypes CDC Bronco, CDC Meadow and CDC Raezer. Seed weight before grinding and weight of pea flour after grinding was recorded and compared. Also, the average particle size was recorded.

Geno Grinder 10

Grinding was evaluated in a Geno Grinder 10 using zirconia balls of 6.5 mm diameter and zirconia cylinders (12*12 mm dimensions). Taking 12 pea seeds of CDC Bronco in 15 mL round bottom capped polycarbonate tubes in combination with zirconia balls/cylinders, grinding was tested at 1500 rpm and 1650 rpm in a Geno grinder 10 for 2

and 4 minutes. Instead of 15 mL, 50 mL flat bottom capped polycarbonate tubes were also tested.

Another experiment on grinding was conducted in a Geno Grinder 10 using metal balls (tungsten and steel balls) (Table C2 and C3). Grinding was evaluated for 30 and 15 pea seeds (CDC Bronco) at 1650 rpm speed and 2 minutes using different combinations of metal balls of varying size. Particle size of ground pea flour were measured and compared through microscopy for different grinding methods (Table C4). Pea seed samples were ground using a metal ball and without a metal ball in a Geno Grinder 10. AAS assay was conducted to evaluate potential metal contamination of seed samples by metal balls (Table C5).

Results and Discussion

Experiments to develop appropriate grinding method for pea seeds

Cryogrinding: Cryogrinding is considered an efficient way of grinding, particularly for heat sensitive and tough materials. Since most materials become brittle when exposed to cold temperatures, cryogenic grinding utilizes this effect prior to and or during the grinding process. In cryogrinding methods, the sample should remain fully frozen throughout the grinding procedure and afterwards, till the ground sample dries fully, under vacuum. Dry pea seeds were first ground at room temperature or at liquid N_2 temperatures in a cryo-block using a Geno Grinder 10 and then transferred to ceramic mortars partially filled with liquid nitrogen for a second manual grinding. Both these protocols resulted in condensation of vapors from room temperature air and gain of moisture by pea flour. Additionally, the polycarbonate cryo tubes became brittle and cracked, so the idea of cryogrinding was abandoned. Adrjanowicz et al. (2011) also

reported that cryogrinding can activate and accelerate not only structural changes, but chemical decomposition in samples.

Cyclone mill: In mill grinding, the screen sizes used were 0.5 mm and 0.4 mm for Retsch and UDY cyclone mills, respectively. Percentage loss in weight was calculated and on average percentage weight loss was approximately 15% and 26-27% for Retsch and UDY cyclone mills, respectively (Table C1). Average particle size obtained by both methods of mill grinding was ~ 100 µm. So, it was concluded that the powder obtained by mill grinding was too coarse for XRF analysis and the loss of powder was significantly high.

Table C1 Grinding evaluation using Retsch mill and UDY cyclone mill.

Cultivar	No. seeds	Total seed wt. (g)	Grinding method	Screen mesh size (mm)	Total flour wt. (g)	% Loss	Mean % loss	Mean Retsch Mean % loss	Mean UDY Mean % loss
CDC Bronco	12	2.4	Retsch	0.5	2.3	7.0	11.8	15.5	26.7
CDC Bronco	12	2.4	Retsch	0.5	2.1	11.9			
CDC Bronco	12	2.5	Retsch	0.5	2.1	16.3			
CDC Bronco	12	2.4	UDY	0.4	1.9	18.3	24.7		
CDC Bronco	12	2.3	UDY	0.4	1.8	23.7			
CDC Bronco	12	2.4	UDY	0.4	1.6	31.9			
CDC Meadow	12	2.4	Retsch	0.5	1.9	18.1	15.1		
CDC Meadow	12	2.1	Retsch	0.5	1.7	16.4			
CDC Meadow	12	2.2	Retsch	0.5	1.9	10.9			
CDC Meadow	12	2.3	UDY	0.4	2.1	9.1	32.5		
CDC Meadow	12	2.2	UDY	0.4	0.9	58.4			
CDC Meadow	12	2.4	UDY	0.4	1.7	30.0			
CDC Raezer	12	2.9	Retsch	0.5	2.5	12.9	19.6		
CDC Raezer	12	2.8	Retsch	0.5	1.9	31.8			
CDC Raezer	12	2.8	Retsch	0.5	2.4	14.1			
CDC Raezer	12	2.7	UDY	0.4	2.1	20.3	23.1		
CDC Raezer	12	2.9	UDY	0.4	2.2	23.9			
CDC Raezer	12	2.8	UDY	0.4	2.1	25.1			

Geno Grinder: Using a Geno Grinder 10, no seed damage was observed, or partially broken seeds were obtained when zirconia balls were used as grinding media at 1500 rpm for 12 pea seeds in 15 mL round bottom capped polycarbonate tubes. Most of the seeds were intact and the cotyledons were barely damaged even when the number of balls was increased from 1 to 3 and grinding time was increased from 2 to 4 minutes. Seed coats of split seeds were present as large flakes. Coarse powder was obtained when more than one zirconia cylinder was used as grinding media for 2 and 4 minutes. Zirconia balls and cylinders individually did not produce the desired fineness of powder, so a combination of zirconia balls and cylinders was also evaluated which failed to give satisfactory results.

It was observed that powder compacted at the bottom in 15 mL tubes due to the narrow cross-section of the tube, so, 50 mL flat bottom polycarbonate capped tubes (OPS Diagnostics LLC, Lebanon, Pennsylvania, USA) were tested for grinding.

Due to the light weight of zirconia balls and cylinders, metal balls were tested for grinding pea seeds. Use of multiple tungsten balls resulted in surface chip off at 1650 rpm speed when grinding was done for 2 minutes in a Geno Grinder 10 (Table C2). The weight of one tungsten ball was not enough to produce fine grinding. It was also observed that grinding of 15 seeds at a time produced finer powder as compared to 30 seeds in 50 mL polycarbonate tubes.

Table C2 Grinding evaluation using tungsten balls.

Trial No.	No. of seeds	Balls	Speed (rpm)	Time (min)	Pea flour	Comments
1	30	1 L T	1650	2	Coarse	
2	30	2 L T	1650	2	Coarse	Tungsten ball surface shatters
3	30	3 L T	1650	2	Large pieces of seeds	Tungsten ball surface shatters
4	30	1 L T + 5 S Z	1650	2	Worse than 1	
5	30	2 L T + 5 S Z	1650	2	Coarse	
6	30	3 L T + 5 S Z	1650	2	Big pieces	
7	30	1 L T + 10 S Z	1650	2	Worse than 1	
8	30	2 L T + 10 S Z	1650	2	Coarse	Tungsten ball surface shatters
9	30	3 L T + 10 S Z	1650	2	Big pieces	Tungsten ball surface shatters
10	15	1 L T	1650	2	Finer than 1	
11	15	2 L T	1650	2	Coarse	Tungsten ball surface shatters
12	15	3 L T	1650	2	Coarse	Tungsten ball surface shatters
13	15	1 L T + 5 SZ	1650	2	Better than 4	
14	15	2 L T + 5 S Z	1650	2	Worse than 11, better than 5	
15	15	3 L T + 5 S Z	1650	2	Worse than 12, better than 6	
16	15	1 L T + 10 S Z	1650	2	Worse than 1	
17	15	2 L T + 10 S Z	1650	2	Coarse	Tungsten ball surface shatters
18	15	3 L T + 10 S Z	1650	2	Big pieces	Tungsten ball surface shatters

L T= large tungsten ball (13 mm diameter); S Z= Small zirconia balls (5mm diameter)

Another experiment involved use of a combination of steel and zirconia balls (Table C3). The first grinding was done using steel balls of 13 mm diameter, and the second grinding was done using zirconia balls of 6.5 mm diameter at 1650 rpm. The finest powder was obtained when the first grinding was done using one steel ball, and the second using 30 zirconia balls. It was observed that the base of the tubes broke in the first grinding when grinding was done at 1650 rpm using a steel ball. So, the first grinding was done at 1350 rpm using a steel ball, and the second grinding was conducted by zirconia balls at 1650 rpm. Epoxy was used to reinforce the base of the 50 mL polycarbonate tubes, but it did not hold for long. Later, new tubes were manufactured with a hard polycarbonate base to resolve this issue.

Table C3 Grinding evaluation using steel and zirconia balls.

Trial No.	Balls (1st grinding + 2nd grinding)	Pea flour	Comments
1	1 S	Fine	Tube base broke
2	2 S	Coarse	Tube base broke
3	1 S + 10 Z	Finer than 1	Tube base broke
4	1 S + 15 Z	Finer than 1 and 2	Tube base broke
5	1 S + 30 Z	Finest among all	Tube base broke
6	2 S + 10 Z	Coarse compared to 3	Tube base broke
7	2 S + 15 Z	Coarse compared to 6	Tube base broke
8	2 S + 30 Z	Coarse compared to 6 and 7	Tube base broke

S= Small steel ball (13 mm diameter); Z= Zirconia balls (6.5 mm diameter)

The average particle size of pea flour (CDC Meadow) obtained by mill grinding (Retsch and UDY cyclone), and Geno Grinder 10 (first grinding using 1 steel ball and second using 30 zirconia balls of 6.5 mm diameter) was measured through microscopy and compared to particle size of pea starch purchased from Parrheim Foods which was fine enough for XRF analysis (Table C4).

Table C4 Mean particle size and standard deviation of randomly measured particles after mill grinding (Retsch and UDY cyclone) and grinding by Geno Grinder 10 (first grinding using 1 steel ball and second using 30 zirconia balls of 6.5 mm diameter) compared to a particle size of pea starch.

	CDC Meadow (Retsch)	CDC Meadow (UDY cyclone)	Geno Grinder 10	Pea Starch (Parrheim)
	µm	µm	µm	µm
Mean large particles	195.1	158.1	30.9	29.6
Standard deviation (Large particles)	116.9	69.0	8.1	7.8
Mean small particles	60.9	41.1	7.5	12.3
Standard deviation (Small particles)	15.1	14.4	4.3	5.2

Nineteen pea seed samples randomly selected from the Calibration Set were analyzed using AAS after grinding without using steel ball and with one steel ball in a Geno Grinder 10 and no significant iron contamination was observed. (Table C5).

Table C5 **Paired t-test for means of Fe concentrations with and without using steel balls for grinding 19 pea seed samples. Critical two-tail t value is greater than t stat value indicating no difference in Fe concentrations in both cases at *P*<0.05.**

	Fe conc. (mg/kg) without steel ball	Fe conc. (mg/kg) with steel ball
Mean	43.7	43.8
Variance	48.7	48.0
Observations	19	19
Pearson Correlation	0.99	
Hypothesized Mean Difference	0	
Degrees of freedom	18	
t Stat	-0.2	
P(T<=t) two-tail	0.8	
t Critical two-tail	2.1	

Appendix D: Concentration Predictions Based on Standard curves

Standard curves in solid matrix

Pure elements or compounds containing the elements were used for standard curves. Fine powders of iron sulphate ($FeSO_4$, CAS# 7720-78-7, Ameresco), selenium powder for selenium (Se, CAS# 7782-49-2 and Aldrich), manganese carbonate ($MnCO_3$, CAS# 598-62-9, Aldrich), copper oxide for copper (Cu_2O, CAS# 1317-39-1, Alfa Aesar), potassium phosphate dibasicanhydrous (HK_2O_4P, CAS# 7758-11-4, Fluka) and zinc powder (Zn, CAS# 7440-66-6, Aldrich) were mixed with a pea starch fraction to prepare master stock of known concentration of the element of interest, and diluted further in pea starch as required (Table D2). The powders of the standard compounds and the starch matrix were thoroughly mixed by shaking with 30 zirconia balls in a 50 ml tube in a Geno Grinder 10 for 2 minutes at 1650 rpm. Three pellets of 0.7 mm thickness were prepared for each dilution of each element using 120 mg pea flour and stored in dark in vacuum chambers till further use. Sample discs were irradiated using instrument settings and parameters listed in table D1. The average peak areas of each element were plotted against the concentrations to obtain standard equations which were used for predicting concentrations in Subset of Calibration Set (Appendix E). XRF predicted concentrations were correlated to AAS concentrations.

Table D1 XRF instrument set up and conditions for the analysis of zinc, selenium, calcium, manganese, copper, potassium and iron for sub set of Calibration Set.

Condition	Set Up
Atmosphere	Vacuum
Voltage (eV)	13800
Highest beam Current (mA)	220
Acquisition time (secs)	260
Detector	Silicon Drift

Table D2 Standard concentrations for each element in the solid matrix for standard curve preparation.

Element	Concentrations (mg/kg)
K	0, 1000, 3000, 6000, 9000, 12000, 15000, 20000
Ca	0, 10, 100, 500, 1000, 1500
Mn	0, 1, 2, 4, 8, 12, 20
Fe	0, 10, 30, 50, 80, 120, 150, 200
Cu	0, 1, 2, 3, 5, 8, 12, 30
Zn	0, 5, 10, 20, 30, 60, 80
Se	0, 1, 4, 6, 8, 12, 16

Standard curves in solution

For preparation of standard curves in solution, liquid NIST standards used for ICP-MS analysis were obtained from Tissue Culture lab, Plant Sciences, University of Saskatchewan. Standard dilutions were prepared by mixing known quantities of the liquid standards in deionized water (Table D4). A slit of 2 mm thickness was used to hold 150-micro liter liquid and covered by Kapton tape from both sides. Standards were also

analyzed in air with instrument settings and parameters listed in table D3. Three spectra were recorded for each dilution and the average areas were plotted against the concentrations to obtain standard equations which were used for predicting concentrations in Validation Set. XRF predicted concentrations were correlated to AAS concentrations.

Table D3 XRF instrument set up and conditions for the analysis of K, Ca, Mn, Fe, Cu, Zn and Se.

Condition	Set Up
Atmosphere	Air
Voltage (eV)	13000
Highest beam Current (mA)	220
Acquisition time (secs)	260
Detector	Silicon Drift

Table D4 Standard concentrations for each element in solution for standard curve preparation.

Element	Concentrations (mg/kg)
Potassium	0, 1000, 3000, 5000, 8000, 11000, 14000, 17000, 20000
Iron	0, 20, 40, 50, 60, 70,80,90,100, 150
Zinc	0, 20, 30, 40, 50, 60
Copper	0, 1, 2, 3, 5, 7, 9
Manganese	0, 4, 8, 12, 16, 20
Selenium	0, 1, 1.5, 2, 2.5, 5

Results

Standard curves (In solid matrix and solution)

Standards in solid matrix were prepared by mixing known quantities of solid compounds or pure elements with pea starch (Roquette America, Inc.). Preparation of well homogenized solid samples for development of calibration curves is technically challenging and time consuming. For this reason, standard curves in solution were evaluated as an alternative. The advantage of liquid standard curves is attainment of a high degree of homogeneity of element in the matrix and possibility of safe and quick preparation of numerous standard samples. Use of liquid standards also eliminates specific material properties like grain size effects and packing density (Jenkins, 1995).

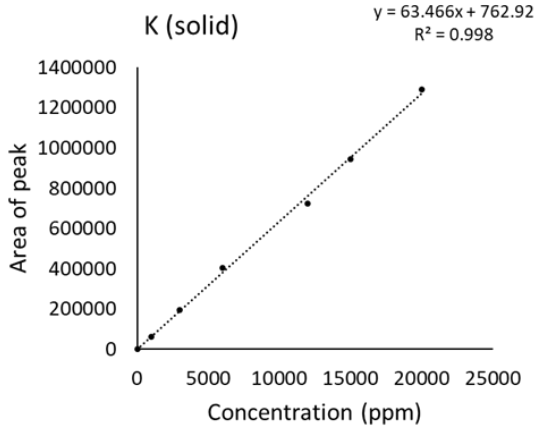
K (solid)
y = 63.466x + 762.92
R² = 0.998
Area of peak
Concentration (ppm)
1400000
1200000
1000000
800000
600000
400000
200000
0
0
5000
10000
15000
20000
25000

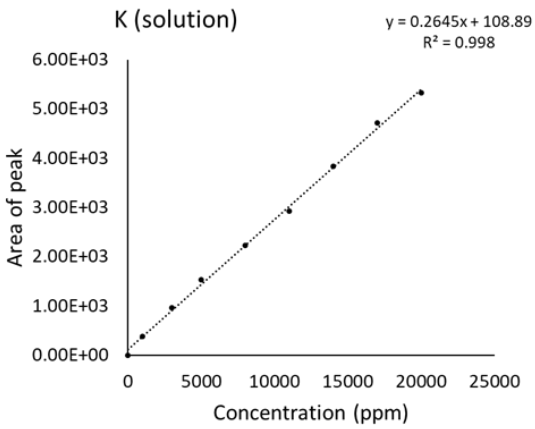
K (solution)
y = 0.2645x + 108.89
R² = 0.998
Area of peak
Concentration (ppm)
6.00E+03
5.00E+03
4.00E+03
3.00E+03
2.00E+03
1.00E+03
0.00E+00
0
5000
10000
15000
20000
25000

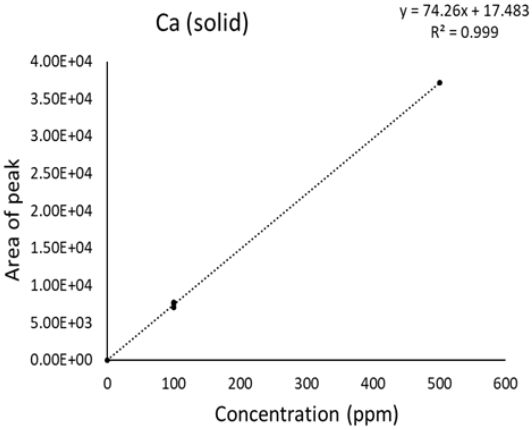
Ca (solid)
y = 74.26x + 17.483
R² = 0.999
Area of peak
Concentration (ppm)
4.00E+04
3.50E+04
3.00E+04
2.50E+04
2.00E+04
1.50E+04
1.00E+04
5.00E+03
0.00E+00
0
100
200
300
400
500
600

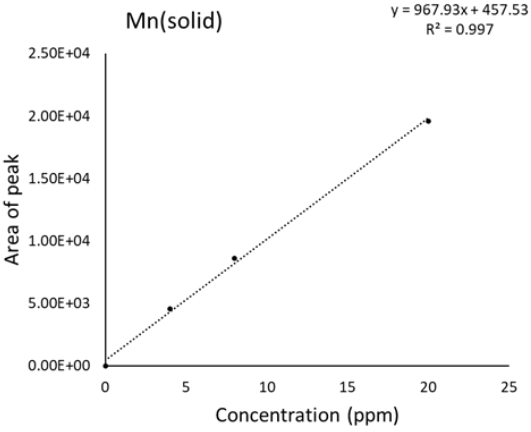
Mn(solid)
y = 967.93x + 457.53
R² = 0.997
Area of peak
Concentration (ppm)
2.50E+04
2.00E+04
1.50E+04
1.00E+04
5.00E+03
0.00E+00
0
5
10
15
20
25

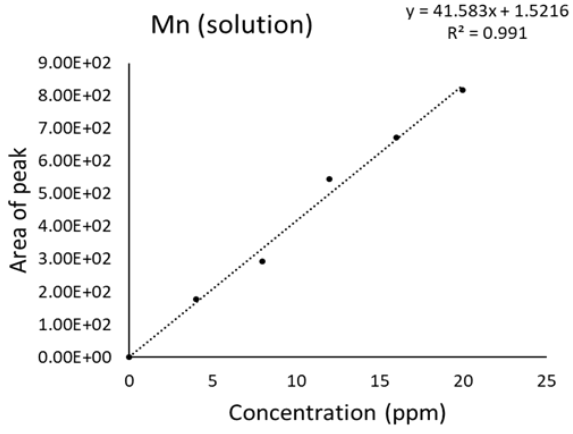
Mn (solution)
y = 41.583x + 1.5216
R² = 0.991
Area of peak
Concentration (ppm)
9.00E+02
8.00E+02
7.00E+02
6.00E+02
5.00E+02
4.00E+02
3.00E+02
2.00E+02
1.00E+02
0.00E+00
0
5
10
15
20
25

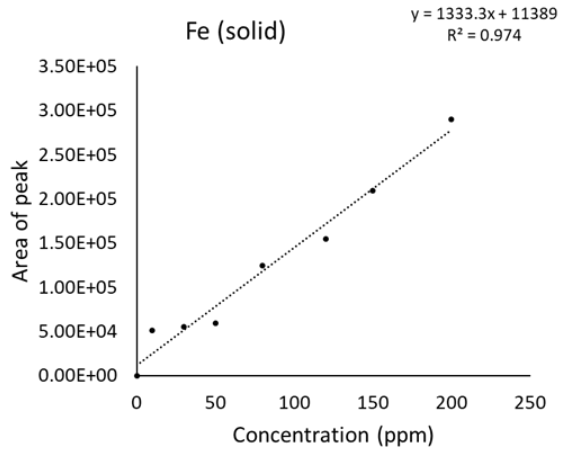
Fe (solid)
y = 1333.3x + 11389
R² = 0.974
Area of peak
Concentration (ppm)

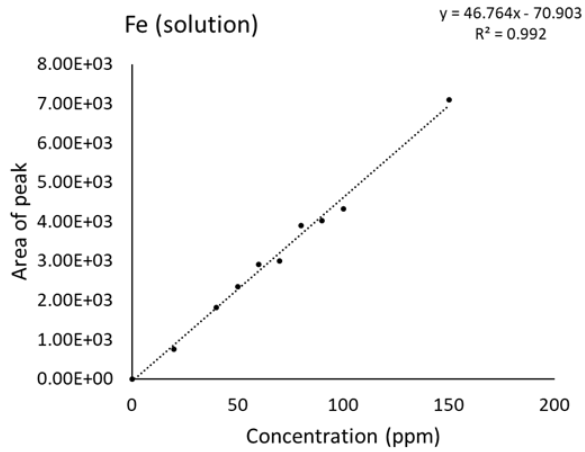
Fe (solution)
y = 46.764x - 70.903
R² = 0.992
Area of peak
Concentration (ppm)

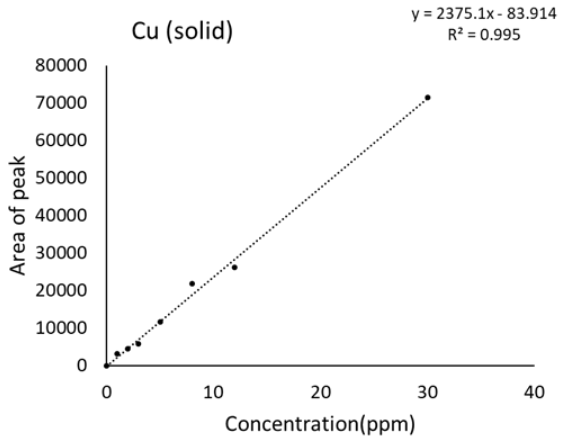
Cu (solid)
y = 2375.1x - 83.914
R² = 0.995
Area of peak
Concentration(ppm)

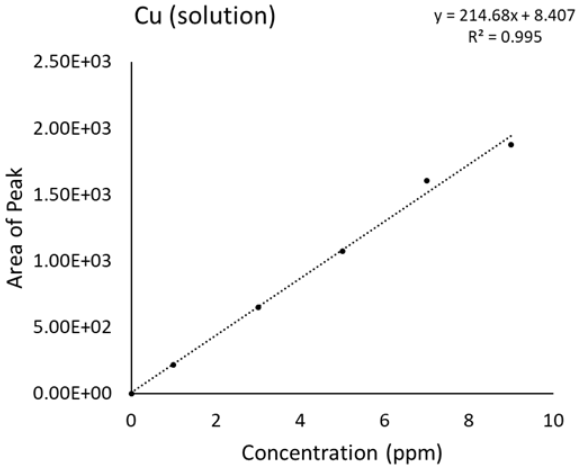
Cu (solution)
y = 214.68x + 8.407
R² = 0.995
Area of Peak
Concentration (ppm)

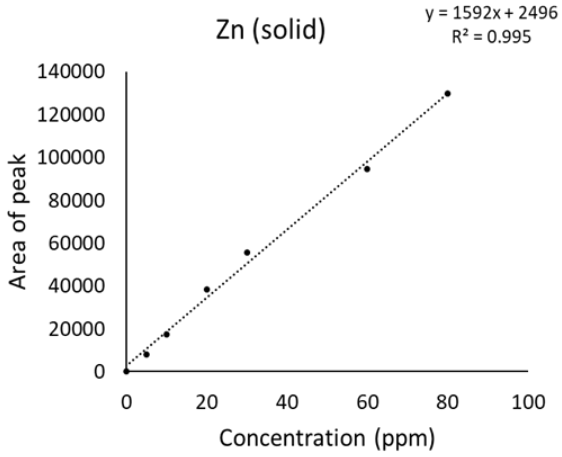
Zn (solid)
y = 1592x + 2496
R² = 0.995
Area of peak
Concentration (ppm)

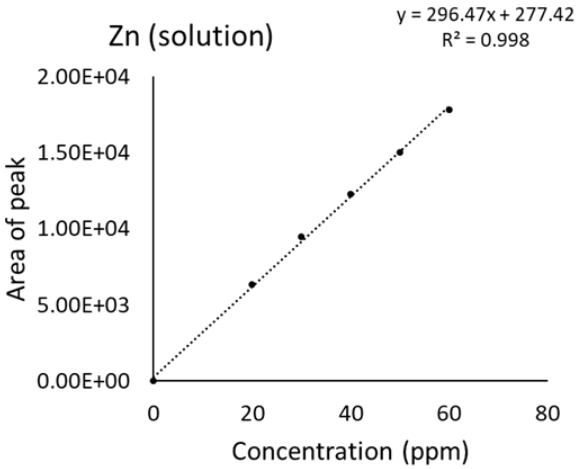
Zn (solution)
y = 296.47x + 277.42
R² = 0.998
Area of peak
Concentration (ppm)

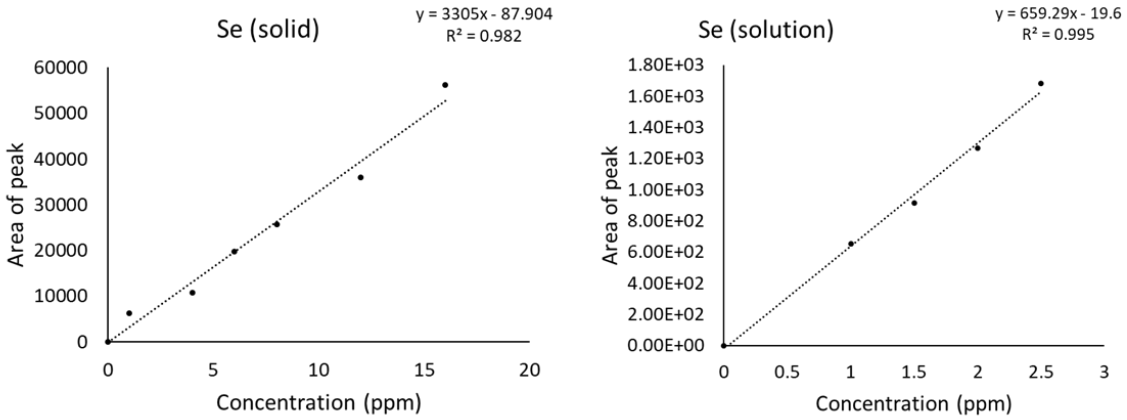

Figure D1 Element-specific standard curve plots by correlating known concentrations and area of the peak. Solid and solution in headings indicate the standard in solid matrix and solution respectively.

The standard curves were plotted by correlating plot peak areas and known concentrations of standards as shown in Figure IV.1 (for solid matrix and liquid standard curves). Standard curves in solid matrix and solution cover the range of element concentrations in seed samples. R^2 value for Ca standard curve in solid matrix was 0.999. Only three data points are shown in Ca standard curve due to loss of spectra files. R^2 value for Mn are 0.997 and 0.991 for standard curve in solid matrix and solution, respectively, 0.995 and 0.998 for Cu and K, respectively for both solid matrix and solution standard curve. For Zn, correlation coefficient was 0.995 for standard curve in solid matrix and 0.998 for standard curve in solution. R^2 values are 0.974 and 0.992 for Fe standard curve in solid matrix and solution, respectively. For Se standard curves correlation coefficient is 0.982 and 0.995 for solid and solution standard curve, respectively. Though, R^2 values are comparable in both type of standard curves, slopes

are significantly different depending on the standard compounds or standard solutions used for preparation of standard curves.

Table D5 Characteristics of standard curves obtained from the solid matrix with units expressed in mg/kg for Min, Max, and RSD.

Parameter→ Element↓	Min (mg/kg)	Max (mg/kg)	Slope	Intercept	R^2	RSD (mg/kg)
K	1000	20000	63.46	762.92	0.998	354.02
Ca	100	500	74.26	17.48	0.999	3.76
Mn	5	20	967.93	457.53	0.997	1.05
Fe	10	200	1333.3	11389	0.974	13.14
Cu	1	30	2375.1	-83.91	0.995	0.93
Zn	10	80	1592	2496	0.995	2.98
Se	1	15	3305	-87.904	0.982	0.84

Table D6 Characteristics of standard curves obtained from solutions with units expressed in mg/kg for Min, Max, and RSD.

Parameter→ Element↓	Min (mg/kg)	Max (mg/kg)	Slope	Intercept	R^2	RSD (mg/kg)
K	1000	20000	0.26	108.89	0.998	272.65
Mn	4	20	41.58	1.52	0.991	0.67
Fe	20	150	46.76	-70.90	0.992	3.64
Cu	1	9	214.68	8.41	0.995	0.28
Zn	20	60	296.47	277.42	0.998	0.78
Se	1	5	659.29	-19.6	0.995	0.06

Prediction of element concentrations in Subset of Calibration Set using standard curves in solid matrix

Using the standard equations obtained from standard curves in solid matrix, XRF predicted concentrations of Subset of Calibration Set were correlated with AAS concentrations. These plots were statistically analyzed using linear regression. For comparison, R, intercept (A) and slope (B) were evaluated. Intercept and slope were evaluated at 95% confidence interval. If the results (concentrations for seed samples) from two different methods are not significantly different, these parameters should have R ~1, confidence interval for intercept (A) should contain 0 and confidence interval for slope (B) should contain 1. Figure IV.2 shows the correlation plots between XRF predicted concentrations and AAS concentrations for Subset of Calibration Set. Table IV.7 summarizes the characteristic parameters for these correlation plots.

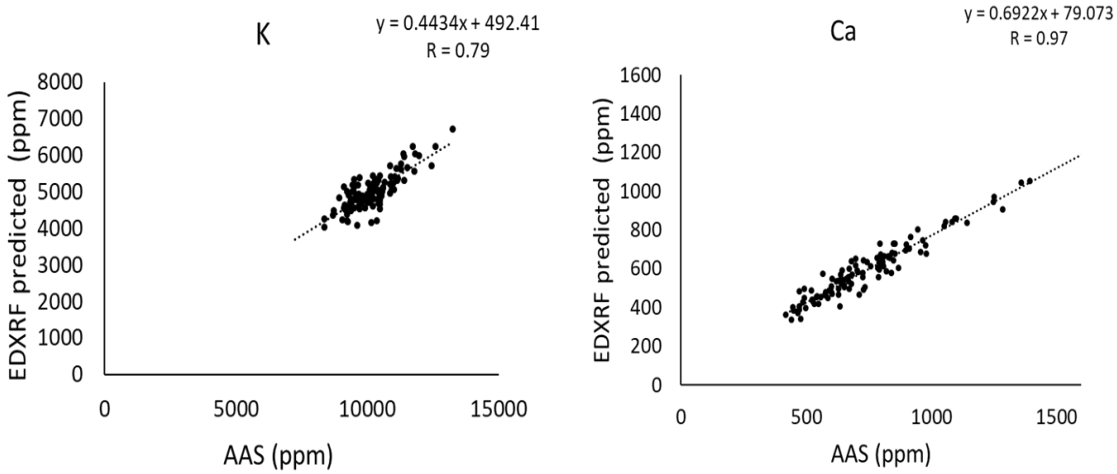

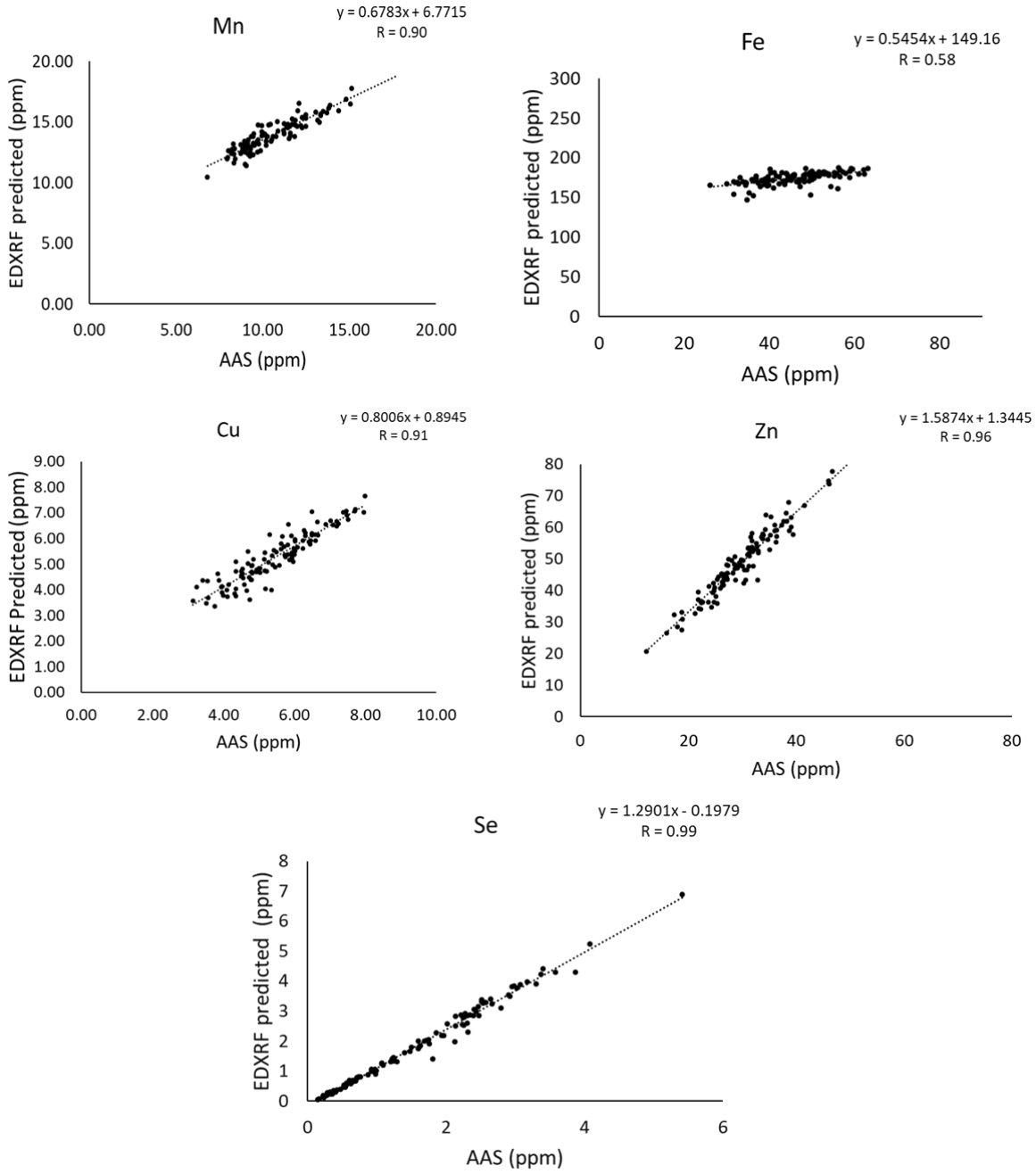

Figure D2 Correlation plots between XRF predicted values using standard curves in a solid matrix and AAS concentrations for Subset of Calibration Set.

Table D7 Characteristic of correlation plots between XRF predicted and AAS concentrations (mg/kg), SD= Standard deviation of differences (mg/kg), SEP = Standard error of prediction (mg/kg).

Analyte	SD (d)	Bias	R	CI of slope	CI of Intercept	SEP
K	604.28	-5182.4	0.79	0.48 to 0.57	-761.25 to 113.97	5099.14
Ca	103.47	-154.74	0.97	0.68 to 0.74	38.12 to 89.20	180.21
Mn	0.78	3.19	0.90	0.77 to 0.85	4.90 to 5.79	3.33
Fe	19.06	127.53	0.58	1.34 to 1.81	91.24 to 113.01	126.79
Cu	0.45	-0.18	0.91	0.82 to 0.90	0.33 to 0.78	0.46
Zn	4.94	19.1	0.96	1.66 to 1.76	-3.91 to -0.72	19.39
Se	0.64	0.2	0.99	1.29 to 1.32	-0.24 to -0.19	0.67

The slope of the curve could not be considered 1 and intercept 0 for any of the elements. Strong R values indicate a relationship between two methods, but the values obtained from both methods were not the same. Bias was significant for K, Ca, Fe, and Zn. Negative bias indicates under-prediction of the XRF method in comparison to the reference method, whereas, positive bias is the indication of overprediction. SEP indicates average deviation of XRF predicted values from AAS concentrations. Bias and standard error of prediction in terms of coefficient of variation or percent bias would allow comparison of deviation between the elements. Systematic bias of 127 mg/kg and 3 mg/kg in Fe and Mn, respectively, were the result of scatter contribution from the steel vacuum chamber.

Prediction of element concentrations in the Validation Set using standard curves in solutions

Standard equations obtained from the liquid standard curves were used for predicting element concentrations in the Validation Set and predicted concentrations were compared with AAS concentrations (Figure D3). Since, the Validation Set was irradiated in air (outside the vacuum chamber), the systematic bias due to the steel chamber

contamination in the Subset of Calibration Set was not an issue in the Validation Set. Correlation between XRF predicted concentrations using the standard equations from standards curves in solution for Validation Set and AAS concentrations was ~ or > 0.7 for Mn, Fe, Cu, Zn and Se and 0.55 for K. XRF underpredicted all the elements except K which was over predicted three times. The slope can be considered 1 for Fe and intercept 0 in comparison with AAS concentrations. This leads to the conclusion that concentrations predicted using liquid standard curves are biased in one way or other except in the case of Fe.

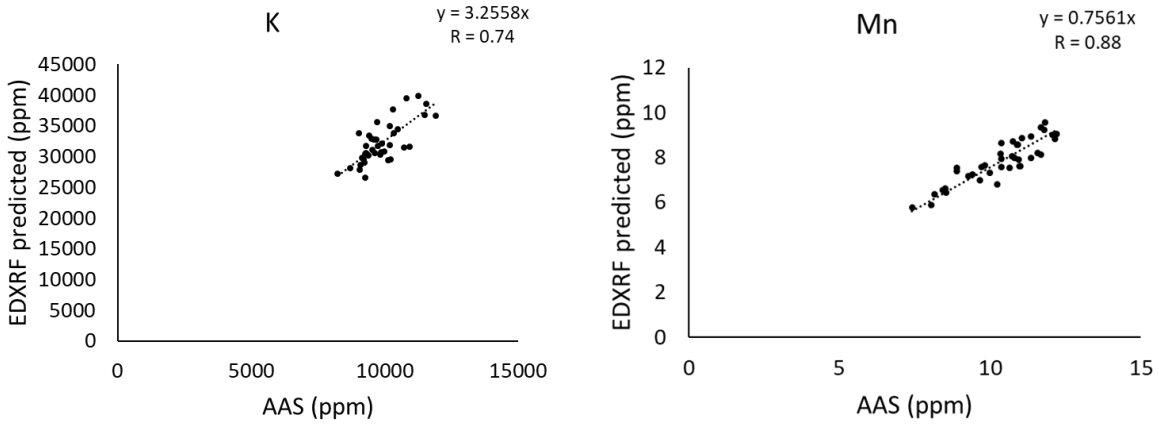

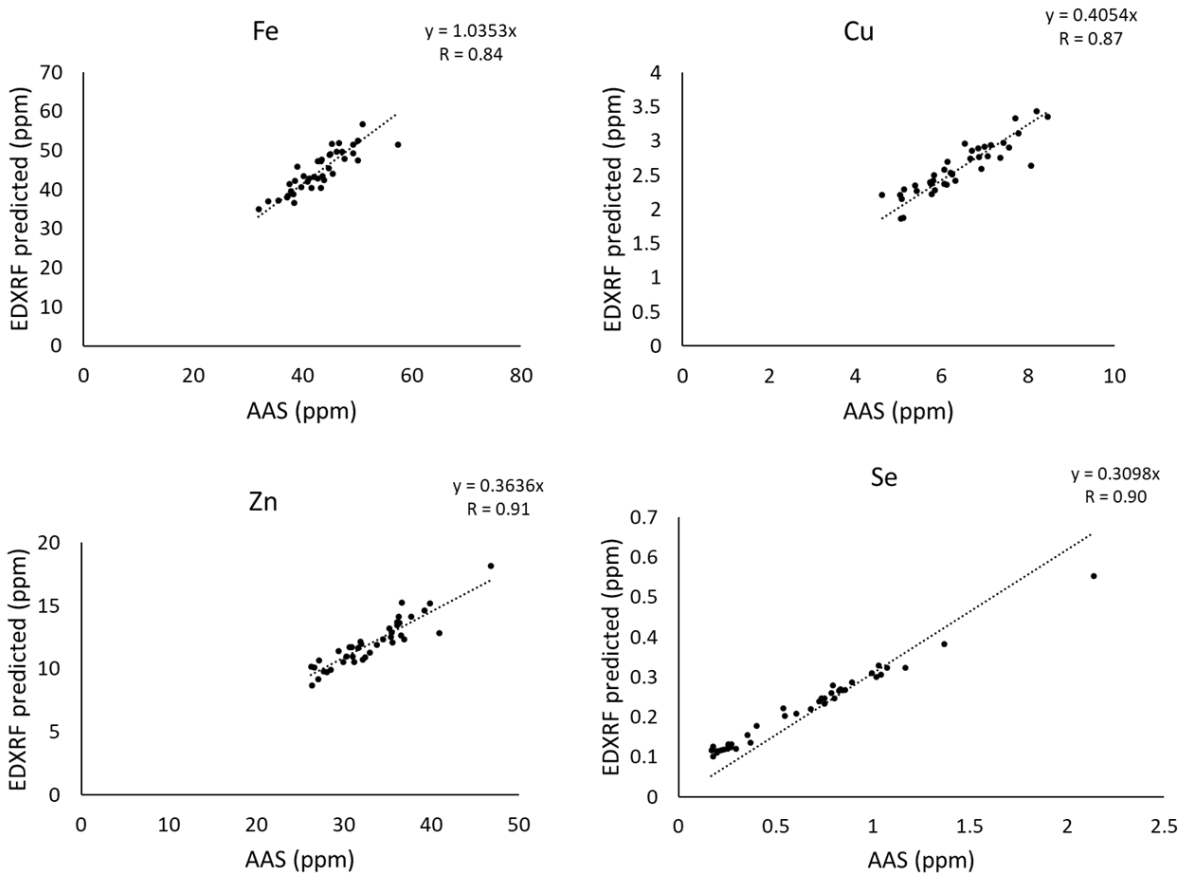

Figure D3 Correlation between XRF predicted concentrations using standard curves in solution and AAS concentrations for Validation Set.

Table D8 Slopes and R values of correlation plots between XRF predicted concentrations using standard curves in solutions and AAS concentrations for Validation Set.

Element	Validation Set	
	Slope	**R**
K	3.255	0.74
Mn	0.756	0.88
Fe	1.035	0.84
Cu	0.405	0.87
Zn	0.363	0.91
Se	0.309	0.90

The prediction of element concentrations in pea seed samples using standard curves, prepared in solid matrix or solutions, was not satisfactory. Though R values were not low for most of the elements (<0.5), the slope ≠ 1 indicated significantly biased prediction compared to the reference method (AAS). This can be attributed to the fact that the matrix of standard curves prepared in pea starch, and matrix of standard curves prepared in solution was significantly different compared to matrix of seed samples, which were prepared from whole pea seeds. Thus, using the matrix similar to unknown samples (pea seed samples) to prepare the calibration curves was recommended as a better solution. The other possible solution was to try a standard less approach (XRF-FP).

Appendix E: List of Subset of Calibration Set Used for Predicting Concentrations from Standard Curves in Solid Matrix

Sample No	Year	Expt.	LOC	ENTRY	NAME
1700001	2013	GWAS Sutherland	Sutherland	73	KASPA
1700002	2013	GWAS Sutherland	Sutherland	12	Avantgarde
1700003	2013	GWAS Sutherland	Sutherland	26	Camry
1700004	2013	GWAS Sutherland	Sutherland	161	Torsdag
1700005	2013	GWAS Sutherland	Sutherland	22	Neon
1700006	2013	GWAS Sutherland	Sutherland	146	CDC Golden
1700007	2013	GWAS Sutherland	Sutherland	176	Aragorn
1700008	2013	GWAS Sutherland	Sutherland	161	Torsdag
1700009	2013	GWAS Sutherland	Sutherland	40	AMPLISSIMO ZAZERSKIJ
1700010	2013	GWAS Sutherland	Sutherland	141	MPG87
1700011	2011	PAM_Rosthern	Rosthern	8	TMP 15159
1700012	2011	PAM_Rosthern	Rosthern	80	Laxtons-Superb
1700013	2012	PAM_Rosthern	Rosthern	13	TMP 15202
1700014	2012	PAM_Rosthern	Rosthern	34	MFR043
1700015	2013	PAM_Rosthern	Rosthern	81	Superscout
1700016	2013	PAM_Rosthern	Rosthern	49	Trapper
1700017	2013	PAM_Rosthern	Rosthern	15	MPG87
1700019	2013	PAM_Rosthern	Rosthern	15	MPG87
1700021	2012	PAM_Rosthernhern	Rosthern	53	MI3391
1700022	2012	PAM_Rosthernhern	Rosthern	46	CDC Acer
1700023	2012	PAM_Rosthernhern	Rosthern	85	Rally
1700024	2012	PAM_Rosthernhern	Rosthern	53	MI3391
1700025	2011	PAM_Sutherland	Sutherland	63	Lucky
1700026	2011	PAM_Sutherland	Sutherland	19	CDC Bronco
1700027	2011	PAM_Sutherland	Sutherland	27	CDC Striker
1700032	2011	PAM_Sutherland	Sutherland	51	CDC Vienna
1700033	2011	PAM_Sutherland	Sutherland	29	Nitouche
1700034	2011	PAM_Sutherland	Sutherland	94	Aragorn
1700036	2011	PAM_Sutherland	Sutherland	22	CDC Mozart
1700037	2011	PAM_Sutherland	Sutherland	50	Radley
1700038	2011	PAM_Sutherland	Sutherland	89	P0321-08
1700039	2011	PAM_Sutherland	Sutherland	30	SW Sergeant
1700040	2011	PAM_Sutherland	Sutherland	28	Cooper
1700044	2011	PAM_Sutherland	Sutherland	1	TMP 15116
1700047	2011	PAM_Sutherland	Sutherland	54	MI3360
1700048	2011	PAM_Sutherland	Sutherland	42	Espace
1700049	2011	PAM_Sutherland	Sutherland	39	SW Marquee
1700050	2011	PAM_Sutherland	Sutherland	37	Orb
1700052	2011	PAM_Sutherland	Sutherland	41	CDC Sage
1700053	2011	PAM_Sutherland	Sutherland	80	Laxtons Superb
1700054	2011	PAM_Sutherland	Sutherland	77	PS05100632
1700055	2011	PAM_Sutherland	Sutherland	28	Cooper

1700056	2011	PAM_Sutherland	Sutherland	56	CDC 1-150-81
1700059	2011	PAM_Sutherland	Sutherland	46	CDC Acer
1700060	2011	PAM_Sutherland	Sutherland	30	SW Sergeant
1700061	2011	PAM_Sutherland	Sutherland	5	TMP 15133
1700064	2011	PAM_Sutherland	Sutherland	40	CDC Montero
1700065	2011	PAM_Sutherland	Sutherland	86	FDP2010
1700067	2011	PAM_Sutherland	Sutherland	34	MFR043
1700068	2011	PAM_Sutherland	Sutherland	21	CDC Golden
1700069	2011	PAM_Sutherland	Sutherland	85	Rally
1700070	2011	PAM_Sutherland	Sutherland	8	TMP 15159
1700072	2011	PAM_Sutherland	Sutherland	33	Rambo
1700073	2011	PAM_Sutherland	Sutherland	94	Aragorn
1700074	2011	PAM_Sutherland	Sutherland	23	CDC Meadow
1700075	2011	PAM_Sutherland	Sutherland	63	Lucky
1700076	2011	PAM_Sutherland	Sutherland	79	PS05101142
1700077	2011	PAM_Sutherland	Sutherland	54	MI3360
1700078	2011	PAM_Sutherland	Sutherland	62	Woody
1700083	2011	PAM_Sutherland	Sutherland	6	CDC Patrick
1700084	2011	PAM_Sutherland	Sutherland	20	CDC Centennial
1700086	2011	PAM_Sutherland	Sutherland	82	Lacy Lady
1700088	2011	PAM_Sutherland	Sutherland	53	MI3391
1700089	2011	PAM_Sutherland	Sutherland	77	PS05100632
1700092	2011	PAM_Sutherland	Sutherland	3	TMP 15121
1700095	2011	PAM_Sutherland	Sutherland	44	Torsdag
1700096	2011	PAM_Sutherland	Sutherland	7	TMP15155
1700097	2012	PAM_Sutherland	Sutherland	85	Rally
1700098	2012	PAM_Sutherland	Sutherland	13	TMP 15202
1700099	2012	PAM_Sutherland	Sutherland	26	Reward
1700100	2012	PAM_Sutherland	Sutherland	49	Trapper
1700101	2013	PAM_Sutherland	Sutherland	68	Hardy
1700102	2013	PAM_Sutherland	Sutherland	7	TMP 15155
1700104	2010	PR-07_SPG	SPG	144	3005-188
1700105	2010	PR-07_SPG	SPG	38	3005-51
1700106	2010	PR-07_SPG	SPG	38	3005-51
1700107	2010	PR-07_SPG	SPG	7	3005-7
1700108	2010	PR-07_SPG	SPG	15	3005-24
1700109	2010	PR-07_SPG	Rosthern	28	3005-40
1700110	2010	PR-07_SPG	SPG	29	3005-41
1700111	2010	PR-07_SPG	SPG	30	3005-42
1700113	2010	PR-07_SPG	SPG	34	3005-47
1700114	2010	PR-07_SPG	SPG	59	3005-86
1700115	2010	PR-07_SPG	SPG	74	3005-102
1700116	2010	PR-07_SPG	Rosthern	99	3005-132
1700117	2010	PR-07_SPG	SPG	135	3005-177
1700118	2010	PR-07_SPG	Rosthern	137	3005-181

1700120	2011	PR-07_SPG	SPG	8	3005-8
1700121	2011	PR-07_SPG	SPG	13	3005-21
1700122	2011	PR-07_SPG	SPG	66	3005-93
1700123	2011	PR-07_SPG	SPG	72	3005-100
1700124	2011	PR-07_SPG	Rosthern	16	3005-25
1700125	2011	PR-07_SPG	SPG	23	3005-33
1700126	2011	PR-07_SPG	Rosthern	106	3005-140
1700127	2012	PR-07_SPG	SPG	109	3005-144
1700128	2012	PR-07_SPG	SPG	3	3005-1
1700129	2012	PR-07_SPG	SPG	43	3005-56
1700130	2012	PR-07_SPG	Rosthern	55	3005-72
1700131	2012	PR-15_Rosthern	Rosthern	89	CDC Meadow
1700132	2012	PR-15_Rosthern	Rosthern	88	1-2347-144
1700133	2012	PR-15_Rosthern	Rosthern	2	CDC Meadow
1700134	2012	PR-15_Rosthern	Rosthern	107	PR-15-256
1700135	2012	PR-15_Rosthern	Rosthern	8	PR-15-24
1700136	2012	PR-15_Rosthern	Rosthern	105	PR-15-248
1700137	2012	PR-15_Rosthern	Rosthern	169	CDC Meadow
1700138	2012	PR-15_Rosthern	Rosthern	102	PR-15-244
1700139	2011	PR-15_Sutherland	Sutherland	1	1-2347-144
1700140	2011	PR-15_Sutherland	Sutherland	2	CDC Meadow
1700141	2011	PR-15_Sutherland	Sutherland	45	PR-15-64
1700142	2011	PR-15_Sutherland	Sutherland	51	PR-15-70
1700143	2011	PR-15_Sutherland	Sutherland	216	PR-15-318
1700144	2011	PR-15_Sutherland	Sutherland	221	PR-15-325
1700145	2011	PR-15_Sutherland	Sutherland	228	PR-15-336
1700146	2011	PR-15_Sutherland	Sutherland	282	1-2347-144
1700147	2011	PR-15_Sutherland	Sutherland	283	CDC Meadow
1700148	2012	PR-15_Sutherland	Sutherland	1	1-2347-144
1700149	2012	PR-15_Sutherland	Sutherland	58	PR-15-149
1700150	2012	PR-15_Sutherland	Sutherland	46	PR-15-113
1700151	2012	PR-15_Sutherland	Sutherland	35	PR-15-93
1700152	2012	PR-15_Sutherland	Sutherland	104	PR-15-246
1700153	2012	PR-15_Sutherland	Sutherland	88	1-2347-144
1700154	2012	PR-15_Sutherland	Sutherland	89	CDC Meadow
1700155	2012	PR-15_Sutherland	Sutherland	168	1-2347-144
1700156	2012	PR-15_Sutherland	Sutherland	128	PR-15-307

PAM: Pea Association Mapping panel, Crop Development Centre, University of Saskatchewan
SPG: Saskatchewan Pulse Growers located near Floral, Saskatchewan
PVRT: Pea Variety Regional Trial